



UNIVERSITATEA
DE MEDICINĂ ȘI FARMACIE
„VICTOR BABEȘ” DIN TIMIȘOARA

Dr. TRUȘCULESCU ANA ADRIANA

Co-autors:

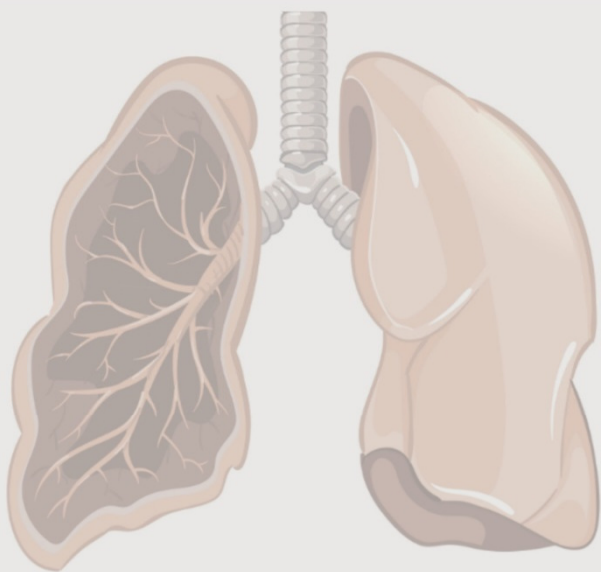
Dr. ing. Versavia ANCUȘA

Dr. Diana MANOLESCU

Dr. Daniel TRĂILĂ

Dr. Camelia PESCARU

Dr. Cristian OANCEA



COMPUTER-AIDED IMAGISTIC DIAGNOSIS IN DIFFUSE INTERSTITIAL LUNG DISEASES

Monograph after the doctoral thesis



HIPPOCRATE

Editura „Victor Babeș”
Timișoara, 2025

II

Editura „Victor Babeș”

Piața Eftimie Murgu nr. 2, cam. 316, 300041 Timișoara

Tel./ Fax 0256 495 210

e-mail: *evb@umft.ro*

<https://www.umft.ro/ro/organizare-evb/>

Director general: Prof. univ. dr. Sorin Ursoniu

Colecția: HIPPOCRATE

Coordonator colecție: Prof. univ. dr. Andrei Motoc

Referent științific: Prof. univ. dr. Claudia Borza

© 2025 Toate drepturile asupra acestei ediții sunt rezervate.

Reproducerea parțială sau integrală a textului, pe orice suport, fără acordul scris al autorilor este interzisă și se va sancționa conform legilor în vigoare.

ISBN 978-606-786-510-3

TABLE OF CONTENTS

LIST OF ABBREVIATION.....	VI
LIST OF FIGURES	VII
LIST OF TABLES	IX
PREFACE	X
INTRODUCTION.....	XI
1. THE MOTIVATION FOR CHOOSING THIS RESEARCH TOPIC	XI
2. THE IMPORTANCE AND TOPICALITY OF THE THEME	XII
3. FRAMING THE TOPIC IN THE INTERNATIONAL, NATIONAL, AND ZONAL CONCERNS OF THE RESEARCH GROUP	XIII
4. THE SCIENTIFIC OBJECTIVES TO BE SOLVED WITHIN THE DOCTORAL RESEARCH	XIII
5. BRIEF PRESENTATION OF THE WORK'S CONTENT	XIV
6. SYNTHETIC COMMENTS REGARDING THE RESEARCH METHODOLOGY AND THE MAIN RESULTS	XIV
GENERAL PART.....	1
1. ILD BACKGROUND	1
1.1. PULMONARY INTERSTITIAL FIBROSIS PATHOGENESIS.....	1
1.2. ILD CLASSIFICATION AND EPIDEMIOLOGY	2
1.3. ILD PROGRESSIVE PHENOTYPES.....	5
1.4. ILD TREATMENT	7
1.4.1. PHARMACOLOGICAL TREATMENT	8
1.4.2. NON-PHARMACOLOGICAL TREATMENT	8
2. ILD IMAGISTIC PATTERNS.....	10
2.1. WHAT ARE THE SIGNIFICANT CT FEATURES FOR MAKING A DIAGNOSIS OF ILD?.....	10
2.1.1. RETICULAR PATTERN	12
2.1.2. MICRONODULAR PATTERN	13
2.1.3. HIGH ATTENUATION.....	14
2.1.4. LOW ATTENUATION.....	16
2.1.5. OVERLAPPING MODELS	18
2.2. INTERCONNECTING HISTOPATHOLOGY WITH HRCT IMAGISTIC APPEARANCE.....	19

IV

3. IDIOPATHIC PULMONARY FIBROSIS (IPF)- THE REFERENCE DISORDER FOR PULMONARY FIBROSIS.....	29
3.1. THE SPECTRUM OF HRCT FINDINGS IN IPF.....	29
3.2. IPF DIAGNOSTIC	33
4. ILD COMPUTER AIDED IMAGISTIC DIAGNOSTIC.....	36
RESEARCH PART	39
5. CHAPTER 1: FACILITIES AND PITFALLS FOR USING CAD FOR ILD DIAGNOSIS.....	39
5.1. DEEP LEARNING IN INTERSTITIAL LUNG DISEASE – HOW LONG UNTIL DAILY PRACTICE.....	39
5.1.1. INTRODUCTION	39
5.1.2. COMPUTER-AIDED DIAGNOSIS HISTORY	40
5.1.3. INTERSTITIAL LUNG DISEASE-SPECIFIC CAD	43
5.1.4. HOW SOPHISTICATED SHOULD THE CNN BE?.....	44
5.1.5. IDIOPATHIC PULMONARY FIBROSIS – THE CHALLENGE OF ALL ILDS.....	46
5.1.6. DISCUSSION.....	47
5.2. COMPUTER-AIDED TECHNIQUES.....	48
5.2.1. REGRESSION	50
5.2.2. LINEAR REGRESSION	51
5.2.3. LOGISTIC REGRESSION.....	51
5.2.4. HIDDEN MARKOV MODELS	51
5.2.5. NEURAL NETWORKS.....	52
5.2.6. COMPLEX NETWORKS	52
5.2.7. LAYOUT ALGORITHM SELECTION	54
6. CHAPTER 2: A NOVEL METHOD FOR LUNG IMAGE PROCESSING USING COMPLEX NETWORKS.....	58
6.1. INTRODUCTION.....	58
6.2. USING HRCT – HUMANS & COMPUTERS	59
6.3. MATERIALS AND METHODS.....	60
6.3.1. LOT SELECTION.....	60
6.3.2. IMAGING PARAMETERS	61
6.3.3. IMAGE LOT SELECTION	62
6.3.4. IMAGE PROCESSING METHOD	63
6.4. RESULTS.....	66

6.4.1. Normal and ILD case sample results.....	67
6.4.2. Additional lot analyzation-results.....	71
6.5. DISCUSSION.....	72
6.5.1. NETWORK SYSTEM SCIENCE.....	72
6.5.2. MEDICAL SCIENCE.....	75
6.5.3. COMPARISON WITH OTHER HRCT ANALYSIS METHODS.....	79
7. CHAPTER 3: ENHANCING IMAGISTIC INTERSTITIAL LUNG DISEASE DIAGNOSIS BY USING COMPLEX NETWORKS.....	81
7.1. INTRODUCTION.....	81
7.2. ILD EARLY DIAGNOSIS.....	81
7.3. ILDs EVOLUTION AND IMAGISTIC DIAGNOSIS.....	82
7.4. COMPUTER-AIDED DIAGNOSIS.....	83
7.5. HYPOTHESIS TO BE EXPLORED.....	83
7.6. MATERIALS AND METHODS.....	84
7.6.1. LOT SELECTION.....	84
7.6.2. IMAGING PARAMETERS.....	86
7.6.3. SELECTING THE PATHOLOGICAL IMAGISTIC ALTERATIONS	86
7.6.4. COMPUTER-ENHANCING THE DATA.....	87
7.6.5. SELECTING RELEVANT METRICS.....	88
7.7. RESULTS.....	91
7.7.1. CASE REPORTS.....	91
7.7.2. PROGRESSION SPEED.....	94
7.7.3. TESTING FOR EARLY DETECTION.....	95
7.8. DISCUSSION.....	96
CONCLUSION AND PERSONAL CONTRIBUTION.....	100
Conclusions study 1.....	100
Conclusions study 2.....	100
Conclusion study 3.....	101
PERSONAL CONTRIBUTION.....	102
BIBLIOGRAPHY.....	105

LIST OF ABBREVIATION

AIP	– acute interstitial pneumonia
CAD	– Computer-Aided Diagnosis
CN	– Complex Networks
CPFE	– combined pulmonary fibrosis and emphysema
CT	– Computer Tomography
ILD	– Diffuse interstitial lung diseases
DIP	– desquamative interstitial pneumonia,
ILD	– diffuse interstitial lung diseases
DLco	– diffusing capacity of the lungs for carbon monoxide
FVC	– forced vital capacity
GE	– General Electrics
GGO	– Ground Glass Opacity
HRCT	– High Resolution Computed Tomography
HPc	– Chronic Hypersensitivity Pneumonitis
HU	– Hounsfield Unit
ILA	– Interstitial lung abnormalities
ILD	– Interstitial Lung Diseases
IPF	– Idiopathic Pulmonary Fibrosis
LAM	– lymphangiomyomatosis
LCH	– Langerhans cell histiocytosis
LIP	– lymphoid interstitial pneumonia
NSIP	– Non-Specific Interstitial Pneumonia
MDD	– Multidisciplinary discussion
OP	– Organizing Pneumonitis
PAP	– Pulmonary Alveolar Proteinosis
PCR	– Polymerase Chain Reaction
PFT	– Pulmonary Function Test
PF-ILD	– progressive fibrosing interstitial lung disease
PPF	– pulmonary progressive fibrosis
PPFE	– pleuroparenchymal fibroelastosis
RB-ILD	– respiratory bronchiolitis-associated interstitial lung disease
ROI	– region of interest
S	– Sarcoidosis
SPL	– Secondary Pulmonary Lobule
UIP	– Usual Interstitial Pneumonia

LIST OF FIGURES

Fig. 1 Interstitial Diffuse Lung Disease Classification.....	4
Fig. 2 Diagnostic criteria for progressive pulmonary fibrosis (PPF)	6
Fig. 3 HRCT, a thin axial section of the lung –with emphasis on the secondary pulmonary lobule (revealed structure and vascularization)	11
Fig. 4 Logical flow for HRCT interpretation	12
Fig. 5 Axial thin-section CT -Reticulation pattern	13
Fig. 6 Axial thin-section CT -Micronodular pattern	14
Fig. 7 Axial thin-section CT -High attenuation pattern.....	15
Fig. 8 Axial thin-section CT -Low attenuation pattern.....	17
Fig. 9 Axial thin-section CT - -injury patterns: high density, low density, reticular and nodular pattern, and overlapping	19
Fig. 10 Simplified representation of a typical HRCT appearance of the most common interstitial lung disease. Idiopathic pulmonary fibrosis	28
Fig. 11 Axial HRCT of UIP pattern.....	32
Fig. 12. Axial and coronal thin-section CT of probable UIP pattern	32
Fig. 13 Axial HRCT of upper and lower lobes marking the indeterminate for UIP pattern;	32
Fig. 14. The proposal flowchart for the diagnostic algorithm of idiopathic pulmonary fibrosis (IPF);	34
Fig. 15 Artificial intelligence progression diagram (AI, artificial intelligence; CNN, convolutional neural network	40
Fig. 16 Convolutional neural network architecture	42
Fig. 17 Difficult ILD patterns	45
Fig. 18 ILD-specific algorithms	49
Fig. 19 Bio Disease network rendered with a hybrid layout algorithm	55

VIII

Fig. 20 DNA network of genes with respiratory function – Force Atlas 2 layout55

Fig. 21 Using multiple layout algorithms throughout the identical research material – reproduced with permission from (243)56

Fig. 22 HRCT parameters61

Fig. 23 Splitting CT sample into layers.64

Fig. 24 Degree distributions for various Rd.....65

Fig. 25 Algorithm processing -step 1- sample selection (a) Normal sample (b) ILD (IFP) sample67

Fig. 26 Emphysema processing68

Fig. 27 GGO processing.....69

Fig. 28 Consolidation processing.....70

Fig. 29 Population distribution comparison according to specific complex network parameters.....71

Fig. 30 Distributions of normal and ILD patients72

Fig. 31 Average coefficient of determination (R^2) for logarithmic and power distributions relative to radial distance (Rd).73

Fig. 32 Relative percentage of standard deviation for ILD vs. normal lungs on all the pathological HU bands.74

Fig. 33 Stepwise analyze HRCT patterns.77

Fig. 34 Box plot for ILD (left) VS Normal (right) for complex network parameters (a) maximum degree (b) total count (c) average degree78

Fig. 35. Simple example to illustrate CN measurements and biological counterparts89

Fig. 36 Case report for a lung axial HRCT, UIP + E pattern (CPFE) patient progression92

Fig. 37 Case report for a NSIP + E patient progression.94

Fig. 38 CNs on Borderline normal versus normal layer distribution;.....96

LIST OF TABLES

Table 1. Interstitial lung diseases (ILDs), other than IPF, demonstrating progressive pulmonary fibrosis (PPF)features	7
Table 2.-ILD-sex, age, smoke, lung, and secondary pulmonary lobule distribution.....	21
Table 3. Classifying ILDs on clusters colors by histopathological pattern;	21
Table 4. ILD-Imagistic Pattern, clinical syndrome, and differential diagnosis ..	22
Table 5. Comparison between 2018 Fleischner (38) and ATS/ERSJRS/ALAT(10)	30
Table 6. HU intervals from Lin Li et al. and Maria Paola Belfiore et al. reports	62
Table 7. Statistical comparison.....	78
Table 8. Methodology comparison.....	80
Table 9. t-test results for relative speed in HU bands parameters VS DLco....	94
Table 10. Statistical t-tests results between borderline and normal lungs.	96

PREFACE

This monograph presents a comprehensive investigation into applying computer-aided diagnosis (CAD) techniques for imaging interstitial lung diseases (ILD). The research focuses on leveraging complex network analysis methods to enhance the early detection and monitoring of ILD patterns in high-resolution computed tomography (HRCT) scans.

The work begins with a critical analysis of the existing literature, highlighting the potential and the challenges associated with using CAD for DILD diagnosis. It then delves into developing novel algorithms integrating visual-based complex network approaches to analyze HRCT images. The monograph explores the correlation between DILD functional and imaging characteristics and the application of these visualization-based techniques. A vital aspect of the research is the provision of early detection and progression monitoring of DILD-related HRCT lesions using computer-aided methods. This presents a detailed examination of the specific HRCT findings in idiopathic pulmonary fibrosis (IPF), which serves as the reference disorder for pulmonary fibrosis.

This treatise's findings contribute to advancing ILD management and imaging diagnosis, offering valuable insights for clinicians and researchers in the field. The integration of complex network analysis with HRCT imaging holds promise for enhancing the early identification and monitoring of these complex lung diseases. The book is structured into several chapters, beginning with an introduction to ILD and the role of HRCT imaging in their diagnosis. It then provides an overview of the current CAD techniques for ILD, highlighting the potential and challenges of deep learning approaches. The core of the research is presented in the subsequent chapters, detailing the development and evaluation of novel complex network-based algorithms for ILD detection and monitoring.

Throughout the treatise, the author has made significant efforts to bridge the gap between the technical aspects of CAD and the clinical needs of ILD management. The work is further enriched by including detailed case studies and comparative analyses with established diagnostic methods. The preface concludes by emphasizing the potential impact of this research on the field of ILD imaging diagnosis and the author's hope that the findings will contribute to the improved care and management of patients suffering from these complex lung diseases.

INTRODUCTION

1. THE MOTIVATION FOR CHOOSING THIS RESEARCH TOPIC

Pulmonary interstitial pathology presents a particularly complex problem caused by the diversity of pathological entities that make up this group. Although these entities have low individual prevalence and are considered rare diseases, they represent an essential part of pulmonary medicine practice; above 200 disorders can lead to interstitial lung injury, often with similar presentations, presenting difficulties in diagnosis and treatment, frequently requiring a multi-disciplinary approach to the case. The difficulty of diagnosing them can arise primarily in the imaging domain - a central analysis element. The broad spectrum of imaging patterns and the presence of a similar appearance of different types of tissue or, conversely, imaging variations of the same type of tissue/lesion create diagnostic variability among specialists in the field. This variability can lead to rare cases, difficulty specifying a diagnosis, and grave confusion in classifying a patient according to a disease pattern, even after multi-disciplinary discussion sessions between medical specialists.

Idiopathic pulmonary fibrosis (IPF) is the most often encountered diffuse interstitial lung disease (ILD), a progressive fibrosing interstitial lung disease (PF-ILD), with a characteristically poor outcome and an amplified early death risk without treatment. There is particular interest in the pulmonology community for this pathology and, more recently, for all ILD with progressive fibrotic character.

In the last decade, substantial progress has been made in understanding pathogenic mechanisms, defining diagnostic criteria, and developing effective medication for treating ILDs. Computer-aided diagnosis (CAD) is often employed in ILD management during the diagnosis and treatment phases. However, CAD has several facets that need careful consideration: selecting the proper technique for the medical needs and conveying the answers in a manner accessible to persons without an information technology (IT) background.

The motivation for choosing this research theme - computer-aided HRCT imaging diagnosis of ILD- resulted from further exploring this patient population group of interstitial pathology, which remains underdiagnosed. The multi-disciplinary approach with colleagues from the IT department emerged as a necessity in the age of digitization and technology.

Thus, this research paper aims to bring new visions of imaging evaluation in interstitial lung pathology based on analytical methods CAD, increasing accuracy in assessment and diagnosis.

2. THE IMPORTANCE AND TOPICALITY OF THE THEME

Diffuse interstitial lung pathology, a diverse group of diseases that manifest common clinical, functional, imaging, and pathological aspects, has consistently raised problems of classification and definition due to the nosological diversity, variable terminology, and imprecise diagnostic criteria.

In recent decades, significant progress has been made in understanding pathogenic mechanisms and diagnostic methods. Although the diagnosis of ILDs was revolutionized by the introduction of high-resolution computed tomography (HRCT) and the precise definition of histological criteria specific to each entity, currently, there is no gold standard diagnostic test. In most cases, the diagnosis represents an intellectual challenge for clinicians, radiologists, and pathologists, and the solution can be found in the multi-disciplinary approach of the patients.

Because of case management and treatment response variability, the gold for the pulmonologist is to identify the distinguished ILD forms in the early stages without an invasive procedure such as a lung biopsy. Within this framework, high-resolution computed tomography (HRCT) remains the predominant method for diagnosing ILD due to lung tissue-specific radiation attenuation properties and maximum spatial resolution.

More than a few approaches to computer-aided diagnosis (CAD) for lung HRCTs are available or developed based on different techniques. Whether built on artificial intelligence, neural networks, or machine learning, these software applications fail to capture the dynamics of a pathology evolution. Therefore, a math-based method of CAD image visualization could be the answer.

The acceptance of antifibrotic therapies for IPF has led to the investigating of such treatments in other fibrotic lung diseases. Today, more than ever, when the beneficial effect of antifibrotic medication in interstitial lung diseases (ILDs) other than IPF manifesting progressive pulmonary fibrosis has been embraced, an early accurate diagnosis of ILD and quantification of fibrosis progression is vital.

3. FRAMING THE TOPIC IN THE INTERNATIONAL, NATIONAL, AND ZONAL CONCERNS OF THE RESEARCH GROUP

The Pneumology Department of the "Dr. Victor Babeş" Clinical Hospital for Infectious Diseases and Pneumophthisiology Timișoara is a national center of expertise for diffuse interstitial lung diseases, most patients being referred by the pneumology community from the western region of the country. Starting in January 2010, patients with ILD were recorded based on a register of diffuse interstitial pneumopathy, where all patients who consented to the registration were entered, creating a viable research database. The medical team managing ILD cases actively participates in the National Registry of Diffuse Interstitial Pneumopathy and Sarcoidosis (REGIS). This project is carried out in collaboration with the "Marius Nasta" Institute of Pneumophysiology, supported by the working group for diffuse interstitial pneumopathy and sarcoidosis within the Romanian Society of Pneumology. The objectives of this initiative are the creation of a national registry of patients suffering from diffuse interstitial pneumopathy and sarcoidosis for clinical research, improvement of the early identification and diagnosis of patients with ILD and sarcoidosis, unification of the diagnostic criteria and the terminology used to describe the cases; creation of an educational platform for resident doctors and specialists, pulmonologists but also rheumatologists or other specialties, improving the care of patients with diffuse interstitial pneumopathy and sarcoidosis, popularizing information related to these diseases among patients.

4. THE SCIENTIFIC OBJECTIVES TO BE SOLVED WITHIN THE DOCTORAL RESEARCH

The objectives proposed in the present research paper were:

1. Critical analysis of data from the specialized literature with an emphasis on facilities and pitfalls for using CAD for ILD diagnosis.
2. Creating valid algorithms for the specific field of ILD management and imagistic diagnostic, emphasizing visual-based complex network methods. The application of CAD systems in the imaging diagnosis of ILD requires submission to the rules of medicine and the science of systems for algorithm validation.
3. Analysis of ILD functional and Imaging HRCT facets and correlation with visualization-based complex network methods.
4. Providing early detection and progression of the imagistic HRCT lesions computer-aided.

5. BRIEF PRESENTATION OF THE WORK'S CONTENT

The present paper describes the general framework of diffuse interstitial pneumopathy (PID) in the first section, including the classification system related to the incidence, imaging patterns, and interconnections with computer-aided techniques. The description of idiopathic pulmonary fibrosis (IPF) and the diagnostic algorithm for this interstitial entity is slightly detailed.

The special part analyses computer-aided HRCT imaging diagnosis's impact on the ILD patient population. Later, a proposed complex networks (CN) model was tested on HRCT scans of normal and ILD patients, establishing quantifiable differences between healthy and affected lungs. The last part of the research paper goes deeper into imaging-aided diagnosis. It quantifies ILD scans' progression and early detection. The groups of patients were selected from the ILD database of the Pneumology Clinic of the "Dr. Victor Babeş" Clinical Hospital for Infectious Diseases and Pneumophthisiology, Timisoara, during January 2010 - 2022.

6. SYNTHETIC COMMENTS REGARDING THE RESEARCH METHODOLOGY AND THE MAIN RESULTS

This retrospective, longitudinal, observational, and comparative study aimed to evaluate the degree of accuracy that the application of complex networks(CN) can additionally provide to diagnose HRCT imaging to obtain an early-stage diagnosis and issue disease progress scores within diffuse interstitial lung pathology. Complex networks (CN), based on the graphical representation of interactions, were used to generate a 3D model of lung imaging contrasts (based on gray tones scale, using Hounsfield units), practically refining the visualization with a mathematical-analytical model. Based on the intrinsic mathematical properties of CN, we sought to determine typical features of healthy and fibrotic lungs. The underlying nature of the degree distribution reflects the intrinsic characteristic of CN; therefore, proliferative or physiological processes have different forms of variation. As a result of this postulate, the pathological processes described by the polynomial distribution can be quantified and/or qualified using the degree of the polynomial as an indicator of distortion and the total number of degrees with the average number as a parameter of intensity. Patients selected to process the images met the inclusion criteria in the study group. The CN algorithm selected and analyzed 65 ILD scans (UIP, NSIP, chronic hypersensitivity pneumonia, organizing pneumonia, and sarcoidosis) and 31 normal high-resolution computed tomography (HRCT)scans. The results obtained by the analytical method were

compared with the initial diagnoses and correlated with scores predicting survival in diffuse interstitial pneumopathies.

Data were collected and analyzed using the Microsoft Office Excel program. They were presented in the box plot format of graphs revealing the statistical distribution, highlighting the four quartiles and the mean value of the distribution. The standard deviation is specified in absolute and percentage values in the proper places compared to other relevant series. The unpaired parametric t-test assessed the significance of differences between groups. If the test statistic is less than the critical value, then the null fails to be rejected. We reject the null hypothesis when the test statistic exceeds the critical value. The p-value could be less than 0.05, and we could still have the test statistic be less than the critical value. This would mean that the α we chose was less than 0.05 and would mean that we would accept the null hypothesis.

GENERAL PART

1. ILD BACKGROUND

Pulmonary interstitial pathology is strongly regulated by various diseases affecting the respiratory system. Even though individual problems have a prevalence close to the cutoff for being considered rare diseases, they constitute a sizeable portion of pulmonary medical practice when taken collectively (1). Diffuse interstitial lung diseases, also known as simply interstitial lung diseases (ILDs), are a heterogeneous group that includes more than 200 different disorders. These diseases are characterized by diffuse damage to the lung parenchyma, with varying degrees of inflammation, fibrosis, and architectural distortion. Even though they start in the pulmonary interstitium, most pathological diseases spread further and affect other parts of the lung, such as the alveolar space, the small airways, the arteries, and/or the pleura. The interstitium extends between the alveolar epithelium and the pulmonary vascular endothelium. It contains different types of cells (fibroblasts, myofibroblasts, macrophages) and extracellular matrix components (collagen, elastin, proteoglycans) (2).

ILDs frequently show signs and symptoms similar to one another, although having distinct patterns of development. It can be challenging to establish the appropriate diagnosis and therapy for an ILD, which usually requires a multi-disciplinary approach (3). Many of these maladies are of unknown cause, and little is understood about their pathogenesis. In this described framework, they are significant causes of morbidity and mortality. (4)

1.1. PULMONARY INTERSTITIAL FIBROSIS PATHOGENESIS

Understanding of the pathogenesis of pulmonary fibrosis has advanced over the last decade. Specific and often unknown triggers initiate lesions, activating distinct pathways that conduct fibrosis of different histological models in genetically susceptible individuals (5). Initially thought of as a mainly inflammatory process, pulmonary fibrosis appears to be driven by persistent injury to the alveolar epithelium and interstitium, leading to an aberrant wound-healing response. Destruction of the alveolar-capillary basement membrane triggers immune cell recruitment and promotes fibroblast differentiation into myofibroblasts, the fundamental effector cell in pulmonary fibrosis. Malfunction of epithelial repair results in scarring of the lung, characterized by excessive collagen deposition, architectural distortion, and irreversible loss of function (6).

1.2. ILD CLASSIFICATION AND EPIDEMIOLOGY

ILD is a suitable "catch-all" for a heterogeneous group of maladies (7). The ILDs have been subcategorized as follows into four categories (8),(9),(10):

- **Those with a known cause** (environmental and occupational exposure, auto-immune disorder, and drug-related (Dr-ILD)) primarily result from connective tissue disorders (11). Prolonged exposure to work and environmental substances can have toxic effects on the lungs. Typical pathogens are mineral or organic dust and toxic gases (12). Epidemiologically, it is difficult to measure the extent of the exposure-related injury. It is probably more common than we know. For this aim, it is imperative to thoroughly search the patient's entire work history and home for clues about possible pathogen-disease relationships. Connective tissue diseases (CTD-ILD) and vasculitis affect all areas of the lung (bronchioles, parenchyma, alveoli). This is why interstitial lung disease is a common feature of rheumatic disease (13), (14). Over 350 drugs have been found to cause pulmonary complications through reactive metabolites or as components of systemic responses (15). Diagnosis is possible with appropriate clinical findings and must be made after other causes have been ruled out in most cases.
- **Those with a granulomatous manifestation**, such as sarcoidosis or hypersensitivity pneumonitis (HP) (or extrinsic allergic alveolitis);
- **Those with unknown causes – without identifiable causes- are** gathered under idiopathic/primary (IIP), which uses the histopathological and radiological approach as its infrastructure. **Major IIP** group includes **chronic fibrosing forms** like-idiopathic pulmonary fibrosis (IPF), Idiopathic non-specific interstitial pneumonia (NSIP) together with **acute/subacute forms-** Acute interstitial pneumonia (AIP), and Cryptogenic organizing pneumonia (COP), and **smoke induces-** respiratory bronchiolitis-associated ILD (RB-ILD) and desquamative interstitial pneumonia (DIP). **Rare IIPs** are Idiopathic lymphoid interstitial pneumonia (LIP) and pleuroparenchymal fibroelastosis (PPFE). **Unclassifiable IIP** causes include inadequate clinical, radiological, or pathological data and significant discordance between clinical, radiological, and pathological findings.

- Furthermore, **the "remainders"** are primarily sporadic diseases with a very low incidence- Langerhans cell histiocytosis (LCH) and lymphangioleiomyomatosis (LAM).

Idiopathic pulmonary fibrosis (IPF, 20.3%), interstitial pneumonia with autoimmune features (IPAF, 17.9%), connective tissue disease-associated ILD (CTD-ILD, 18.3%), and unclassifiable idiopathic interstitial pneumonia (UIIP, 14.7 percent) were identified as the four most prevalent subtypes of ILDs in a recent study (16) involving nearly 2000 participants. IPAF is a provisional category of ILD with subtle characteristics for an autoimmune etiology that does not match the categorization criteria for a particular CTD and is consequently allocated to the subgroup of idiopathic interstitial pneumonia for the time being (IIP) (16),(17).

Idiopathic interstitial pneumonia (IIP) is the most prevalent, with IPF and IPAF being common symptoms. IPF has a chronic/fibrotic manifestation, whereas IPAF has a predominantly inflammatory one, collectively accounting for about 40 percent of total cases (16). IIPs generally account for over 80 percent of ILDs, supporting a Pareto distribution.

Its high incidence and dire prognosis distinguish idiopathic pulmonary fibrosis (IPF). IPF mortality is high, surpassing most tumors, with a median survival period of 3-5 years after diagnosis (18). Due to the extraordinary improvement of antifibrotic medications, an accurate IPF diagnosis in the early stages significantly impacts the patient's prognosis (19).

Figure 1 depicts a Sankey diagram of an ILD categorization based on (20). The node width and flow are proportionate to each disorder class's relative incidence frequency. Recognizing that variances are associated with population ethnicity, age, socioeconomic level, genetic imprinting, geographical location, etc., the values used to indicate the general proportions are not exact numbers. Because individual ILDs are rare, little is known about their actual incidence.

Differential diagnosis of ILD must consider atypical pneumonia (including *Pneumocystis* species), the lymphangitic spread of cancer, and congestive heart failure, all of which may present with similar chest radiographic features; however, numerous paraclinical tests can confirm/disprove these hypotheses (21).

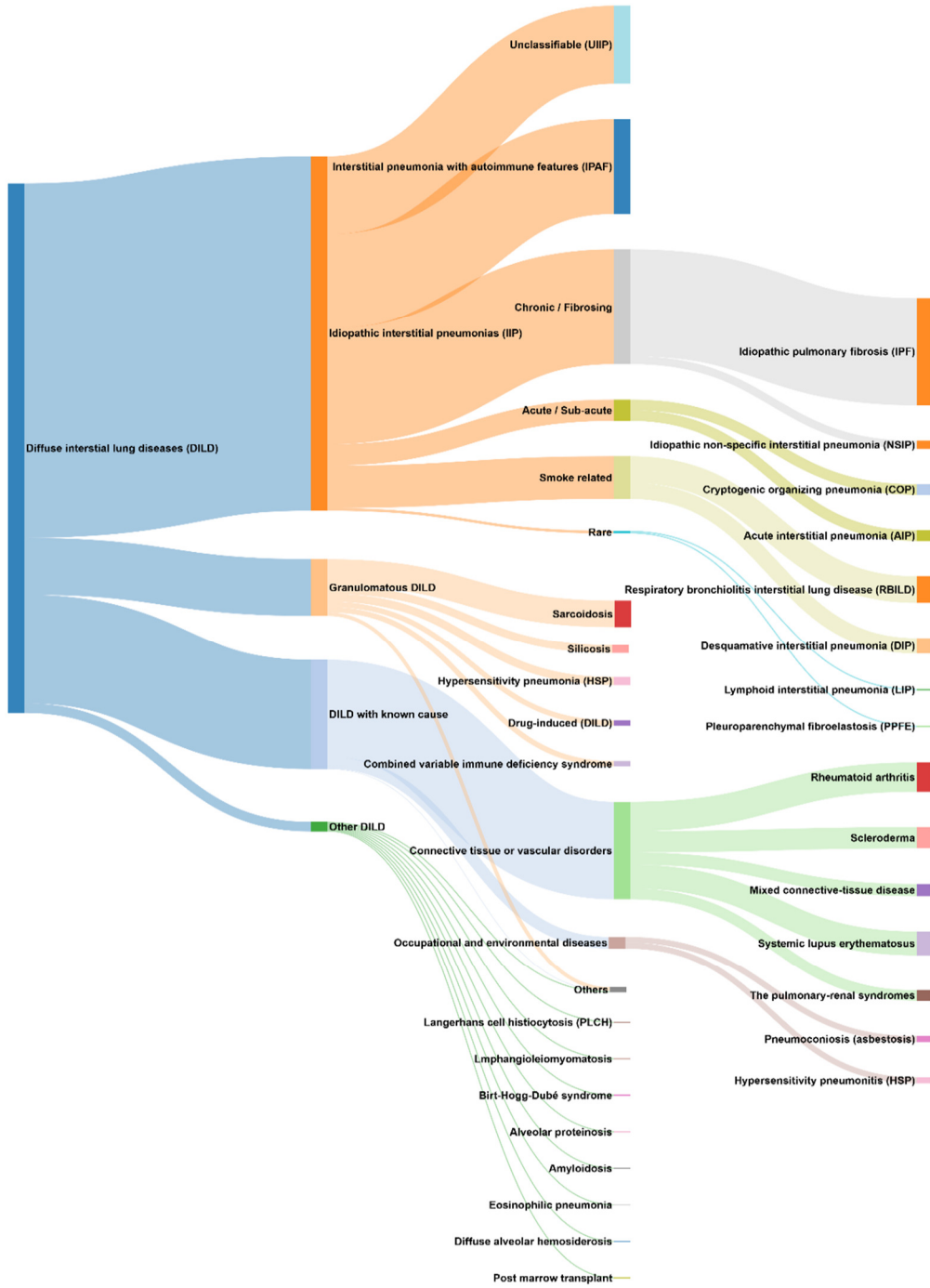


Fig. 1 Interstitial Diffuse Lung Disease Classification

1.3. ILD PROGRESSIVE PHENOTYPES

Establishing findings and patterns specific for diffuse interstitial lung diseases or histopathologic injury based only on one HRCT study is not recommended, especially when an early disease is involved. The accuracy of HRCT for predicting the correct prime diagnosis is improved by the accessibility of several imaging scans spaced over time, as a single HRCT from a one-time point may not represent the true nature of ILD (22).

Suppose IPF evolution is indubitable with progressive fibrosis for other ILDs. In that case, there is consistent variability in the disease course, depending on the predominant slope, inflammation (with a high potential of reversibility), or fibrosis, significantly impacting management and treatment (23). In 2013, Travis et al. (9) proposed five longitudinal behavior pattern categories for ILD evolution, of which three are fibrotic specific. Thus, pulmonary fibrosis may be intrinsically non-progressive and stable, with residual damage after removing a trigger (e.g., Dr-ILD). Alternatively, it could be irreversible fibrosis, progressive, with the potential for stabilization. Progression is stabilized by immunomodulation, at least in the short term. (e.g., mycophenolate mofetil therapy in CTD-ILD (24) and HPc (25)). The third one, the dreaded one, is progressive pulmonary fibrosis (PPF) in non-IPF disorders, characterized by progression regardless of treatment considered appropriate in individual ILDs (IPF-like disease) (26).

All three phenotypes require a constant, long-term follow-up of the HRCT imaging evolution of the disease according to which the case is managed: maintaining the status and preventing or slowing down the progression. (27),(28).

Quantitative imaging techniques can provide significant additional information compared to single time points continuously. They can be used in various ways, including 1) improving the accuracy of initial diagnosis. 2) Assistance with estimating forecasts. 3) identify disease progression; 4) detect new processes in patients with acute or worsening symptoms; 5) detect other abnormalities or complications such as lung cancer. (29),(30).

A trend (26) accelerated by the failure of conventional therapies and the widespread use of antifibrotic therapies in a subset of patients has focused on the progressive fibrotic phenotype of interstitial lung disease. The histologic and imagistic pattern known as usual interstitial pneumonia (UIP) is the hallmark of progressive fibrosis. Nevertheless, progressive fibrosis is not limited to this histological entity. (5)

Fibrosis is the ultimate result of cellular damage, matrix damage, or mutual by various mechanisms, including trauma, thermal injury, chemical injury, hypoxia, and immune-mediated injury (33). Some patients get a progressive

phenotype characterized by self-perpetuating fibrosis, reduced lung function, poor quality of life, and eventually premature death under the umbrella of progressive fibrotic ILD. (34).

The term progressive pulmonary fibrosis (PPF), other than IPF, was proposed by (26) instead of progressive interstitial lung fibrosis, highlighting an underlying ILD condition (IPF-UIP-like) that produces rapid lung deterioration beyond the interstitium. Diagnostic criteria for the PPF phenotype (Fig. 2) definition input clinical, physiological (31), and radiological (32),(33), hasty impairment occurring within the past year with no alternative explanation.

Imagistic HRCT fibrosis progression is usually assessed visually based on the percentage of lung volume with fibrotic features in the upper, middle, and lower lung areas. Side by side, adjacent HRCT sections of the initial and follow-up CT examinations are compared after adjustment for lung volume changes. Increased areas or severity of traction bronchiectasis and bronchiolectasis, novel ground-glass opacity with traction bronchiectasis, novel fine reticulation, augmented lobar volume loss, and new or increased honeycombing are the radiological features that must be carefully screened. Elevated levels of fibrotic features indicate progression (34).

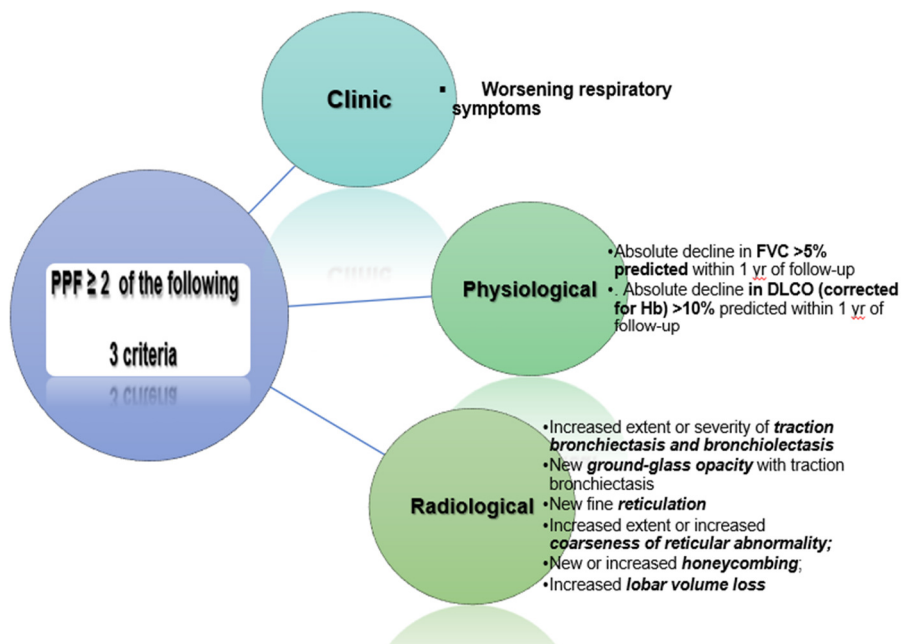


Fig. 2 Diagnostic criteria for progressive pulmonary fibrosis (PPF)

Adapted after (26). PPF Definition is at least 2 of the 3 criteria (clinical, physiological, and radiological mentioned) for the past year. IPF= idiopathic pulmonary fibrosis; ILD=interstitial lung disease; PPF=progressive pulmonary fibrosis., DLco= diffusing capacity for carbon monoxide, FVC=force vital capacity

Several trials (35),(36) suggested that antifibrotic medication has a beneficial effect in interstitial lung diseases (ILDs) other than IPF with PPF phenotype (35),(36). Thus, a scheme for the most prevalent and representative ILDs with PPF features has been proposed in table 1. Accordingly, rapid identification of different types of ILD progression and early imaging HRCT diagnosis are the goals that must be achieved.

In a recent study (37), interstitial lung abnormalities (ILA) progression is relatively common and associated with increased age and an increased mortality rate. Precise imaging findings (e.g., traction bronchiectasis) and patterns (e.g., a probable UIP pattern) (38) are strongly associated with ILA progression, too.

Table 1 Interstitial lung diseases (ILDs), other than IPF, demonstrating progressive pulmonary fibrosis (PPF)features

Interstitial lung Disease(ILD) other than Idiopathic Pulmonary Fibrosis(IPF)				
IIP	Autoimmune-ILDS	Exposure -related	ILD with cysts and/or airspace filling	Granulomatosis
AFOP	↑ SSc	↑ HP	↑ LCH	↑ Sarcoidosis
iPPFE	RA	Occupational- Pneumoconiosis	Lymphoproliferative	
Unclassifiable	MCTD	Illicit Drugs	PAP	
AIP	Vasculitis	Medication	LAM	
iDIP	Sjogren	Radiation	Others	
iNSIP	Myositis	Post Infections		
iLIP	SLE			
COP	Others			

Adapted after (26). The arrows indicate an increase in the incidence of PPF in ILD with disease progression. AIP = acute interstitial pneumonia; AFOP = acute fibrinous and organizing pneumonia; COP = cryptogenic organizing pneumonia; DM= dermatomyositis; HP = hypersensitivity pneumonitis; iDIP = idiopathic DIP; IIP = idiopathic interstitial pneumonia; iLIP = idiopathic lymphoid interstitial pneumonia; iNSIP = idiopathic nonspecific interstitial pneumonia; iPPFE = idiopathic pleuroparenchymal fibroelastosis; MCTD=mixed connective tissue disease; PAP = pulmonary alveolar proteinosis; PM= polymyositis; RA = rheumatoid arthritis; SLE = systemic lupus erythematosus; SSc = systemic sclerosis LCH= Langerhans cell histiocytosis;. LAM= lymphangioleiomyomatosis;

1.4. ILD TREATMENT

The differential diagnosis of fibrosing ILDs is difficult because clinical, radiological, and pathological characteristics often overlap, requiring a multidisciplinary approach (39). In this setting, it is essential to establish a conclusive diagnosis because nonpharmacological and pharmacological treatment approaches (including corticosteroids, immunosuppressants, and, more recently, antifibrotic agents) are disease-specific(40), (41). Histopathologically, all ILDs exhibit varying degrees of inflammation and fibrosis

that are highly variable among ILD subtypes and individuals with the same disease. When the inflammatory pattern predominates, the histology is that of organizing pneumonia (OP) or nonspecific interstitial pneumonia (NSIP), which response well to corticosteroid anti-inflammatory treatment. In contrast, in the fibrosis pattern, the presentation is usual interstitial pneumonia (UIP) with fibroblastic foci and lesser inflammation response, reacting well to anti-fibrotic medication (42).

1.4.1. PHARMACOLOGICAL TREATMENT

Pharmacological treatment is divided into two parts: one that aims to reduce and stabilize disease development and the other that aims to counteract the effects of ILD on the lung. Prednisone or a related derivate substance is the most commonly used oral corticosteroid medicine in treating ILD. ILD progression is considerably slowed or even prevented when combined with certain immunosuppressive medications (such as mycophenolate mofetil, azathioprine, cyclophosphamide, and rituximab). However, the adverse effects must be constantly monitored, and the quality of life may be reduced.

Antifibrotic medications, such as pirfenidone and nintedanib, are aimed at the lung tissue, minimizing the amount of scarring present and preserving lung function- a primary indication in IPF. In contrast, the side effects are significantly more severe than in the preceding selections, and robust doctor-patient dialogue is essential to make this choice (43), (44) summarizes the clinical practice guidelines and statements for ILD. The American Thoracic Society (ATS), the European Respiratory Society (ERS), and the Fleischner Society are critical players in developing the guidelines. If the initial guidelines focused on IPF, the revised guidelines expand beyond IPF management to include treatment recommendations for other ILDs (26).

1.4.2. NON-PHARMACOLOGICAL TREATMENT

Long-term oxygen therapy must be provided to people who have severe chronic resting room air hypoxemia (45). Pulmonary rehabilitation aims to improve daily functioning.

There is a broad spectrum of responses to the medication; some ILDs may not respond at all, while others may react immediately. Even the success criterion is flawed: the treatment is successful if the measurements (symptoms, physiologic, and imagistic data) indicate stabilization. Nevertheless, experience demonstrates that this plateau is only transitory. The deterioration of a patient's condition may be caused by the ILD's natural course, comorbidities, or adverse

drug effects. Osteoporosis, infection, and muscle weakness are typical therapeutic side effects that might lead to condition deterioration.

The progressive fibrosing interstitial lung disease phenotype should consistently and continuously be evaluated for transplantation (46).

2. ILD IMAGISTIC PATTERNS

2.1. WHAT ARE THE SIGNIFICANT CT FEATURES FOR MAKING A DIAGNOSIS OF ILD?

HRCT represents the standard investigation when an ILD is suspected. Compared with chest X-rays, thin-slices computed tomography is more sensitive and specific for diagnosing interstitial lung syndrome. HRCT is indispensable in the exploration of interstitial syndromes. Image acquisition achievable with modern equipment of the tomographic slice is a thickness of 1,5 mm or less. The smaller the distance between the cups, the higher the resolution is. Model-based iterative reconstruction techniques are also used, increasing the image's accuracy. An incremental reduction in overall radiation dose is obtained using spaced axial imaging provided compared with volumetric computed tomography. Volumetric imaging, on the other hand, could give quantitative lung imaging information in the serial follow-up of ILD, able to evaluate the extent of lung damage affected by the disease. (47). A computed tomography performed under standard conditions, with sections of 3 or 5 mm, can be a source of confusion, not detecting the characteristic changes of ILD, resulting in loss of definition of small vessels, airways, nodular infiltrates, and septa. Also, the exam with contrast substance can confuse the visualization of the pulmonary interstitium, keeping its value only for the correct detection of hilar and mediastinal adenopathy (27), (48).

In addition to the obligatory full inspiration to a total lung capacity scan, a "complete" thin-section CT includes two more acquisitions: an expiration and a prone scan. Expiratory sequences are explicitly included to assess the presence of small airway disease and to explore aspects of air trapping for possible obstructive function issues. Some patients require prone imaging to detect early or mild ILD. Dependent position pulmonary atelectasis is often seen on supine inspiratory scans, which may mimic mild subpleural reticular abnormalities and ground-glass opacities (49),(38).

Thin-section CT detects anatomical structures of the lung parenchyma, particularly elements of the secondary lung lobule. It represents the minor pulmonary structure, surrounded by a connective tissue septum. It has a polyhedral shape, 1-2.5 cm in diameter, in the center having the centrilobular arteriole and bronchiole, on the periphery with veins and lymphatics in the interlobular septum (figure 4). The secondary pulmonary lobules are better expressed in the subpleural spaces and along the lung fissures. Under normal

conditions, it cannot be identified on standard chest radiography; however, the interlobular septa is visible on HRCT even on a customarily constituted lung (50).

The pulmonary interstitium can be separated into three compartments: the peribronchovascular or axial interstitium, the centrilobular interstitium with intralobular septa (of the secondary lung lobe), and the peripheral interstitium (which includes the interlobular septa, as is seen in figure 3 with the secondary lung lobe scheme). A close relationship exists between the pulmonary interstitium and the airways, so any lung disease affects the interstitium to some extent. It responds to injuries by thickening.

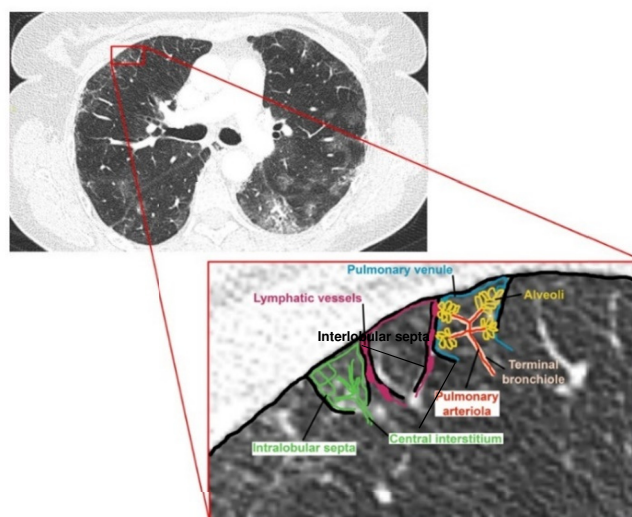


Fig. 3 HRCT, a thin axial section of the lung –with emphasis on the secondary pulmonary lobule (revealed structure and vascularization)

HRCT imaging patterns and their distribution in the lung and the secondary lung lobule are essential to obtain a more truthful diagnosis of ILDs. Understanding secondary lobular anatomy and the appearance of lobular structures are keys to interpreting HRCT. Thin-section CT can show many secondary pulmonary lobule features in both, normal and abnormal lungs. Many lung diseases, particularly interstitial diseases, produce some characteristic changes in the location of lobular structures, helping the ILD subtypes to be highlighted. The distribution pattern is an acknowledged diagnostic criterion (20),(28), which is evaluated in two dimensions: in the apico-basal gradient and concerning the secondary pulmonary lobule (SPL) with the interstitial distribution. Also, HRCT imaging could scan other extra patterns, like the presence of pleural effusion, pneumothorax, costophrenic angle spares, and so

on, narrowing the ILD etiological spectrum. Essentially, we can stratify lung imaging primary lesions into four categories: reticular pattern, nodular pattern, high attenuation, and low attenuation, whose distribution, overlap, and association with other lesions matter (51), (52). The findings are summarized in figure 4.

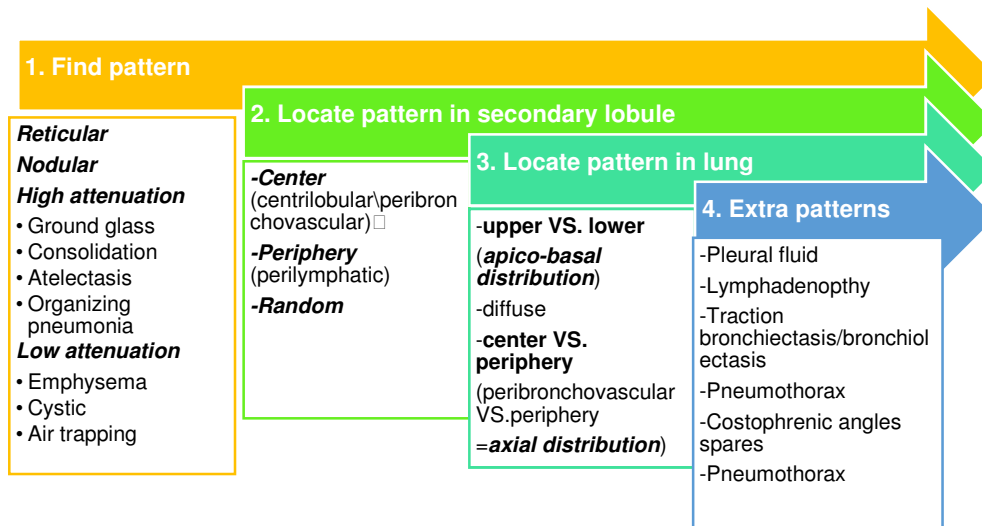


Fig. 4 Logical flow for HRCT interpretation
Adapted after (10)

2.1.1. RETICULAR PATTERN

Reticulation, or simple reticular pattern, is described by all the intersecting lung opacities, giving it the appearance of a network. Varying degrees of inflammation and fibrosis due to interstitium injury cause thickening of the intra and interlobular septa of the secondary pulmonary lobule. Since the septa have an anatomically linear shape, the thickening follows that contour, resulting in intersecting lines. On HRCT scans, aspects of this line network could suggest an etiology or ILD progression to fibrosis (53). For example, the smooth thickening of the interlobular septa from acute pulmonary edema should be differentiated from the arciform thickening shape of the intra/interlobular septa found in idiopathic or secondary pulmonary fibrosis because of the pulmonary scar distortions. UIP pattern is frequently associated with other evidence of fibrosis, including architectural distortion and bronchiectasis (Fig.5 (b)) (54). Therefore, in patients with UIP, reticulation is often irregularly spaced, with a mixture of thick and thin lines, in contrast to CT scans from non-specific interstitial pneumonia, in which spacing is more regular lines and more homogeneous in thickness (Fig.5 (a)) (38).

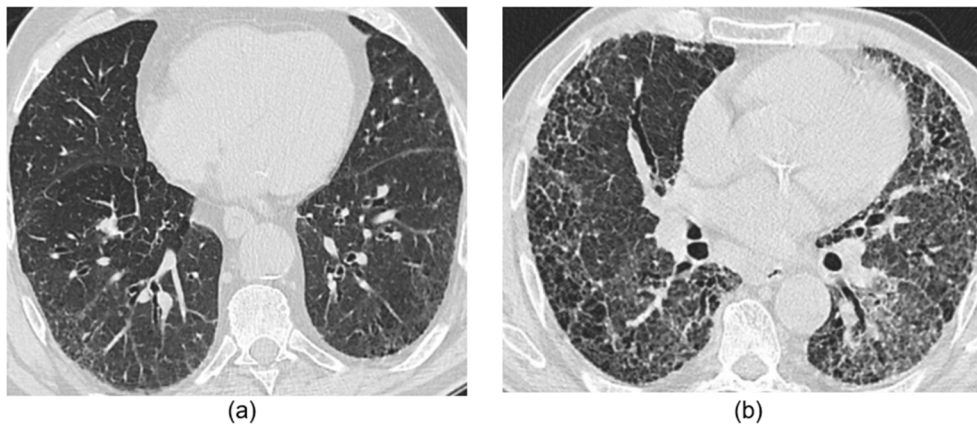


Fig. 5 Axial thin-section CT -Reticulation pattern

Scans belong to the 'Dr. Victor Babes' Infectious Diseases and Pneumoftiziologie Clinical Hospital Timisoara database; Fig. 5 (a) - subpleural smooth reticulation of possible UIP pattern. Fig.5 (b) - Arciform reticulation with architectural distortion and bronchiectasis of fibrosing UIP, IPF case

2.1.2. MICRONODULAR PATTERN

The classification of lung nodules can be done by size, in large (>10 mm and < 30 mm), small (< 10 mm and >3 mm), and micro-nodules (<3 mm) (53). The distribution of micro/nodules shown on thin-section CT is essential in accurately diagnosing the nodular pattern and its impact on ILD classification. Relation to the configuration of the secondary pulmonary lobule and subpleural sparing can place multiple small lung nodules into one of three categories: perilymphatic (with inter lobular septa affinity, linearly interconnected, like appears in sarcoidosis- fig .6 (b), centrilobular (no contact with the pleural surface and with equal distances between them, e.g., hypersensitivity pneumonitis- fig. 6 (a) or random (diffuse, vascular) distribution (e.g., pneumoconiosis, miliary tuberculosis, fungi spread) (55), (54).

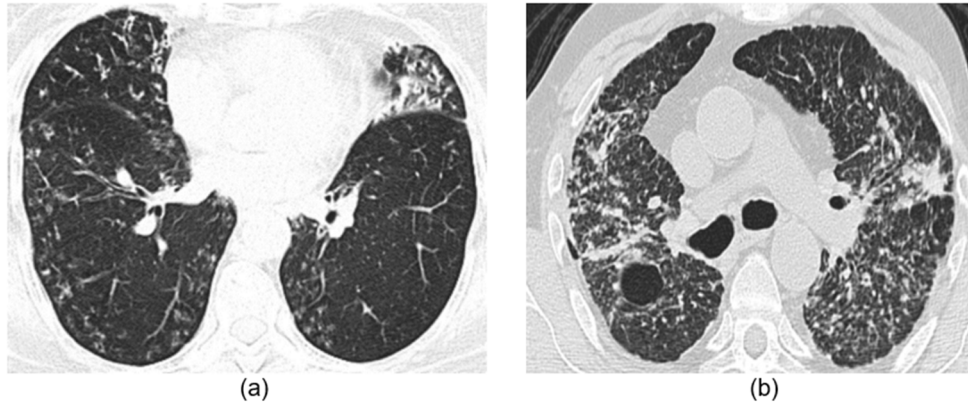


Fig. 6 Axial thin-section CT -Micronodular pattern

Scans belong to the 'Dr. Victor Babes' Infectious Diseases and Pneumoftiziologie Clinical Hospital Timisoara database; Fig.6 (a) -centrilobular micronodules distribution of hypersensitivity pneumonitis patients. Fig. 6 (b)- perilymphatic micronodules distribution of sarcoidosis patient.

2.1.3. HIGH ATTENUATION

Ground-glass opacity (GGO) refers to a homogeneous area of increased lung opacity (a process that partially fills the airspaces). The amplified opacity does not obscure the underlying bronchial and vascular structures (fig.7 (a)). Ground-glass opacification may either be the result of air space disease (partial filling of the alveoli) or early interstitial lung disease (smooth thickening of the interstitium or alveolar walls-e.g., fibrosis) as a result of fluid, cells, and fibrosis presence (54). The GGO pattern is widespread in ILD. However, it is unspecific and may represent a reversible process if not associated with other fibrosis evidence, such as traction bronchiectasis, honeycombing, and reticulation. There is evidence that the HRCT aspect of GGO indicates inflammatory process activity, especially in fibrosing alveolitis, extrinsic allergic alveolitis, and squamous interstitial pneumonia (28). UIP is unlikely when pure ground glass opacity is present as an isolated finding of diffuse ILD. The presence of abundant pure ground glass opacity in a patient with fibrotic ILD, particularly in non-fibrotic lung areas, suggests acute exacerbation or infection (56), (57). In the Hounsfield Unit (HU), the GGO spans an apparent interval [-703,-368], specific to the General Electric Healthcare Optima 520 (58).

Consolidation is denser than GGO and depicts the moment when the airspaces are entirely filled with air. Yet, one can detect the air bronchogram presence (Fig.7 (b)). Alveolar spaces could be filled with pus, edema, hemorrhage, inflammation, or tumor cells (59). It is usually an accumulation of exudate or material in the alveoli, as in chronic obstructive pulmonary disease

(COPD) (60). Still, it can sometimes result from severe pulmonary fibrosis, such as sarcoidosis (61). Consolidation is not characteristic of UIP but may be seen in IPF patients with overlapping infections or malignancies. From a purely visual perspective, the consolidation looks like a visually defined compact opacity in ILD, whose boundaries are poorly defined in other diseases. The density of HU values varies between (-100,5), matching reticulation (62).

Atelectasis refers to lung tissue retraction and reduction, with the absence of air in the alveoli and alveoli collapse. It is a pulmonary volume loss, either entirely or partially. On rare occasions, when the HRCT is made in a prone position, atelectasis and hypoventilation can mimic the fibrosis appearance in its early stage (63).

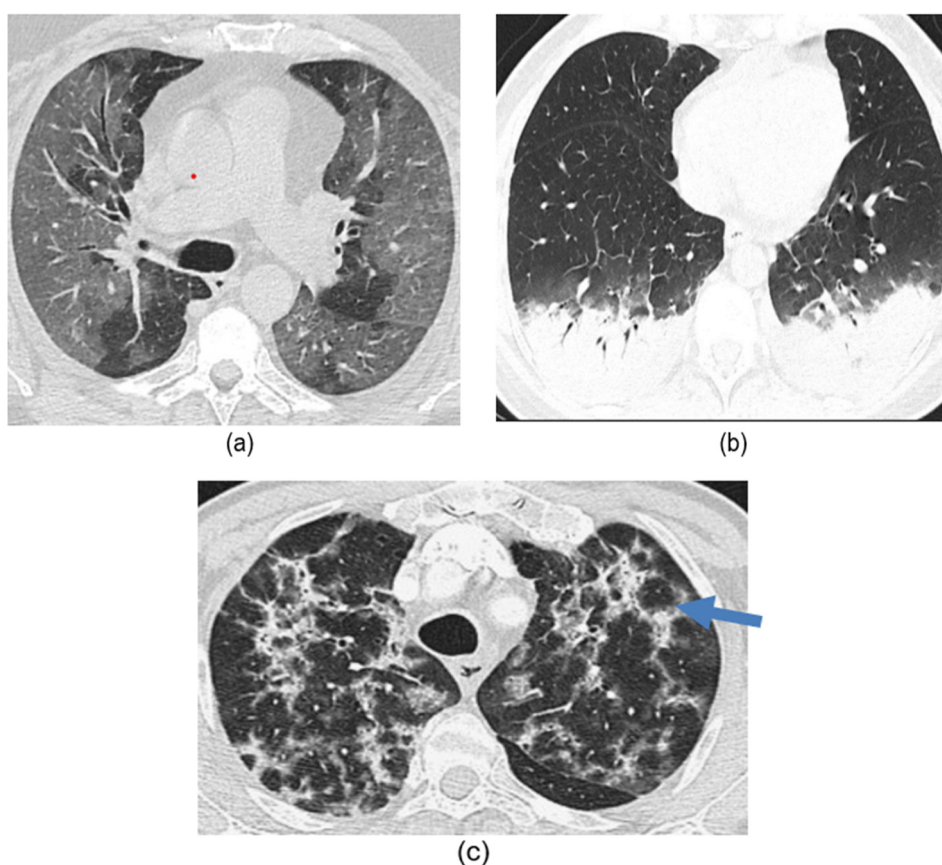


Fig. 7 Axial thin-section CT -High attenuation pattern

Scans belong to the 'Dr. Victor Babes' Infectious Diseases and Pneumoftiziologie Clinical Hospital Timisoara database; Fig.7 (a) -axial HRCT section of extensive GGO areas, with mild reticulation, case of a patient with NSIP cellular pattern, with scleroderma; Fig.7 (b)- double pneumonia, in ILD bacterium suprainfection; Fig.7 (c)- a case of organizing pneumonia after a severe form of SARS CoV2 viral infection- with atoll sign present (blue arrow)

Organizing pneumonia is the usual reaction to lung lesions during the healing process, most likely to a lung infection, but also found after radiation therapy, inhaling injury, neoplasm, and drug toxicity. In HRTC evaluation, it may have a multitude of appearances, including nodular images and irregular GGO patterns, but most often peripheral bilateral consolidation (atoll sign-Fig. 7 (c)) (63), (64). This distribution does not overlap UIP, which has a typical basal and subpleural distribution, which is often heterogeneous.

2.1.4. LOW ATTENUATION

Emphysema appears as polygonal or rounded low-attenuation areas deprived of walls (fig.8 (a)). Interlobular septa surrounding the emphysematous regions of the lung, compressed lung tissue, and perilobular vessels can make the diagnosis hampered and misinterpreted as walls (65). Sometimes, a central white dot representing the pulmonary artery within the secondary pulmonary lobule can be seen (66).

Cysts are round circumscribed areas of lucency or low attenuation of 1 cm or more in diameter, surrounded by an epithelial or fibrous wall, and typically have discrete walls (fig.8 (b)). Cysts, not honeycomb cysts (i.e., do not stack along the subpleural lung), suggest a diagnosis other than IPF. Lung cysts are the principal pattern of specific interstitial diffuse lung diseases, including pulmonary Langerhans cell histiocytosis and lymphangiomyomatosis. Still, they can also be seen in lymphoid interstitial pneumonia and desquamative interstitial pneumonia (67).

Air trapping refers to lung regions that, following expiration, do not show the typical increase attenuation or show little change in the cross-sectional area; the presence of air trapping suggests small airway disease, with excess gas ("air") retention in all or part of the lung. Mild cases of air trapping may be discernible only on expiratory scans, while in more severe cases, inspiratory thin-section CT may show evidence of a mosaic attenuation pattern. Air trapping in ILD is commonly associated with hypersensitivity pneumonia, constrictive bronchiolitis, and sarcoidosis (68).

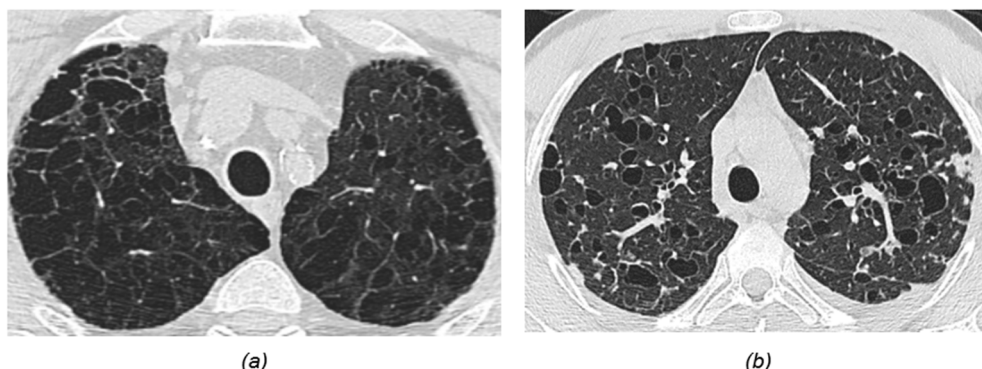


Fig. 8 Axial thin-section CT -Low attenuation pattern

Scans belong to the 'Dr. Victor Babes' Infectious Diseases and Pneumoftiziologie Clinical Hospital Timisoara database; Fig.8 (a) -axial HRCT section of panlobular emphysema, Fig.8 (b)-axial HRCT section of upper distribution cyst of an LCH patient

Honeycombing (fig 9.14) is clusters of small cyst air space (hypolucent areas), ranging in diameter from 0.3 to 1.0 cm (but occasionally as large as 2.5 cm), with well-defined walls linked together, often thick walls, uniformly and multilayer display (69). They could effortlessly be confused with *traction bronchiectasis and bronchiolectasis*. The main difference between them is that while the honeycombing cyst pattern always has a subpleural distribution, with no sparing of the subpleural surface, the irreversible dilated airway connects back to the more central airways, often with irregular and tortuous pathways (54). Interobserver variability burden for the presence or absence of honeycombing, bronchiectasis, or their combination remains a real issue in the practical approach (63). Honeycombing cysts consist of massive dilatation and disruption of peripheral airspaces due to surrounding alveolar septal fibrosis and tangentially viewed traction bronchiolectasis; the remodeling process appears to be a continuum from traction bronchiectasis to honeycombing, and that theoretical separation of the two processes may be confusing (70),(71). Represent the permanent end-stage of parenchymal destruction in patients with interstitial fibrosis. (64). Practical, it is a severe fibrosis feature that typically appears in UIP but is not pathognomonic for IPF because it could translate to final fibrotic stages of sarcoidosis, HP, and NSIP pattern (72),(73).

Architectural distortion Implies any distortion of the normal lung parenchymal anatomy. In the context of ILD, an abnormal appearance of the secondary pulmonary lobule shape or size, with evidence of volume loss demonstrating tethering and warping of the usual hexagonal format, will appear (54).

2.1.5. OVERLAPPING MODELS

In imaging practice, the primary lesions in the appearance of ILD may exist independently, but we often find them in various combinations, **overlapping**, creating accurate models that may be typical or less for a particular ILD entity (74), (75). Examples of this primary elements mixture are offered in Fig. 9.

Mosaicism (fig.9.13) - The term mosaic attenuation is used to describe density differences between affected and non-affected lung areas. The mosaic attenuation pattern is caused by either ventilation deficiency (airway narrowing/air trapping such as RB) or perfusion impairment (reduced perfusion in these pathological areas secondary to vasoconstriction like pulmonary chronic thromboembolism experience)(76). Thin-section CT aspects perform like heterogeneous attenuation of the lung parenchyma, with generally well-defined geographic borders corresponding to the outlines of the pulmonary lobule. These low attenuation areas may only be apparent on expiratory scans. Patchy black and white lung areas may help identify the underlying process (77). Answering the question of which area is abnormal, the black or the white lung, is a significant element of clinical management (56).

Head cheese pattern (fig.9.13)- Multiple areas of mosaic attenuation (low attenuation), ground glass opacities (high attenuation), and normal lung tissue (normal attenuation). Therefore, it reflects a collocation of regions with three (or sometimes more) variable densities of different attenuation within the lungs, with a heterogenous appearance of the parenchyma, and was called the **three-density pattern** (78). It is considered highly specific for chronic hypersensitivity pneumonitis but could appear in other ILDs like sarcoidosis (79).

A crazy-paving pattern (fig.9.12) appears as ground-glass attenuation with superimposed interlobular septal thickening and intralobular lines (80). The crazy-paving pattern is often sharply demarcated from normal lungs. It may have a geographic outline, often with lobular or geographic sparing. It is a hallmark of pulmonary alveolar proteinosis but could be found in acute exacerbation of IPF, diffuse alveolar hemorrhage, and organizing pneumonia, representing an ancillary or uncommon finding (81).

Reversed halo sign (atoll sign) - Fig 9.11 is defined as a central, focal rounded area of ground-glass opacity surrounded by denser consolidation of crescentic shape (forming more than three-fourths of a circle) or complete ring (ring-shaped opacities) of at least 2 mm in thickness (82). The reversed halo sign is a well-recognized CT pattern associated with organizing pneumonia (83), which is most commonly cryptogenic (COOP) but can also be secondary to a wide range of pulmonary diseases (84).

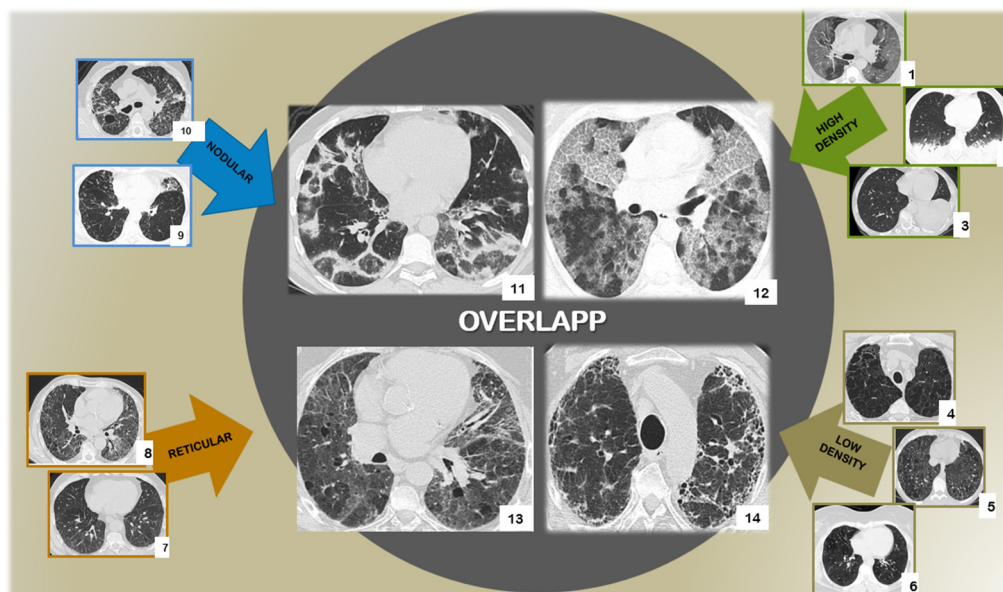


Fig. 9 Axial thin-section CT - injury patterns: high density, low density, reticular and nodular pattern, and overlapping

Scans belong to the 'Dr. Victor Babes' Infectious Diseases and Pneumoftiziologie Clinical Hospital Timisoara database. Primary lesions: Fig.9.1-9.3-GGO, consolidation, atelectasis of LLL; Fig.9.4-9.6- emphysema, Cyst, air trapping; Fig.9.6-Fig.3.8-smooth reticulation, arciform reticulation with parenchymal destruction; Fig.9.9-9.10- perilymphatic and centrilobular micronodules distribution; Overlapping: Fig.9.11- cryptogenic organizing pneumonia (COP), with the atoll sign; Fig. 9.12-Alveolar proteinosis- with the crazy paving pattern; Fig.9.13-Chronic hypersensitivity pneumonia, with the headcheese pattern and mosaicism; Fig. 9.14- idiopathic pulmonary fibrosis with the usual interstitial pneumonia pattern.

2.2. INTERCONNECTING HISTOPATHOLOGY WITH HRCT IMAGISTIC APPEARANCE

Radiological diagnosis of ILD is pattern-based and linked to underlying histology. Findings at HRCT generally reproduce the macroscopic abnormalities seen by pathologists. Thus, working knowledge of the interconnection between histopathological changes and HRCT patterns with the typical appearance of common ILDs is essential in daily practice (85).

Many ILDs prefer certain zones. Evaluation of the dominant distribution is, therefore, an essential tool. For example, it is known that in most patients with idiopathic pulmonary fibrosis (IPF), the disease tends to be most prominent in the middle to lower zone. This contrasts with fibrosis in sarcoidosis patients, who usually favor the upper lobe. In addition, radiologists need to consider axial distribution (i.e., central versus peripheral), which is of potential value. Using the example of IPF and sarcoidosis again, the former is often peripheral (subpleural). At the same time, the disease is more central (and bronchocentric)

in the latter. A final example is seen in patients with organizing pneumonia. In this case, consolidation may be more pronounced in the perilobular trend (64).

In addition to zonal distribution, distribution at the level of secondary pulmonary nodules may also be diagnostic. This is especially true for micronodular disease, where assigning nodules to one of the three centrilobular, perilymphatic, and random distribution types helps narrow the differential diagnosis (63).

As previously mentioned, usual interstitial pneumonia (UIP), non-specific interstitial pneumonia (NSIP), organizing pneumonia (OP), acute interstitial pneumonia (AIP), desquamative interstitial pneumonia (DIP), respiratory bronchiolitis-associated interstitial lung disease (RB-ILD), **as major IIPs**, together with **rare IIPs** such as lymphoid interstitial pneumonia (LIP), pleuroparenchymal fibroelastosis (PPFE) are part of the family idiopathic interstitial pneumonia (IIPs). Unique entities like lymphangiomyomatosis (LAM), Langerhans cell histiocytosis (LCH), Pulmonary Alveolar Proteinosis (PAP), granulomatous disease (like sarcoidosis or hypersensitivity pneumonitis -HP) together with IIPs are included in **diffuse interstitial lung diseases (ILDs)** of unknown cause (86). Each of these entities has typical imaging and histological patterns, although imaging patterns appear to be associated with more significant inter-observer variability in practice (87), (88). Each entity may be idiopathic or secondary to identifiable causes such as collagen vascular disease or inhalation exposure. Diagnosis of idiopathic interstitial pneumonia correlates with clinical, imaging, and pathologic features.

These mentioned findings of ILD are edified in Tables 2,3 and 4. The histopathological pattern that intertwines with the imaging characteristics of HRCT is presented in this multifaceted representation. Color clustering according to the ILD classification (table 3), the histopathological forms and their connections with age distribution, smoking, lung distribution, and the level of the SPL are carefully detailed (table 2). Also, targeted information about the types of primary lesions and how they merge to create specific HRCT models for a particular histopathological ILD form are presented. Last but not least, with value in clinical practice and the management of ILD, the corresponding clinical syndromes and the possible differential diagnosis are revealed, too (table 4).

Table 2.-ILD-sex, age, smoke, lung, and secondary pulmonary lobule distribution

Histological Pattern:	Sex Age Average	Smoke Related	Distribution					
			Lung			PSL		
			I	M	S	Pb	PI	PS
UIP Cert	M, >50y	+/-	+++ Hd□					N
Probable UIP			++ Hd□					N
Indeterminate UIP (Incipient)			+					N
Acute Exacerbation			Hd→ Od					
NSIP Incipient	F, 40-50y		+ Od□	+/-		+		Y
Progressive			+Od□	+/-		+		Y
DAD early	50-60y	+/-	+++ Od/Hd	++ Od/Hd	+			N
DAD Progressive		+/-	+ Hd	+ Hd	+ Hd			N
OP			+/-			+		N
			Hd□			++	+	N
DIP	30-40y	+	++Od	+/-				N
RB		+	+/-	+/-	++			
LIP	F, 50y		++ Od	++ Od	+/-	+		N
PPFE	55-60y				+			N
DAH Acute/Resolution	F					+		Y
Chronic						+		
LAM	F, Fertile		++ Od	++ Od	+/- Od			
LCH Incipient	20-40y	+		+	+			
Progressive		+		+	+			
Sarcoidosis	M	-		+	+		+	N
PAP	M,30-50y		+Od	Od				
HP Acute (Inflammatory)		-		+Hd	+Hd			
Chronic (Fibrosis)				+Hd	+Hd	+		

Table 3 Classifying ILDs on clusters colors by histopathological pattern;

Histopathological pattern	ILD	
UIP / NSIP	chronic fibrosing IIPs	Major IIPs
COP \ AIP	Acute/subacute IIPs	
DIP / RB	Smoking-related IIPs	
LIP / PPFE	Rare IIPs	
LAM / LCH	ILD with unique/specific histology	
Sarcoidosis / PAP / HP	ILD with characteristic complex histology	

Green patterns correspond to chronic fibrosing IIPs; blue patterns correspond to acute/subacute IIPs; purple patterns correspond to smoking-related IIPs; rare IIPs are the grey line of histopathological patterns; orange lines are for ILD with unique histology.

Table 4 ILD-Imagistic Pattern, clinical syndrome, and differential diagnosis

Imagistic Pattern																
Lesion																
Nodules		Reticulation				High attenuation		Low attenuation			HC	TB/b	Mo	Cp	Hc	RHS
Centro lobular	Peri lymphatic	Vascular	Smooth	Nodular	Archiom-fibrotic	GGO	C	E	Cy	At						
					+	+/-fin					+	+/-				
					+	+/-fin						+				
			+			+/-fin						+/-				
					+	+	+/-				+	+/-		+/-		
			+			+++										
					+++	+	+				+/-	+				
						++	++									
					++	+	+					+++				
+/-						+++									+	
						+++										
			+		+/-	+++			+/-			+/-				
+			+		+	+		+		+			+			
+ Small/Variable	+		+			++										
									+1-30 mm						a thin wall of the cyst	
							++					+				
			+			+	+						+	+/-		
				+	+							+				
				+/-		+/-	+/-		+++						A thin wall of the cyst	
+++									+							
+									+++						irregular wall of the cyst	
	+			+	+		+					+			+/-	
			+				+							++		
+							+			+			+			
+					+						+	+/-	+		++	

ILD-diffuse interstitial lung diseases; **IP**- idiopathic interstitial pneumonia; **UIP**: usual interstitial pneumonia; **NSIP**-non specific interstitial pneumonia; **AIP**- acute interstitial pneumonitis; **OP**- organizing pneumonia; **COP**- cryptogenic organizing pneumonia; **DIP**-desquamative interstitial pneumonia; **RB-ILD**-Respiratory bronchiolitis-associated interstitial lung disease; **LIP**-Lymphocytic interstitial pneumonia; **PPFE**- Idiopathic pleuroparenchymal fibroelastosis; **DAH**- diffuse alveolar hemorrhage; **DAD**-diffuse alveolar damage; **LAM**- lymphangiomyomatosis; **LCH**- Langerhans cell histiocytosis; **PAP**- Pulmonary Alveolar Proteinosis; **AE-IPF**-acute exacerbation of idiopathic pulmonary fibrosis; **I**-inferior/Basal; **M**-Medio pulmonary; **S**- superior; **Hd**-Heterogen distribution: distribution variations (occasionally diffuse, can be asymmetric), multifocal distribution; **Od**-(Omogenous distribution)- uniform distribution/diffuse; **PSL**-pulmonary secondary lobule;

Others	Clinical syndrome	Diff Dg
	IPF	- HPc - Dr; - CTD (ScS, PM/DM, BMTC) - asbestosis
	AE-IPF	
	I-NISIP CTD-ScS, PM/DM	- CTD (BMTC) - Dr - HPc
	-AIP-exudative -Dr	some types of infection, irradiation, and oxygen toxicity
	Organizing-AIP	CTC-LES, ARDS
Time-related -migratory- fluctuating	Idiopathic: COP, Secondary: Infection, Drug toxicity Aspiration of gastric contents CTD (PM/DM), Organ transplant Radiotherapy	-Vasculitis (Wegener's granulomatosis) - Tumors (Lymphoma, lung cancer)
	Idiopathic DIP	Dr , CTD
	RB-ILD	
+++ Mediastinal lymphadenopathy	-Sjogren sd. Autoimmune disease -AIDS	
	-infections, - bone marrow transplant, - autoimmune diseases – genetic predisposition	
Spares costophrenic angles -gravity-related (Shift with gravity)	-LES - ANCA vasculitis; -Sd Goodpasture	Coagulation disorders, drugs, inhaled toxins, or transplantation
Nodular calcification		
+/-pneumothorax chylothorax	LAM can be sporadic or associated with tuberous sclerosis	
Spares costophrenic angles +/-pneumothorax	LCH	
Lymphadenopathy: hilarious, bilateral mediastinal, symmetrical, well defined = hilar consolidation	Sarcoidosis	
	Idiopathic	Secondary: in association with malignant diseases, infections, silicon dust, aluminum, and chemical substances exposure)
	HP acute	
	HP chronic	

Pb-Peribronchovascular; **Pl**-perilymphatic; **Ps**-pleural sparing = NY-No/Yes (subpleural/ peripheral distribution); **GGO**- ground glass opacities; **C**-consolidation; **E**-emphysema centrilobular; **Cy**-cyst; **At**-air trapping; **HC**-honey combing; **TB/b**-traction bronchiectasis/bronchiolectasis); **Mo**-mosaicism; **Cp**-Crazy paving; **Hc**-head cheese pattern; **RHS**- Reversed halo sign (atoll sign); **IPF**- idiopathic pulmonary fibrosis; **I**-Idiopathic; **HP**-hypersensitivity pneumonitis (c-chronic); **Dr**-drug related; **ANCA vasculitis**: anti-neutrophil cytoplasmic antibody-associated vasculitis, **Sd** Goodpasture: anti-glomerular basement membrane disease; **CTD-connective tissues diseases**: **ScS** - systemic scleroderma; **PR** - rheumatoid arthritis; **BMTC** - mixed connective tissue disease; **PM / DM** - polymyositis/dermatomyositis; **LES** - systemic lupus erythematosus;

The characteristic computed tomographic (CT) features of **usual interstitial pneumonia (UIP)** are subpleural and peripheric distribution, with an apico-basal gradient (predominantly basal) of the lesions. UIP is the most common form of chronic fibrosing lung disease. Various diseases, including connective tissue diseases, chronic hypersensitivity pneumonia, pneumoconiosis, and, in sporadic cases, sarcoidosis, can produce UIP. Nevertheless, the most common cause of UIP is idiopathic pulmonary fibrosis (IPF), in which no underlying diseases can be diagnosed (89). Characteristic CT findings are reticulations, "honeycombing" cysts (confirming the diagnosis in "typical UIP)-Fig.9.14, traction bronchiectasis, and bronchiolectasis with architectural distortion; focal ground glass could appear (66) (38). The morphological pattern of IPFs represents 55% of IIPs.

Non-usual interstitial pneumonia (NSIP) is predominantly ground-glass opacity and/or reticular pattern. NSIP represents 14-35% of the morphological pattern without obviously apical-caudal HRCT gradient. Lesions distribution is homogeneous, bilateral, and can spare the subpleural space (90). Subpleural sparing of the dorsal regions of the lower lobes is present in approximately 40% of cases and may be a helpful feature in making the diagnosis because it is considered very specific for NSIP (91). NSIP is classified into two subtypes: cellular and fibrotic patterns, depending on which pathological features predominate, inflammation or fibrosis (92). Pure ground-glass without fibrotic changes is the hallmark feature of cellular NSIP, separated from the fibrotic NSIP pattern in which there is reticulation, traction bronchiectasis, and architectural distortion due to fibrosis. Aspects suggestive of progressive NSIP versus UIP include the presence of extensive traction bronchiectasis without or with minimal honeycombing changes (66). The occurrence of GGO in a patient with IPF (UIP) means either an exacerbation of IPF or a lung infection. Finding GGO usually goes with reversible diseases, contrasting with reticulation and traction bronchiectasis, which appear in fibrotic findings. As shown in Table 4, NSIP is usual the imagistic and histopathologic pattern for idiopathic NSIP and connective tissue diseases (CTD), like systemic sclerosis or polymyositis/dermatomyositis (PM/DM). Nevertheless, in mixed connective tissue disease (BMTc), drug-related ILD or chronic hypersensitivity pneumonia could also appear (93).

Morphopathological **acute interstitial pneumonia (AIP)**- also known as Hamman-Rich syndrome) the substrate is diffuse alveolar damage (DAD) due to acute onset and a rapidly progressive course of the disease (9) (94). Typical HRCT settings are bilateral ground-glass opacities (patchy or diffuse) and consolidations, with predominance in the lower lobes. HRCT lesions differ

depending on the evolutionary phase: in the acute exudative phase, GGO and condensation appear, and in the organizing phase, traction bronchiectasis predominates with parenchymal architectural distortion (95). There is clinical, pathological, and radiological overlap with acute respiratory distress syndrome (ARDS), and patients often present with respiratory failure developing over days or weeks (63).

Organizing pneumonia (OP), usually described as predominating in the lower lobes, has peripheral, subpleural, peribronchovascular SPL distribution with bilateral patchy airspace consolidation/ground-glass opacities (multifocal parenchymal consolidation), with or without small nodules around bronchovascular bundles (centrilobular) (96). Abnormal findings like crazy paving, peribronchial nodules, thickening bronchial walls, or ectasia could be seen. Time-related migratory, fluctuating- some abnormalities disappear spontaneously, and new areas of consolidation appear simultaneously in different sites (97). Characteristic is the atoll sign-Fig.7c. Lung architecture is preserved; fibrosis is absent.

Desquamative interstitial pneumonia (DIP) is typically characterized by bilateral ground-glass opacities in the basal parts of the lung (seen in 92% of patients). It is often associated with fine reticulation (98). Irregular reticulation, traction bronchiectasis, and small cysts may occur. Honeycomb's appearance is not usual. In addition to smoking, other factors such as systemic disease, infections, and environmental/occupational exposure to toxic substances and drugs may be associated with DIP (99).

Respiratory bronchiolitis-associated interstitial lung disease (RB-ILD) is a mild inflammatory pulmonary condition. The histopathological substrate of RB-ILD is respiratory bronchiolitis (RB). Thus, this entity is generally viewed as an amplified respiratory bronchiolitis response that, compared to the merely bronchiole-centered lesions seen in RB, leads to interstitial and air space inflammation and fibrosis extending to the nearby alveoli. CT abnormalities come with diffuse or predominantly upper lobes and thickening of the bronchial walls, centrilobular emphysema, GGO, and centrilobular nodules, imprecisely delimited (100). Some voices declare that RB-ILD and DIP represent different points along the same disease spectrum. DIP is the more severe, with panlobular diffuse mild-to-moderate interstitial fibrosis (101),(102). On the other hand, RB-ILD and DIP frequently co-occur (26).

Conform to the international classification of idiopathic interstitial pneumonia (9), DIP, and RB-ILD into companionship with pulmonary Langerhans cell granulomatosis belongs to the group **of smoking-related interstitial pneumonia**. While 100% of respiratory bronchiolitis-associated

interstitial lung disease cases are linked to cigarette smoking, this figure is 90% for DIP (103). Depending on the classification, smoking-related acute interstitial pneumonia and idiopathic pulmonary fibrosis may also be considered smoking-related ILDs (104), differing from hypersensitivity pneumonitis and sarcoidosis, ILDs that may be less prevalent in smokers (105). Smoking-related interstitial lung disease is a problematic subgroup typically showing profound emphysema with milder superimposed fibrotic changes. Smoking cessation is the primary attitude to take to stop the ILD progression. Otherwise, if the patient does not stop smoking, GGO in DIP may evolve into fibrosis or cystic lucencies. Langerhans cell histiocytosis (LCH) nodules may cavitate and evolve into irregular thick wall cysts (106).

Cystic abnormalities features may be the guidance element of several rare lung diseases, such as lymphangioleiomyomatosis (LAM), Langerhans cell histiocytosis (LCH), lymphocytic interstitial pneumonitis (LIP), desquamative interstitial pneumonitis (DIP)(107). Wall thickness (thin or thick) and anatomical distribution (spread or sparing of particular areas of the lung) can be pretty helpful for narrowing the differential diagnosis for diffuse lung diseases. **LAM and LCH are ILDs with unique/specific histology.** If LAM, a rare progressive multisystem disorder, predominantly impacts women of reproductive age, LCH affects young, primarily male smokers. The characteristic abnormality on lung CT scans in patients with LAM is the presence of thin-walled cysts scattered in a bilateral, roughly symmetric pattern without any lobar predominance (108). LCH CT findings reveal centrilobular nodules or/and thick wall cysts with variable size, mid- to upper distribution, and sparing costophrenic angles (109).

New research (26) shows a more grave emphysema type of smoking-related interstitial issue, with interstitial fibrosis, called **airspace enlargement with fibrosis (AEF)**. Axial and sagittal images show clustered asymmetric cysts that are more prominent and irregular than typical honeycomb cysts without traction bronchiectasis or other signs of fibrosis.

Lymphocytic interstitial pneumonia (LIP), one of the rarest of the interstitial lung with female predilection (in the fifth decade of life), is associated with a CT pattern of ground-glass opacity sometimes associated with centrilobular and subpleural micronodules and perivascular cysts(110). Thus, it could surely be included in the group of ILD with a cystic pattern.

Enlarged mediastinal lymph nodes are the mutual element of LIP with **sarcoidosis**, a granulomatous disorder of unknown etiology. Thin-section CT of sarcoidosis findings usually follows a perilymphatic distribution pattern, with a predilection for the upper and mid-lung fields. Imaging evaluation can be complicated, as the manifestations are variable and depend on the stage of the

disease. It is often labeled as the "great mimicker" (111), with a large spectrum of image features. Symmetric hilar/mediastinal lymphadenopathy and nodules infiltrate (presumably reflecting conglomerate granulomata) reflect among the first disease stages. Perilymphatic nodules are mainly grouped along the bronchial vascular bundles, interlobular septa, interlobar fissures, and subpleural areas (112),(113). Pulmonary fibrosis represents the end stage-IV, with central bronchial distortion and diffuse linear fibrotic pattern (typically radiating away from hila in all directions) (114).

Pulmonary alveolar proteinosis (PAP) is classically associated with the **lung crazy paving sign** on CT. The smooth thickening of interlobular and intralobular septal lines and ground glass opacities, patchy or geographic distribution, may have a slightly lower lobe predilection (115).

High-Resolution CT is preferred in the radiologic evaluation of **hypersensitivity pneumonitis (HP)**- one of the ILDs with known etiology. In acute HP, HRCT may be normal or show diffuse ground glass or centrilobular ground glass nodules, poorly defined centrilobular nodules, and areas of air trapping at the level of the secondary pulmonary lobule with mid- and upper-lung zone predominance (116). Chronic HP (HPc), fibrotic changes such as septal thickening, traction bronchiectasis, and honeycombing are seen classically in a peribronchovascular distribution with a mid- and upper-lung zone predominance. Airspace consolidation may be seen in chronic HP but is felt to represent superimposed infection and is not intrinsically related to HP pathophysiology. The headcheese sign is relatively specific for HP (117).

To better understand how HRCT elements can combine and create accurate interstitial lung disease models, which can be very suggestive for a type of illness, a simplified diagram is presented for the most commonly encountered interstitial lung diseases (fig. 10 (a) and fig. 10 (b)).

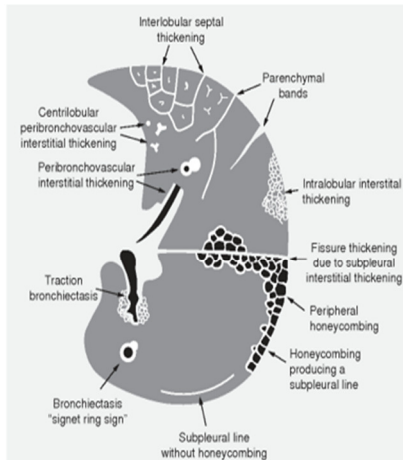


Fig 10(a)- Types of linear, reticular opacities and lucency cystic lesion

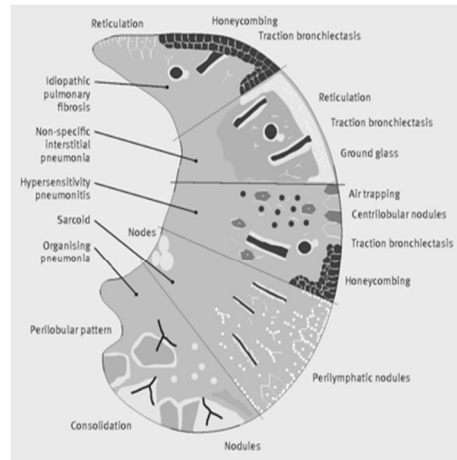


Fig.10(b)- Overlapping primary lesions in creating HRCT models for IPF, NISIP, HP, Sarcoidosis, OP

Fig. 10 Simplified representation of a typical HRCT appearance of the most common interstitial lung disease. Idiopathic pulmonary fibrosis

(taken from (118))

(taken from (119)).

The typical pattern of usual interstitial pneumonia is a predominance of subpleural reticular elements in the lower lung, traction bronchiectasis, and honeycombs with mild ground-glass opacities). Nonspecific interstitial pneumonia (subpleural ground-glass opacities, fine reticulations in the lower lung, fibrotic traction bronchiectasis at the final stage, typically without honeycomb formation). Hypersensitivity pneumonitis: acute- Centrilobular or geographic ground-glass opacities and air trapping (mosaic attenuation), chronic: fibrosis with reticulation, traction bronchiectasis, and possibly honeycombing. Sarcoidosis (mediastinal and bilateral pulmonary lymphadenopathy, perilymph distribution of the nodes; fibrous, often perihilar, mass, or honeycombing). Organizing pneumonia (nodule or consolidation, frequently perilobular pattern, fluctuating).

3. IDIOPATHIC PULMONARY FIBROSIS (IPF)- THE REFERENCE DISORDER FOR PULMONARY FIBROSIS

3.1. THE SPECTRUM OF HRCT FINDINGS IN IPF.

UIP is the histopathological and imagistic pattern of IPF. If IPF is equal to UIP, vice versa, UIP is not equal to IPF. In other words, IPF diagnosis needs obligatory UIP models, but the UIP pattern can also appear secondary to underlying diseases. Patients with fibrotic chronic hypersensitivity pneumonitis, connective tissue disease (e.g., rheumatoid arthritis, systemic sclerosis, polymyositis/dermatomyositis), exposure-related ILDs (e.g., asbestosis, drug amiodarone toxicity), radiation, ANCA-associated vasculitis's could provide UIP patterns. HP-UIP and CTD-UIP may be suspected based on their imaging appearance but are often imagistic and indistinguishable from IPF-UIP. In 6–10% of IPF cases, PPFE is seen (120), (121). It may be associated with a rapid decline in lung function, increased risk of pneumothorax and pneumomediastinum, and decreased survival (120).

Clustering under the UIP framework pattern, we can find four categories of facets: UIP model, probable UIP, indeterminate for UIP, and considering another diagnostic (89),(10),(38).

The updated clinical practice guide proposals were assigned and merged to better understand the UIP spectrum (table). Fleischner's statement (38) and ATS/ERS/JRS/ALAT guidelines (10) validate that honeycombs are a hallmark of UIP and must be present to make a final thin section CT diagnosis of **typical UIP** (fig.11). While (10) associate reticulation with peripheral traction bronchiectasis or bronchiectasis, at (38), this feature is not mandatory. Fleischner consensus also mentions the absence of inconsistent features like cysts, consolidation, and alveolar infiltrates. The typical distribution of UIP is subpleural and basal dominant, although upper lobe involvement is joint. Despite heterogeneous distribution, In some cases, the craniocaudal distribution of UIP can be relatively uniform. Lung fibrosis reflects lung architectural distortion and, in more severe forms, lobar volume loss with the displacement of the oblique fissures to posterior segments (122).

Probable UIP also has predominantly subpleural and basal distribution, often heterogeneous, with reticulation and traction bronchiectasis or bronchiolectasis (fig.12); (10) suggests that it may also have mild GGO, but it is not a dominant feature. Instead, Fleischner's statement shows that the honeycomb cyst formation may be absent. Both assign that reticulation with some inconspicuous or minor findings suggests an alternative diagnosis, which

indicates the lesions as indeterminate for UIP. This is inconsistent with UIP but not suggestive of an alternative diagnosis (123). Also, (10) suggests possible mild GGO or architectural distortion as distinctive features that do not indicate a particular fibrotic pattern. This category includes a subgroup of patients with very restricted subpleural ground-glass opacification or reticulation without noticeable CT features of fibrosis, for whom there is a suspicion that early UIP or probable UIP is present. In such cases, it should be set with prone inspiratory views that the subpleural opacities do not represent dependent atelectasis. Opposite, when features and distribution of features do not have any specific etiology, it is genuinely indetermined UIP (fig.13) (10).

Table 5 Comparison between 2018 Fleischner (38) and ATS/ERS/JRS/ALAT(10)

HRCT diagnosis	Overlapping findings	ATS/ERS/JRS/ALAT guidelines	Fleischner Society Statement		
Typical UIP	Distribution: -Subpleural and basal predominant; -Often heterogeneous, it can be diffuse				
	Features: -Honeycomb cyst formation; -Reticulation;				
	- <i>Traction bronchiectasis or bronchiolectasis</i> ;			with	-With /without
					-Absence of features to suggest an alternative diagnosis
Probable UIP	Distribution: -Subpleural and basal predominant; -Often heterogeneous.				
	Features: -Reticulation -Traction bronchiectasis or bronchiolectasis			-May have mild GGO;	-Absence of honeycombing; -Absence of features to suggest an alternative diagnosis
Indeterminate for UIP	Distribution:	-Subpleural and basal predominance	-Variable or diffuse; -not predominantly subpleural or basal		
	Features: -Reticulation -with some inconspicuous or minor findings that suggest an alternative, non-IPF diagnosis		-Possible mild GGO or architectural distortion□		

HRCT diagnosis	Overlapping findings	ATS/ERS/JRS/ALAT guidelines	Fleischner Society Statement
Alternative diagnosis □	Distribution: -Upper or mid lung Predominant; - peribronchovascular		-Areas of subpleural sparing
	Features: - Predominant consolidation; - Widespread pure GGO (without acute exacerbation)		
	Distribution:	-Perilymphatic	
	Features: - Widespread mosaic attenuation; - Diffuse nodules or cysts	*	□

Statement and guidelines in Diagnostic Categories of UIP Based on CT Patterns adapted after (66)ATS = American Thoracic Society, ALAT = Latin American Thoracic Society, ERS = European; Respiratory Society, GGO = ground-glass opacity, JRS = Japanese Respiratory Society, UIP = usual interstitial pneumonia, CTD = connective tissue disease, IPF = idiopathic pulmonary fibrosis, □ ATS/ERS/JRS/ALAT guidelines had other distributions listed that were different from the Fleischner Society Statement, which included: (a) dilated esophagus (consider CTD), (b) pleural plaque (consider asbestos exposure), (c) distal clavicle erosions (consider RA), (d) clinically significant lymphadenopathy, and (e) pleural effusions and/or thickening (consider CTD, drugs). □-Distribution/features that are not indicative of a particular fibrotic pattern; * with substantially sharply defined lobular expiratory air trapping; □ including micronodules, centrilobular.

An alternative diagnosis should be considered when the distribution is predominantly in the upper or middle lung or peribronchovascular, with features suggesting predominant consolidation, widespread pure GGO or mosaic attenuation, with nodules or cysts. In daily practice, a chest x-ray of ILD appearance and clinical findings could mimic a suspicion of idiopathic pulmonary fibrosis. Still, the HRCT pattern suggests an alternative diagnosis of fibrotic lung disease. Examples comprise bronchocentric fibrosis in the upper lobes or profuse mosaic attenuation that indicates hypersensitivity pneumonitis, posterior fibrotic retraction of the hila in sarcoidosis, or widespread ground-glass opacification with subpleural sparing in NSIP.



Fig. 11 Axial HRCT of UIP pattern

The Hallmarked honeycombing cyst; has subpleural, basal, and heterogenous distribution; with secondary traction bronchiectasis and bronchiolectasis.

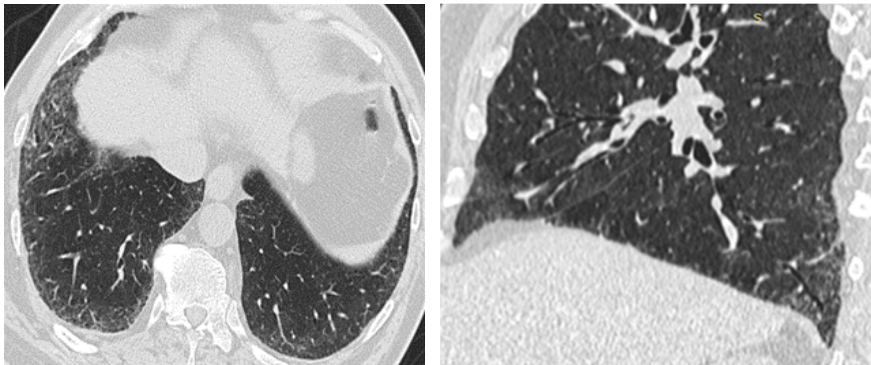


Fig. 12. Axial and coronal thin-section CT of probable UIP pattern

Has subpleural, basal, and heterogenous distribution; with reticulation with peripheral traction bronchiectasis and bronchiolectasis;-mild GGO

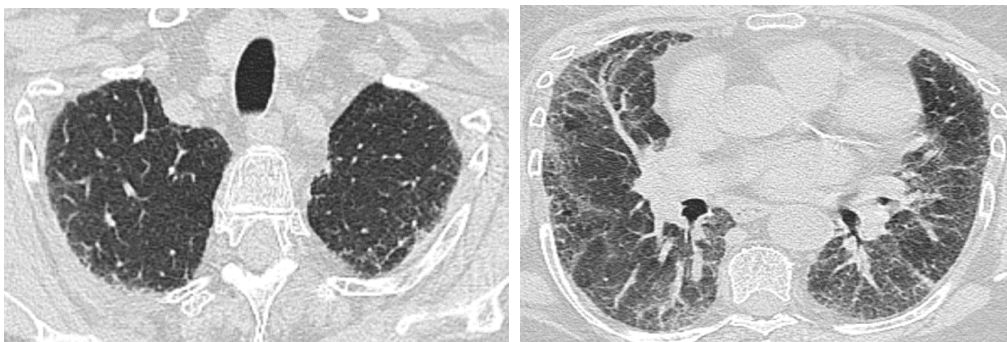


Fig. 13 Axial HRCT of upper and lower lobes marking the indeterminate for UIP pattern;

Has subpleural distribution with mild reticulation in upper lobes and reticulation and GGO in the lower areas; features and distribution of features do not have any specific etiology-truly indetermined UIP

3.2. IPF DIAGNOSTIC

The progressive aspect of ILD offers a tantalizing and terrifying challenge: early and accurate diagnosis can dramatically increase survival rate and life quality by promptly employing the proper treatment, consequently doubling the survival rate (124). As previously stated, clinical signs and symptoms overlap, so paraclinical methods are crucial to diagnosing ILD correctly. However, the more commonly used investigations, like chest X-Ray (CXR), peripheral blood tests, and spirometry, need to be complemented with the more specialized High-Resolution Computer Tomography (HRCT), lung ultrasound, and, in particular cases, bronchoscopy and surgical lung biopsy (125), (126).

As it was overwritten, IPF is the typical progressive chronic interstitial fibrotic lung disease, most frequently ILD, with an abysmal prognosis (16). Age is typically older than 60, and the etiology is unknown (7). Median survival after diagnosis is 3 to 5 years, with some patients progressing more rapidly or slowly, surviving more than ten years (38),(10),(127). Early imaging diagnosis of IPF using thin sections of CT is critical to guide the selection of patients for antifibrotic drugs (pirfenidone and nintedanib) that can mitigate the decline in lung function due to the high risk for early death without treatment (7),(10),(40). On the other hand, the precise ILD diagnosis is essential as well (89),(128), as medication that is beneficial for one ILD may be highly harmful to another (e.g., steroid administration in IPF is harmful due to the underlying mechanism of fibroblast activation and proliferation (129); essentially IPF it is considered to be unresponsive to “standard” therapies. Despite promising antifibrotic treatment, currently, no treatment can stop or reverse the scarring of the lungs. The aim is to slow pulmonary fibrosis progression.

HRCT plays a central role in diagnosing and treating all interstitial lung diseases, especially fibrotic diseases. In appropriate clinical circumstances, idiopathic pulmonary fibrosis (IPF) diagnosis can be made without surgical lung biopsy when HRCT features are consistent with common interstitial pneumonia (UIP) (130)

A thin-section CT, inspiratory, expiratory, prone sequence is the most sensitive radiological examination to assess the lung parenchyma for evidence of ILD. The key anatomical components of the lung parenchyma assessed in interstitial lung pathology are the interstitium and the secondary lung lobes (SPL) (66). Consequently, the histologic phenotype, lesion type (primary lesion and/or overlapping model), and its pulmonary and SPL distributions may compete and cooperate in developing the precise clinical syndrome.

The future of radiological diagnosis in ILD may be identifying disease behavior-based radiological phenotypes that predict disease results, which will be the

cornerstone **in** determining clinical management (131). Classifying the intrinsic CT features of fibrosis according to (38) and/or (10) is an essential role for radiologists, and it may detect progression early and make a significant contribution to the multidisciplinary debate (MDD) on this vital diagnosis.

According to (26) (132), (89), (133), (134), (135), (136), (122), (137), (138), (16), a proposed diagnosis algorithm for IPF is as follows (Fig.):

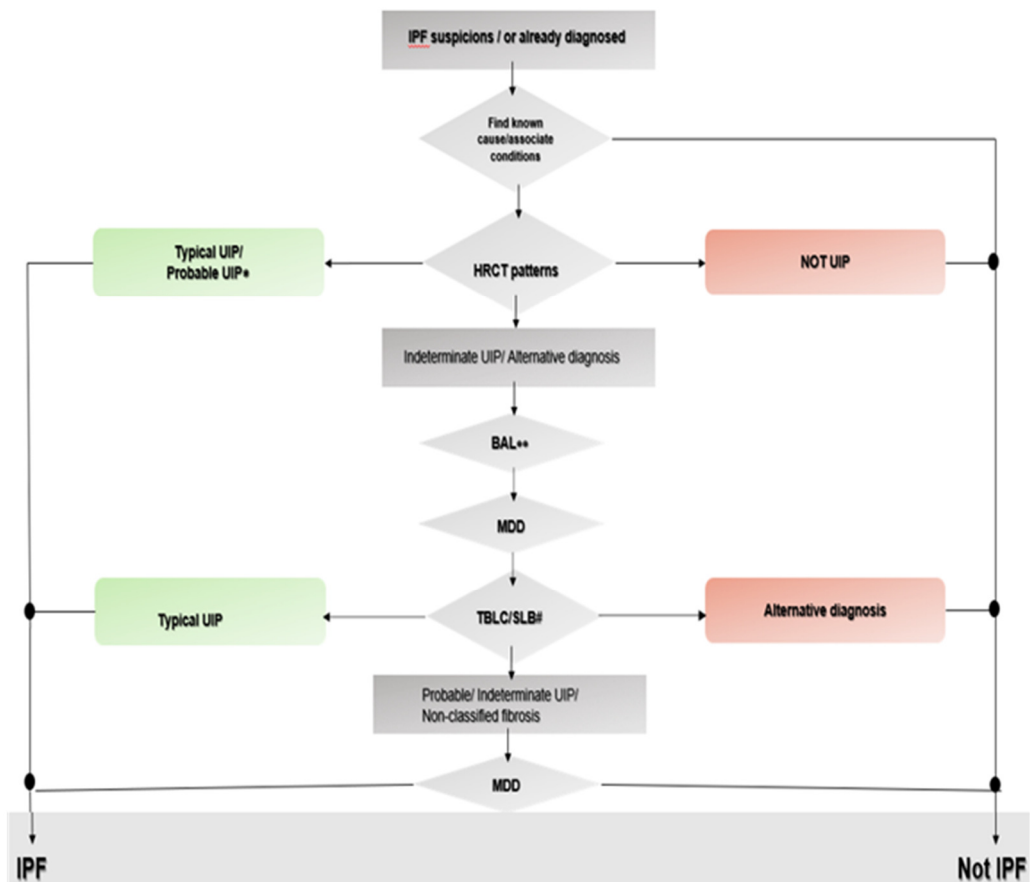


Fig. 14. The proposal flowchart for the diagnostic algorithm of idiopathic pulmonary fibrosis (IPF);

Usual interstitial pneumonia (UIP); Transbronchial lung cryobiopsy (TBLC); surgical lung biopsy (SLB); high-resolution computer tomography (HRCT); bronchoalveolar lavage (BAL); multidisciplinary discussion (MDD). □ Patients with a radiological pattern of probable UIP can receive a diagnosis of IPF after MDD without validation by lung biopsy in a proper clinical context (e.g., 65 yr old males, smokers). □ □ BAL may be performed before MDD in some patients evaluated in experienced centers. # TBLC is the preferred lung biopsy procedure in centers with appropriate expertise and/or in some patient populations. SLB may be explained in some patients with nondiagnostic findings on TBLC.

Even considering the current state of practice, ILD diagnosis is a developing field. In practice, there is a precise sequential algorithm to diagnose ILD. Initial clinical evaluation includes history and physical examination, which can find a potential cause and/or an associated condition leading from the start to another diagnosis. In many circumstances where a biopsy was once regarded as required, HRCT can now be used as a substitute. For instance, in certain patients with IPF, the HRCT appearance may be sufficiently distinctive to obviate the need for a biopsy (where UIP criteria are met) (7),(139),(140). Conform (26) Patients with radiological findings of probable UIP can receive a diagnosis of IPF after MDD without validation by lung biopsy in a proper clinical context (e.g., 65-year-old male, smoker). In the few remaining instances where a radiological diagnosis is not possible, In the rare remaining instances when a radiological diagnosis is not attainable, HRCT is still extremely valuable, but only as a guide for determining the optimal surgical biopsy site. Even techniques recommend HRCT for prognostic assessment and illness staging (141),(142),(143) .

The indeterminate UIP pattern or alternative diagnosis on chest HRCT pattern will lead to a multi-disciplinary discussion (MDD) that might suggest a lung biopsy and a new MDD post-biopsy result. Some patients could perform BAL for supplementary assessment before MDD in qualified centers. For lung biopsy samples in patients with ILD of undetermined type, TBLC is the preferred maneuver if possible (144). The HRCT and histopathological patterns label the diagnosis.

4. ILD COMPUTER AIDED IMAGISTIC DIAGNOSTIC

Computer-aided techniques (CAD) can be broken down into learning and discovery. Both can be carried out under supervision or independently; nevertheless, the results of computer techniques are primarily data-based.

Artificial intelligence (AI) is the intelligence displayed by machines, as opposed to the natural intelligence exhibited by animals and humans. AI research is defined as the field of study of intelligent algorithms related to systems that distinguish their environment and take actions that increase their chances of achieving their goals.

"Artificial intelligence" describes machines that mimic and represent "human" cognitive abilities related to the human mind, like "learning" and "problem-solving" based on the concept of rationality (145). An algorithm is a way of processing data. In other words, artificial intelligence represents algorithms that train the computer to have its own new algorithms according to complex rules that are not based on mathematical analysis. They auto-adapted after they received the data set human input. Subcategories of AI are machine learning (ML) and deep learning (DL). ML consists of a set of algorithms designed to improve their performance with the help of training data. The primary purpose of these algorithms is to predict specific characteristics of the analyzed data and/or to make independent decisions based on it (without the help of human input) – to cluster it. This model is generated to fit the analyzed sample data best. For example, if it receives information about the axial plane HRCT image of the chest, it processes and later groups which images are part of the axial section and which are not. Alternatively, clusters the diseases where cough appears as a common element (146), (87).

Based on the data set provided, DL goes deeper and learns to recognize autonomously (without human input) based on segmentation rules, the number of categories in the database, and what features create a category. For the same example with thorax HRCT, DL could tell which findings belong to the axial plane, a sagittal or longitudinal image, based on its autonomous algorithm. Complex neuronal networks (CNN) are the engines that run DL, which is a structure of algorithms and data (87), (147). Usually, they are used for second opinions computer-aided.

A relatively new approach uses visual aids in which data is processed and abstracted in the background to provide valuable clues and condensed information to allow autonomous human judgments. Complex networks (CN) are expressive interconnected visual representations and data modeling as

networks. Clinical and functional data, thoracic HRCT pathways, and disease networks form structures that can be visually represented as networks (148). On the other hand, there is clear synergy and dynamism among the elements of these data sets. The connections between data entities are static and represent transformation relationships or, better yet, convey the influence that nodes assert over one another (149), (150). CN represents a quantitative analytic method that does not influence the outcome as a second opinion but enhances the medical HRCT judgment as an alternative diagnosis.

The technique used in human-based diagnosis starts with pattern recognition, defining their location in the lung, gathering this data into an identifiable disease configuration, and solo throw visualization. The high-resolution computed tomography (HRCT) detection and diagnosis of diffuse lung disease are primarily based on the recognition of a limited number of specific abnormal features, specific combinations or patterns of these abnormalities, one or more specific distributions of abnormal findings, and the use of basic history and clinical information.

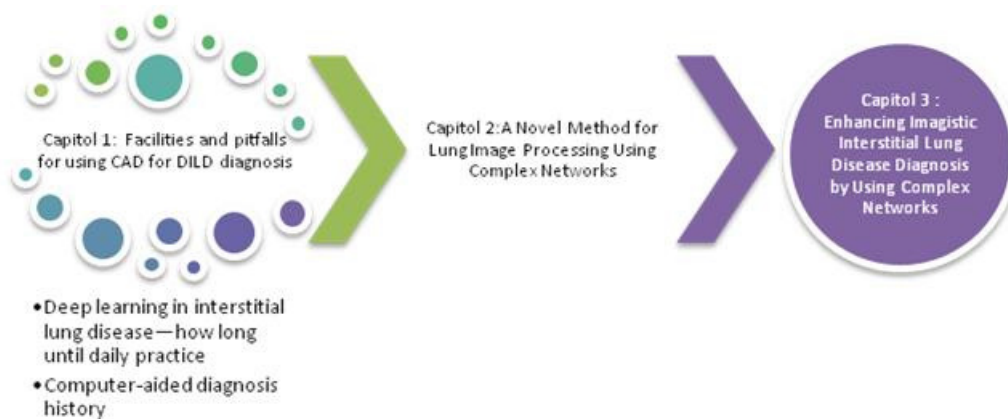
This is vastly different from the way computer-aided diagnosis (CAD) works. Most CAD uses heuristics and machine learning with no analytical process, being interested in the proper classification and not the reasons why this occurs. A hybrid method, including heuristics and analysis, is described in (151) to bridge the gap. Computer-based Quantitative assessment of progression of pulmonary fibrosis can provide a more objective and reproducible measure of progression than visual assessment (152), (153).

Due to the lung tissue-specific radiation attenuation qualities and maximal spatial resolution, HRCT, since 2011 (145), has been the central noninvasive instrument in analysis, offering crucial details and insights that can lead to diagnosing ILDs (138). The imaging results are analyzed based on distinct textural patterns in the lung window's distribution and extent. The evaluation focuses on the picture's grayscale tones (in terms of HU) and geometrical structures, essentially a repeating pattern-matching challenge, offering the ideal setting for computer-aided diagnostic (CAD) systems. Texture recognition is highly accurate when a complex network approach is used because of its analytic properties (146),(147).

As with any diagnostic tool, there can be intricacies that require a specialized technician and/or further, more invasive investigations. Furthermore, this is quite challenging for the practitioner, given that human error is still not negligible. Substantial inter-observer inconsistency, even between experienced radiologists, confuses the process (157), (128), (149),(87). The present-day approach is to try and supplement human analysis of HRCT with automated

tools, like the CALIPER program (150), or various AI-based tools, like (151), (152), (153), (154).

With information technology (IT) procedures, CAD allows medical professionals to comprehend and employ distinct imagistic investigations (155). The objective is to increase the speed and accuracy of diagnosis, with IT as a supplement or even an independent diagnostic alternative. (156) The CAD algorithms are part of artificial intelligence (AI) since they imitate human thought (157). Essentially, the ILD diagnosis is an algorithm with the following workflow: If physical examination outcomes and paraclinical studies (chest X-ray, lung function measures, routine and specialized blood tests) suggest ILD based on a complete history, an HRCT is conducted (158). The human aspect then intervenes by validating the quality of the resulting data and, if no issues/artifacts are discovered, looking for patterns in particular regions. If the data are conclusive, a diagnosis may be established. Still, if they are ambiguous, a list of potential diagnoses will be generated, needing more talks and more sophisticated, invasive investigations. The individual executing these algorithms is crucial to accurate and rapid diagnosis since they introduce an overall inherent variance. As CAD can emulate the algorithm, it would be a perfect option for this step as it would eliminate deviations. Well-conducted research intends to comprehensively examine how artificial intelligence (AI) enhances ILD diagnosis, focusing on convolutional neural networks (CNNs) as described in (159),(160). CNN may reduce human resources and cut the costs associated with this fatal disease's social and medical elements.



RESEARCH PART

5. CHAPTER 1: FACILITIES AND PITFALLS FOR USING CAD FOR ILD DIAGNOSIS

5.1. DEEP LEARNING IN INTERSTITIAL LUNG DISEASE – HOW LONG UNTIL DAILY PRACTICE

5.1.1. INTRODUCTION

Interstitial lung diseases (ILDs) refer to about 200 distinct lung illnesses that include inflammation and fibrosis of the interstitium, with associated clinical, radiological, and pathological characteristics and are significant causes of morbidity and mortality. (4)

Due to the lung tissue-specific radiation attenuation qualities and maximal spatial resolution, high-resolution computed tomography (HRCT) is the technique of choice in diagnosing ILD. The imaging results are analyzed based on distinct textural patterns in the lung window's distribution and extent. The evaluation focuses on the picture's grayscale tones and geometrical structures, which is essentially a repeating pattern-matching challenge, offering the ideal setting for computer-aided diagnostic (CAD) systems. With information technology (IT) procedures, CAD allows medical professionals to comprehend and employ distinct graphical investigations (155). The objective is to increase the speed and accuracy of diagnosis, with IT providing a supplement or even an independent diagnostic alternative (156).

The CAD algorithms are part of artificial intelligence (AI) since they imitate human thought (157). Essentially, the ILD diagnosis is an algorithm with the following workflow: An HRCT is conducted (158) if physical examination results and paraclinical studies (chest X-ray, lung function measures, routine and specialized blood tests) suggest ILD based on a complete history. The human aspect then intervenes by validating the quality of the resulting data and, if no issues/artifacts are discovered, looking for patterns in particular regions. If the data are conclusive, a diagnosis may be established, but if they are ambiguous, a list of potential diagnoses will be generated, needing more talks and more sophisticated, invasive investigations. The individual executing these algorithms is crucial to accurate and rapid diagnosis since they introduce an overall inherent variance. As CAD can emulate the algorithm, it would be a

perfect option for this step as it would eliminate deviations. This research will comprehensively examine how AI enhances ILD diagnosis, focusing on convolutional neural networks (CNNs).

5.1.2. COMPUTER-AIDED DIAGNOSIS HISTORY

The virtual subclass of an AI component is machine learning (Fig. 1), which consists of mathematical algorithms used by computer systems to learn a specific task via experience without explicit human instructions (149). This advancement is represented by the concept of deep learning (DL), which is comprised of a multi-layer representation learning architecture.

Through a sensor, the representation stimulates the first layer of neurons, which activates the next layer through complicated connections.

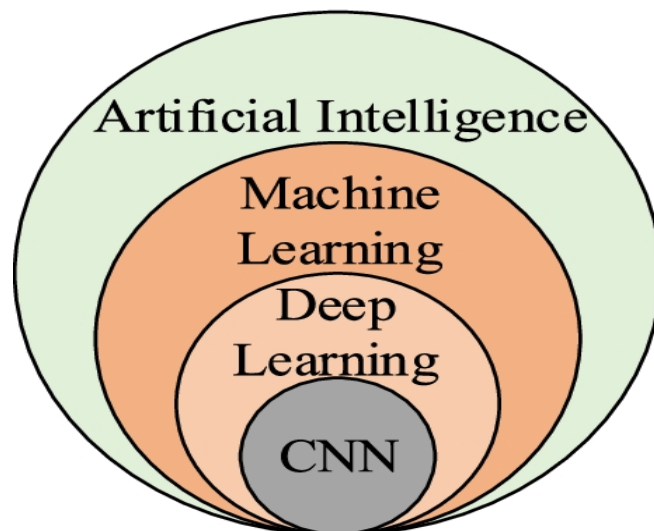


Fig. 15 Artificial intelligence progression diagram (AI, artificial intelligence; CNN, convolutional neural network)

Each layer analyzes the representation non-linearly, resulting in an increasingly complicated schema and a departure from the general task-specific algorithm for machine learning (161,162). The primary benefit of DL is that it can improve autonomously and without human input. It can execute arbitrary parallel computations more efficiently than other algorithms (163,164) from an application viewpoint. Among other applications, DL is used in visual object identification (161), voice recognition (165), driving assistance (166), and language categorization (164).

Neocognitron combined neurophysiological architecture (162,167,168) was the first algorithm effectively employed for pattern recognition in 1980. As shown by the advent of the backpropagation technique in 1989, which enabled handwritten digit identification and became a landmark reference (167), the key to effective feature extraction is the design of adequate network architecture.

CNNs demand big, well-balanced datasets and complex algorithms, which affect processing power and storage capacity (162,163). Krizhevsky et al. created the Alex Net CNN model by amassing the most extensive training set of 1.2 million pictures. The system categorized the photos into 1000 nature categories with the lowest error rate possible (168), making it the most advanced database for training CNNs.

The first neural network to reach superhuman performance in visual pattern recognition emerged in 2011 when Ciresan et al. employed a deep neural network on a graphics processing unit to detect photos of traffic signals (<http://people.idsia.ch/juergen/superhumanpattern.html>). In the last ten years, graphics processing units have enabled lower calculation times for complicated operations in a typical scenario, facilitating the development of CNN (162,169).

As shown in Fig. 2, each CNN has a complicated architecture with an initial picture input as a pixel array from a receptive field and multiple hidden computational connection layers (161,170).

The CNN's core component, the convolutional layer, comprises many weighted individual filters (161). Multiple filter sets detect distinct visual patterns. Small patterns like corners, lines, and edges are seen before forms and objects.

A CNN needs numerous layer types and communication between them to function (170). The last step predicts the picture category probabilities. It determines the active feature class with the most robust and relevant features (168).

The first CNN Healthcare application goes back to the early 1990s. Lo et al. used the CNN algorithm to identify lung nodules on chest X-rays, achieving an 80 percent true-positive detection rate (171). Sahiner et al. (172) employed CNNs to distinguish bulk from normal breast tissue on mammograms, achieving a 90% positive predictive value. In 2008, brain MRIs effectively diagnosed hippocampal sclerosis (173). Due to the short size of the database and the simplicity of detecting specific lesions, the high favorable rates seen in these first investigations are skewed.

There are several obstacles to getting medical pictures for deep learning:

- (1) They are difficult and expensive to acquire compared to typical images.
- (2) Valid annotation of bio-images requires the assistance of professionals.

- (3) The scale of the medical database is often inadequate, but state-of-the-art image analysis datasets (ImageNet, AlexNet, GoogLeNet, VGGNet) include hundreds or millions of natural image instances.

A possible solution is transfer learning, in which weights from a CNN trained on a natural dataset are transferred to a CNN learned on a separate dataset (170,174). Despite the stark differences between natural photography and medical images—the former being colored and the latter being grayscale—all have the same descriptions. Histograms of directed gradient and scale-invariant feature transform have been utilized effectively to segment and detect medical images. Bar et al. (175) corroborated this in chest pathology using CNNs trained on nonmedical image datasets to analyze 93 chest X-ray pictures. The area under the curve (AUC) was 0.93 for identifying right pleural effusion, 0.89 for detecting heart enlargement, and 0.79 for classifying normal vs. abnormal chest X-rays. All values are significantly over 0.5, indicating that the model is accurate.

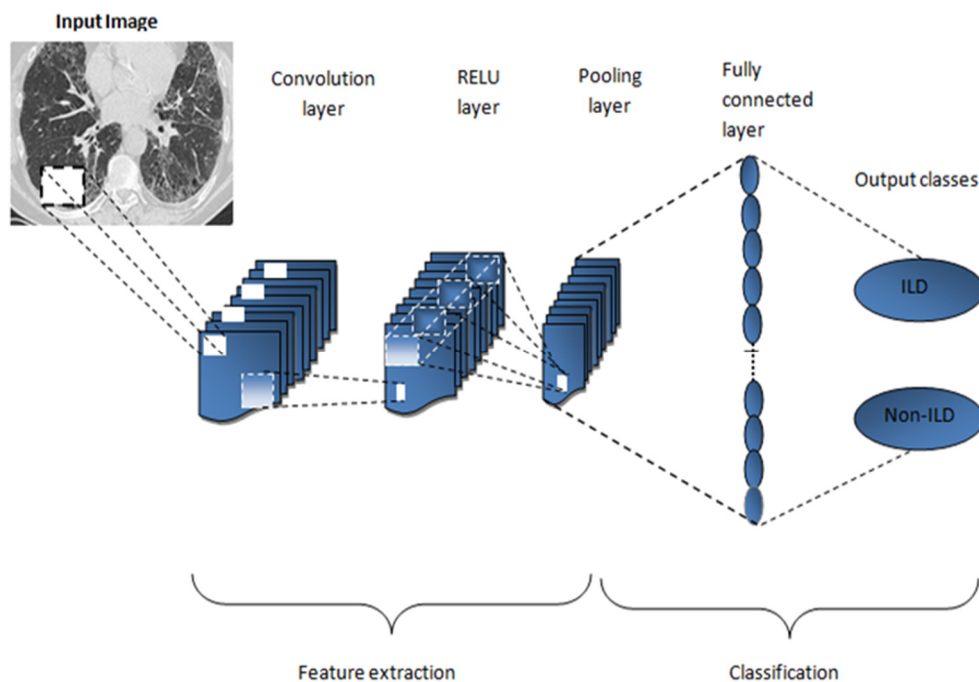


Fig. 16 Convolutional neural network architecture

CNN applications in bio-imaging research flourished in segmentation, detection, and classification applications beginning in 2014, including lung nodule detection and classification, colon polyp detection, coronary calcification detection (169,176), skin cancer classification (177), knee cartilage segmentation (178), brain tumor segmentation (179), and breast lesions classification (180,181).

The goal is to acquire more precision and superior performance than human counterparts. Even though artificial intelligence research has been primarily focused on neurology (157), oncology, and cardiovascular diseases (170), the first three leading causes of death, the chest imaging field is also of interest for lung nodule detection and classification (182,183), tuberculosis lesion classification (184), lesion detection (185), and parenchymal pulmonary disease classification (153).

5.1.3. INTERSTITIAL LUNG DISEASE-SPECIFIC CAD

Reticulation (RE), honeycombing (HC), ground-glass opacity (GGO), consolidation (CD), micronodules (MN), and emphysema (EM), or combinations of the above, are typical ILD patterns in high-resolution (HR) CT scans. The challenge arises when the outcomes are contradictory or ambiguous (Fig. 3). CNNs require large image sets because normal lung or distinct tissue categories may display similar appearances (Fig. 3a, b or c, d), yet considerable changes across people for the same tissue class may be observed (Fig. c–e).

Anthimopoulos M. et al., excluding unclear lung regions and the broncovascular tree, experienced radiologists annotated and employed 120 HRCTs for training and testing a CNN. Due to the hyper-parameters generated for the ILD pattern characterization, the suggested algorithm outperformed the state-of-the-art approaches (Alex Net, VGG-Net-D). Due to the overlapping appearance, the combination of GGO/ RE and individual GGO and RE patterns also displayed a significant misclassification rate. An accurate description of texture distinct from gray-scale intensity value has clinical implications in distinguishing between idiopathic pulmonary fibrosis (IPF) and non-specific interstitial pneumonia. In response to these obstacles, Christodoulidis S. et al. (174) introduced a CNN architecture that could extract the textural variation of ILD patterns. Just a two percent improvement in CNN performance was realized, using transfer learning from many non-medical source datasets. The significant drawback in (174) is using CT scans instead of HRCT.

The few applications that employ HRCT, such as (151,152,154), all use CNNs for classification. Even though Li et al. (152) and Li et al. (154) use a proprietary architecture in an unsupervised method, their performance is inferior to that of other possibilities (174,186).

5.1.4. HOW SOPHISTICATED SHOULD THE CNN BE?

In pattern classification, Kim et al. (199) compared shallow learning (SL) to deep learning (DL). In their work, they employed four convolutional layers and two fully connected layers to create a CNN architecture that improved accuracy from 81.27 to 95.12 % by increasing the number of convolutional layers. This reduced the misclassification rate between ambiguous instances such as HC/RE (Fig. 3e) or NL/EM and highlighted the need for more complicated DL approaches in ILD diagnostics. Differentiating between distinct lung tissue patterns on HRCT images is difficult, particularly when utilizing limited samples for region-of-interest (ROI)-based classification. This might lead to mismatches since lung tissue may have a similar look among distinct tissue categories despite substantial heterogeneity between people within the same category.

In addition to grayscale differences, image processing also includes object identification, independent of other factors. Wang Q. et al. (187) presented a multi-scale rotation-invariant CNN method to address this bias, considering that patient movement during scanning and breathing may impact lung volume size. This method employs a Gabor filter, which evaluates the precise frequency and directions in a confined area, simulating the human visual brain. This algorithm's performance accuracy categorizes all ILD patterns above 85 percent, reaching 90 percent for N, GGO, and MN patterns. Similar to the earlier work, increasing the number of CNN layers has reduced the error rate. This technique is flawed by the exponential complexity of the Gabor filter implementation, which requires considerable computing resources.

All other research (174,186–188) that classified ILD patterns used a patch-based approach to picture representation. Their drawback was the tiny picture portions (31 pixels), which led to the loss of fine detail. In addition, the image patch had to be manually annotated, resulting in a laborious procedure for radiologists. Recognizing the difficulty in manually identifying ROIs for automated pulmonary CAD systems, Gao M. et al. (189) attempted an alternative classification method for ILD patterns.

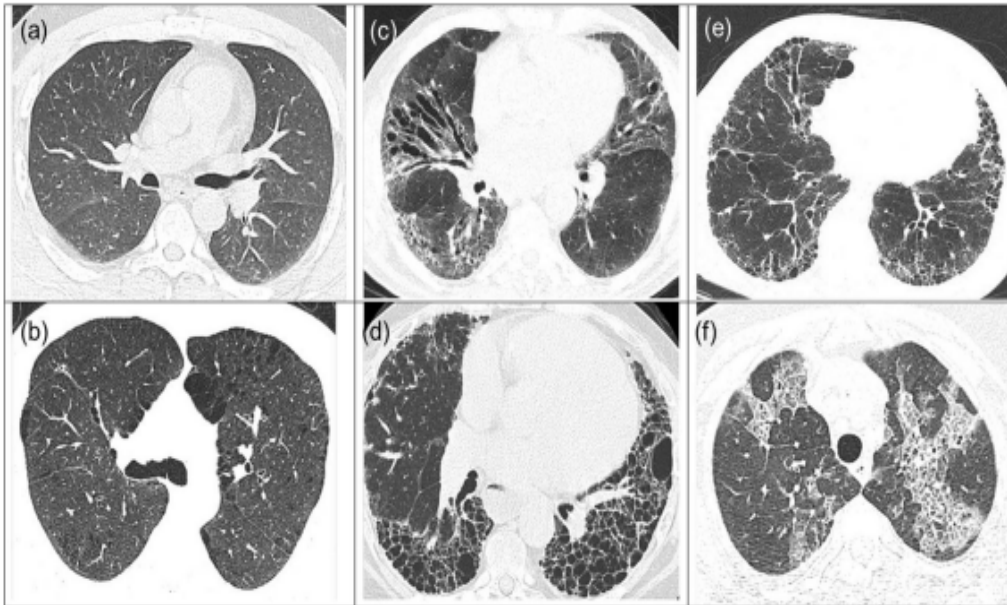


Fig. 17 Difficult ILD patterns

a) NL in subject 1. b) EM in subject 2. c) RE in subject 3. d) HC in subject 4. e) Mixed HC/RE in subject 5. f) Mixed RE/GGO in subject 6. Source: "Victor Babes" Database

Similar to emphysema quantification (190), but with more autonomy, they suggested a technique for global picture identification based on grayscale level. This viewpoint caught more information and used slice-level picture labels or tags without defining ILD areas. Rescaling the CT picture in Hounsfield units (HU), the approach expresses three distinct attenuation scales concerning the lung ILD pattern: low attenuation pattern (HU = 1400 and 950) for EM, high attenuation pattern (HU = 160 and 240) for CD, and typical lung attenuation (HU = 1400 and 200). The patch-based categorization obtained 87.9 percent accuracy compared to the holistic approach's 68.6 percent accuracy. The findings are deceptive: the holistic technique correctly recognized EM but had difficulty distinguishing between normal lung (NL), MN, and CD patterns. The ideal EM categorization needs more investigation, maybe using a mixed-method technique. The dataset continues to be the Achilles' heel of each approach.

Bae HJ. et al. (191) offered an intriguing technique by generating an unlimited number of arbitrarily distinct ILD patterns from 2D HRCT images, which improved the classification accuracy of CNN for lung tissue patterns. The algorithm avoided over-fitting, stabilizing accuracy loss for the validation set and offering various ILD patterns. The accuracy of a particular area of interest or the whole lung was 89.5 %, which was greater than the accuracy of traditional CNN

data augmentation (82,1%) and comparable to the human ability. The most effective ROIs were NL, GGO, RE, and EM. The algorithm's randomization of ILD patterns cannot technically guarantee a hypothetically ideal level of accuracy. In addition, the algorithm's repetitive nature necessitates excessive computational resources, making it unsuitable for a typical computer.

5.1.5. IDIOPATHIC PULMONARY FIBROSIS – THE CHALLENGE OF ALL ILDS

HRCT must diagnose and treat all interstitial lung illnesses, particularly fibrotic lung disease. In a clinically suitable setting, idiopathic pulmonary fibrosis (IPF) can be diagnosed without a surgical lung biopsy when HRCT signs of typical interstitial pneumonia (UIP) are present (89). Based on expanding data, a Fleischner Society statement broadened this recommendation to cover individuals with suspected UIP symptoms (38,192).

Despite this paradigm, the radiological evaluation of ILD remains challenging due to high inter-observer variability, especially among experienced radiologists (128,149). This might be a barrier in clinical practice since imaging expertise is not always available, particularly at non-academic sites. This could lead to delayed diagnosis and unnecessary interventional procedures, such as surgical lung biopsies, which may present unacceptable risks, especially for elderly patients with severe disease.

Walsh et al. (153) presented a CAD that could be quickly installed on conventional computer equipment to solve these restrictions. A total of 1157 HRCT scans were pre-processed to generate a maximum of 500 distinct four-slice montages (concatenations) per CT scan, yielding a dataset of multiplied images with 420,096 unique montages for the training algorithm and 40,448 for the validation set. This investigation employed the convolutional neural network Inception-ResNet-v2 as the particular neural network architecture (193,194). An experienced thoracic radiologist classified each HRCT into one of three categories: UIP, potential UIP, or inconsistent with UIP (89), with the corresponding diagnostic prediction outcome. Neural network training becomes an interactive process using a specific optimization approach to change the network's internal parameters and eliminate scan errors. Tested on 139 HRCT (68,093 distinct test montages), the algorithm's accuracy was 76.4 %, with 92.7 % of diagnoses falling inside one group. The program evaluated 150 four-slice montages in 2.31 seconds.

Another approach (153) was evaluated clinically on a second sample of 150 HRCT scans with fibrotic lung disorders. Numerous patients with IPF, chronic fibrotic hypersensitivity pneumonitis, or connective tissue disease-related fibrotic interstitial lung disease were assessed by 91 thoracic radiologists

(not participating in the training process). The average performance vs. the radiologists' assessment was 73,3 % (93.3 % within one category). The median diagnostic accuracy of thoracic radiologists in this sample was 70.7%. This technique is a useful diagnostic tool for IPF since it provides consistent, nearly immediate reports with human-level accuracy. Since the UIP pattern is associated with high mortality rates in ILD, the distinction between UIP and non-UIP is crucial. The algorithm and the majority opinion of the radiologists produced the same prognostic differentiation ($p = 0.62$) between these two groups (195). When Fleischner criteria for IPF diagnosis were considered, a solid interobserver agreement was seen between the algorithm and the radiologists. CNN is not programmed to detect basal honeycombing as a distinguishing feature of UIP. Still, it appears capable of learning to do so. This autonomous activity may provide a foundation for identifying new imaging biomarkers for fibrotic lung disease. The difficulty with this algorithm is that it only evaluates one tissue subtype per slice, thereby removing any mixed patterns. However, the fact that it is easily accessible and requires only a small amount of local resources is a huge advantage.

5.1.6. DISCUSSION

The lack of big imaging datasets for training is a significant obstacle to developing accurate deep-learning algorithms for diagnosing fibrotic lung disease. An international collaborative effort is required to establish a centralized image repository to solve this issue. In addition, the photos must be standardized using a suitable format, HRCT. There are too few algorithms that deal with certain picture types, such as (151–154), and since 1-mm-thick slices might reveal lesions that would be overlooked, this format is essential. Since the images will likely be collected from numerous sources, the resolution, grayscale, and annotations must also have a standardized format.

The "Next Generation" of clinical AI is a CNN that can be placed on any computer station and is accessible to non-academic institutes. In the realm of ILDs, specifically, AI can aid in the differentiation and early diagnosis of individuals with the most severe type, namely IPF. Early identification of IPF will result in tailored antifibrotic treatment that significantly prolongs survival and minimizes acute exacerbations, which are not only fatal but also expensive (195–199). To meet such lofty standards, a hybrid algorithm should be devised.

A combination of several CNNs may be the answer to decreasing the expenditures associated with social and healthcare elements (217,218) since specific algorithms, such as (202), display exquisite accuracy in certain areas. The CNN combination might have various configurations and begin creating the same input or have similar configurations and produce distinct inputs. Even more

intriguing would be merging many AI approaches, such as CNN, with clustering and classification algorithms, maybe in parallel or sequential stages. The objective is to minimize local area computing regardless of the technique, leaning toward a cloud architectural style.

Legal considerations such as data privacy and security become crucial in this instance, and security protocols may impede communication between the local and computational nodes.

5.2. COMPUTER-AIDED TECHNIQUES

In every computer application, one must remember that a computer is essentially a machine that performs what it is programmed to do; therefore, picking the appropriate program is essential. One must specify inputs, desired outputs, and generating methods to choose a program.

In ILD diagnosis, the inputs are those available during the multidisciplinary discussion: patient-generated information (the initial clinical evaluation, high-resolution computerized tomography (HRCT), and biopsy) and literature- or practice-generated information (ILD classification, diagnosis criteria, statistical and historical data). The outcome is either (ideally) a diagnosis for the current patient or (at the very least) a valuable recommendation for the clinician to consider.

Early computer applications in medical diagnosis began in the 1990s, with an initial precision below or, at best, equal that of medical practitioners. As Computer Science progressed, so did their precision (176).

The ethical implications of employing computers for a second or even first opinion, how much one should rely on them, whether or not their engineer developers are responsible for their outputs over time, and to what extent must at least be stated here. Who is responsible for any medical act if a computer performs it? This examination is beyond the scope of this paper (which is to highlight ILD management-specific methods). Still, before implementing such algorithms, their performance and reliability enhancements (200) should be weighed against their legal consequences, as discussed in (201).

Returning to the technical features of ILD management computer-aided applications, two types can be defined: the first analyzes data and provides a conclusion based on it, whereas the second conjugates complex data sets and displays its depiction, allowing humans to generate a conclusion.

The first category employs the computer as a second opinion maker, focusing on learning and reasoning applications. In contrast, the second category primarily uses the computer as an enhancer, inventing new methods to visualize facts that help humans understand them better.

Figure 18 gives a classification of ILD-specific algorithms along three axes: conclusion maker (machine/human), goal (finding, learning, and reasoning), and human supervision dependence (supervised, unsupervised, reinforced).

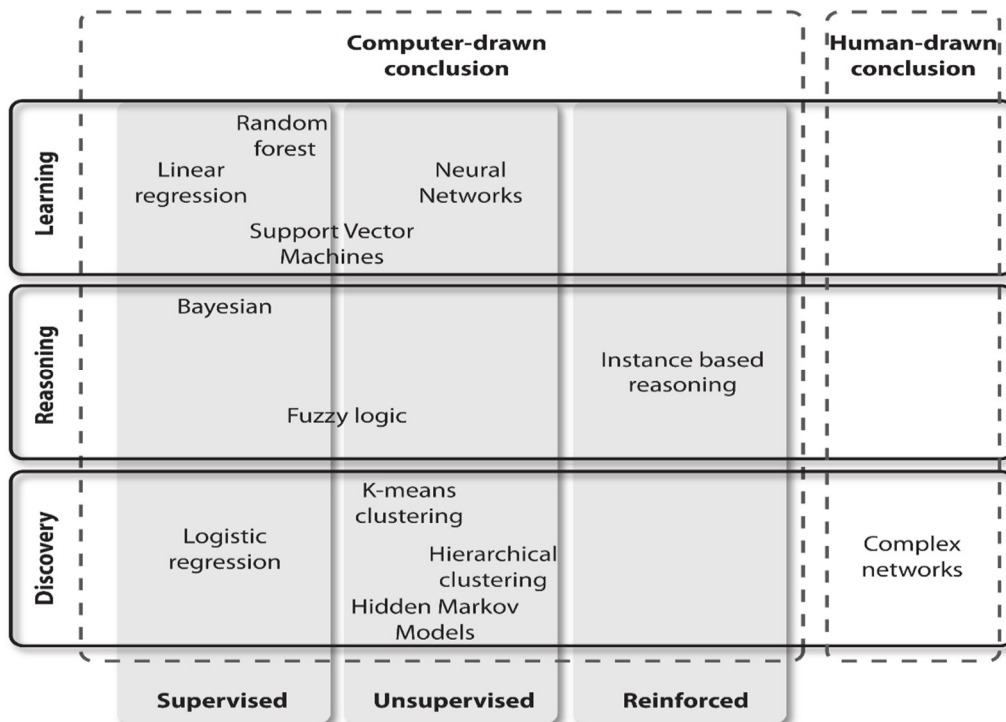


Fig. 18 ILD-specific algorithms

Figure 18 provides a fast reference for selecting an algorithm class. For instance, if we want to construct a diagnosis model that recognizes existing patterns, learning algorithms are the obvious choice because they learn from the data provided. Nonetheless, if a new diagnostic parameter is desired, the discovery section contains the necessary algorithms. When we need a consensus between inputs and rules, we employ reasoning algorithms, sometimes allowing for uncertainty or statistical judgments. Consequently, these algorithms help develop a diagnosis or treatment algorithm with quantifiable input rules.

As its name suggests, supervised machine learning entails training a model by providing it with input data and the expected output values (known beforehand). The algorithm then produces a model (formula) that fits the input data and may be used to analyze new input data (202).

The two most prevalent applications of supervised learning are linear regression and classification. In unsupervised machine learning, no training set instructs the algorithm on generating results; instead, the algorithm is responsible for discovering commonalities across data. They are utilized chiefly for grouping, anomaly detection, and neural networks. K-means clustering, hierarchical clustering, DBSCAN clustering, and the hidden Markov Model are among the most common unsupervised ML methods.

The reinforcement learning (RL) algorithms are based on a trial-and-error methodology. The learner is not told what to do but instead learns good and bad acts based on the rewards or punishments it receives in response to its activities. Consequently, it will always choose the movements that maximize its benefits (203).

When clinicians are faced with a lengthy therapeutic procedure, these algorithms can be used in conjunction with medical imaging for medical diagnosis. Multiple application directions exist for reinforcement learning algorithms, including ILD, dynamic therapy regimes, automated medical diagnostics, and more general domains (204,205).

The following parts will focus on the most ILD-specific applications implemented, as shown in Figure 18.

5.2.1. REGRESSION

Regression models are primarily concerned with establishing the relationships between input and output values, where input values represent a variety of characteristics of the analyzed data. Continuous values constitute the output values. Linear regression, logistic regression, polynomial regression, and support vector machine(SVM) are among the most frequently used regression models. SVM can also be used for unsupervised machine learning; however, ILD-specific applications have yet to be developed.

The primary distinction between linear and logistic regression is in their respective applications. Linear regression is used to determine continuous values that are reliant on the input data. This algorithm aims to estimate the training data best by fitting a straight line to the data. Logistic regression is used for classification, which involves assigning input data to one of two categories with a specified probability or level of confidence. Both algorithms have been utilized successfully in the medical industry to diagnose various diseases. Given the vast number of biomarkers and indications collected by medical devices and software, it can be challenging to establish meaningful connections between all these factors. A regression method can improve data interpretation and correlation if these indicators are viewed as interdependent characteristics.

5.2.2. LINEAR REGRESSION

For the identification of ILD, linear regression models are widely used. It has been demonstrated that such models can incorporate multiple features (some of which are directly measured through lung function testing, while others are calculated or observed through medical imaging), including pulmonary artery (PA) diameter, mean pulmonary arterial pressure (mPAP), HRCT-determined ILD severity, forced vital capacity (FVC), transfer factor of the lungs for carbon monoxide (TLCO), age, sex, and body surface area (BSA). By utilizing these algorithms, parameters such as PA diameter have been shown to play a significant part in the diagnostic process, revealing a novel association with ILD (206,207).

5.2.3. LOGISTIC REGRESSION

On the other hand, logistic regression models can be used to predict the chance that certain factors influence disease. In the case of elderly pneumonia patients, for example, factors such as mean age, pulmonary severity index, concomitant disorders (diabetes mellitus, high blood pressure), and QTc interval prolongation could be used to predict the chance of mortality (208).

These regression algorithms are often utilized with medical imaging techniques, resulting in a more precise diagnosis. (209,210). Also, techniques for estimating the risk of breast cancer have been created using mammography, artificial neural networks, and logistic regression.

Another regression algorithm, random forest, was used to concentrate on pulmonary regions from distinct topographic regions by analyzing and simultaneously extracting data from the three sections (upper, medial, and lower), thereby significantly increasing the probability of correct detection of ILD lesions (211).

5.2.4. HIDDEN MARKOV MODELS

Hidden Markov Models are frequently employed in the decision-making process, predicated on the premise that a patient is in one of a finite number of health states at any time. These states are referred to as Markov states.

K-means clustering, hierarchical clustering, and hidden Markov model algorithms have been used frequently in evaluating disease progression, including Chronic Obstructive Pulmonary Disease (COPD), Interstitial Lung Disease (ILD), tuberculosis surveillance, Huntington's disease, and Diabetes Mellitus. (212–214).

5.2.5. NEURAL NETWORKS

Neural networks are algorithms that attempt to replicate human neuron's function by developing a complicated architecture that begins with an image as input and divides it into numerous layers (convolutional, fully connected) arranged in a particular sequence. These methods have been utilized successfully for lung nodule detection and classification (182,183), tuberculosis lesion classification (184), lesion detection (185), and parenchymal pulmonary disease classification (153).

Typical ILD patterns readily obtain a classification accuracy of 85.5% (188), whereas other methods, such as (202), attain near-perfect accuracy in particular circumstances.

The number of HRCT-specific applications is restricted, e.g., (154,215) and, despite enhancements, alternative implementations, e.g., (161,170), provide significantly superior performance.

The most challenging aspect of ILD neural networks is not the algorithm but rather the training set (161,170). Large, well-balanced HRCT imaging datasets reveal lesions that would otherwise go unnoticed, but they are not publicly available and are insufficiently extensive (153,154).

5.2.6. COMPLEX NETWORKS

The human capacity to monitor the volume of all available data begins to lag. No single researcher can be entirely up to date, and they cannot manually analyze the accuracy and authenticity of information because each research center pursues its investigations, develops its data, and, as a result, its findings. This necessitates big storage media and rapid processing power (205).

Information stored in a specified data format is one of the medical domains in which software could be helpful. Even though standard concepts have a few common medical representation formats (216), meta-data and informal information are always kept in a human language unique to each institute or researcher. Each entity is allowed to use the format that best suits its purposes.

On the other hand, whenever one wishes to begin modeling data based on existing medical databases, the researcher must typically 'cure' the data or submit it to a 'harmonization' process that either restructures the data or removes the unnecessary details that could slow down any subsequent data analysis (217).

Processing power is another method of medical science using IT tools. Given the massive quantity of available data, modeling it would require significant time without assistance. This is where processing power could intervene in several areas, such as modeling data according to data type-

specific models (218), producing prediction algorithms based on statistics and probabilities (219), and programmatically investigating various scenarios based on data confidence level, etc.

There have been various ways regarding data modeling and visual display. Visualizing and interpreting healthcare data employing complex networks has been increasingly popular (239). This is an alternative technique to the all-too-familiar bar charts, graphs, pie charts, and squares schemas, and the reason for this is that this style of representation offers several additional characteristics (220,221).

Due to the nature of data, a couple of crucial intrinsic traits make network science an excellent tool for medical research: interconnectivity and link dynamics.

Not only are the relationships between data entities static, but they also indicate transformation relationships or, more precisely, they convey the effect that nodes exert over one another. A hospital's patient flow is an example of data that could be represented as a complex network. Metabolic processes and elements are potentially viable for network representation data source usage.

The more information a graph represents, the more a viewer can comprehend at a glance instead of verifying many spreadsheets or examining simple figures or statistics.

A vast selection of network visualization tools and techniques regarding data representation are available. Bioinformatics' most popular visualization tools include Gephi, Cytoscape, NetworkX (Python library), iGraph (R and Python), and Pajek. In addition to providing a network visual representation, these programs also implement various visualization techniques from which the user can select: Force Atlas 2, Fruchterman-Reingold, Kamada Kawai, OpenOrd, Circular layout, etc. (73),(74). This multiplicity of possibilities ultimately results in distinct perceptions of the same network. This means that the user does not have to worry about organizing components on a blank canvas but instead utilizes pre-programmed algorithms for this purpose and then watches the finished product to better understand the data.

Depending on their primary purpose, network visualization tools fall into two groups. The first group of tools comprises those with a visually appealing user interface and an intuitive mode of use. This consists of Gephi, Pajek, and Cytoscape. The second group emphasizes efficiency and rapid delivery of results through a scalable design. This first group demands higher technical expertise from the end user, who may need specialized support to fully harness these technologies' benefits. This is the cost of speed-oriented and highly customized network visualization tools such as NetworkX and iGraph, which lack a visual interface.

5.2.7. LAYOUT ALGORITHM SELECTION

There are several network visualization techniques, depending on the necessity and the intended output: force-directed algorithms, circular layout, arc layout, and an adjacency matrix. However, not all are suitable for all medical data types and sizes. Matrix layout is almost too mathematical and abstract to perceive interactions clearly. In contrast, arc layout and simple circular layout become too congested for massive networks. Force-directed layouts are adaptable, scalable, and, most importantly, functional from a medical standpoint. However, some ordering between nodes is lacking in this scenario, so the user can quickly determine the node rankings or hierarchy visually (148).

We can consider the following four factors while determining the optimal network layout:

- The network's characteristics - the available data attributes
- The desired features to emphasize - what the user hopes to achieve by employing a specific layout.
- The layout algorithm's specifications, or what the algorithm claims to perform most effectively.
- Previous research or performance evaluations.

Fortunately, medical data possesses a variety of network features and data properties. If we take a metabolic network comprised of genes and proteins, it is safe to state that most of these networks are dense; they contain many edges and nodes. Node size (which may be proportionate to its degree or the number of connections), node color (which may reflect a certain cluster or function/role it performs within the network), edge width, and others may all be used in such a network to highlight the relevance of each piece.

Depending on the researcher's demands, the desired output may be a perfect clustering – to delimit groups of nodes with a high degree of similarity, the delimitation of odd nodes, or the discovery of patterns that would otherwise be undetectable without an appropriate visual representation (Fig.19).

While the first two aspects rely solely on the user's judgment, the third and fourth aspects – algorithm specifications and review documentation – are based on available documentation provided by their creators, as well as the experience of others (user feedback) who have tried, tested, reviewed, and shared their results with the community.

There are several studies on the performance and effectiveness of visualization tools and layout algorithms, and the data sets, which frequently include medical data, are diverse (241).

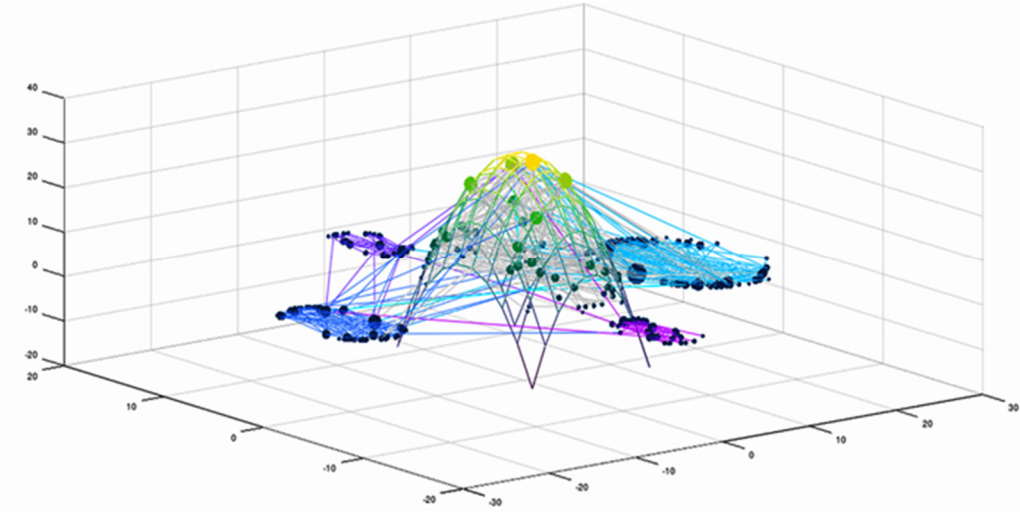


Fig. 19 Bio Diseases network rendered with a hybrid layout algorithm

In fact, layout selection is a trial-and-error process in which experimenting with layouts may provide extraordinary outcomes based on the network's characteristics. Cluster separation, node spacing or proximity, varied node colors and sizes, and edge length and weight are all visual cues that show and emphasize the connectedness between network nodes (Fig. 20).

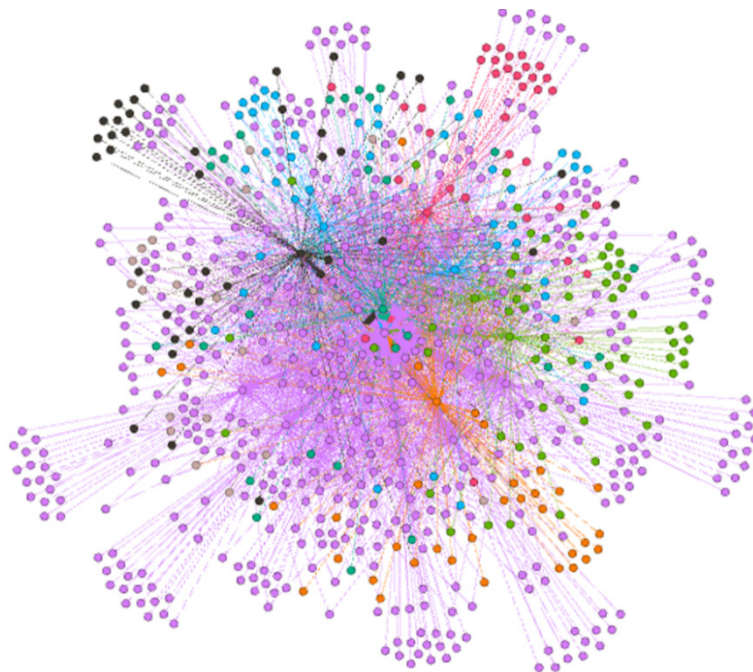


Fig. 20 DNA network of genes with respiratory function – Force Atlas 2 layout

Beyond the characteristics of each layout, the discussion focuses on the effectiveness and speed of these algorithms. Given the amount of data that must be processed and shown, case studies have demonstrated that some of them cannot handle such a workload beyond a certain magnitude and volume. It may take hours to build a proper layout if the user does not possess the necessary processing capacity for such activities; alternatively, the application may crash before completing the rendering process. Metabolic networks, such as genetic pathways, are examples of dense networks with many nodes and edges.

There is an apparent distinction between them, and choosing user-friendly technologies is costly.

Although there have been studies on the performance of such tools (222,223), from a performance standpoint, there does not appear to be a clear preference for a particular algorithm among medical professionals; in fact, some studies do not even mention the type of algorithm used to generate one specific network. At best, it may describe the clustering algorithm employed for community detection.

Once a viable visualization algorithm has been identified, the researcher does not devote further effort to a comparative investigation of numerous similar tools but focuses on achieving the best possible outcome with the chosen method (Fig. 21).

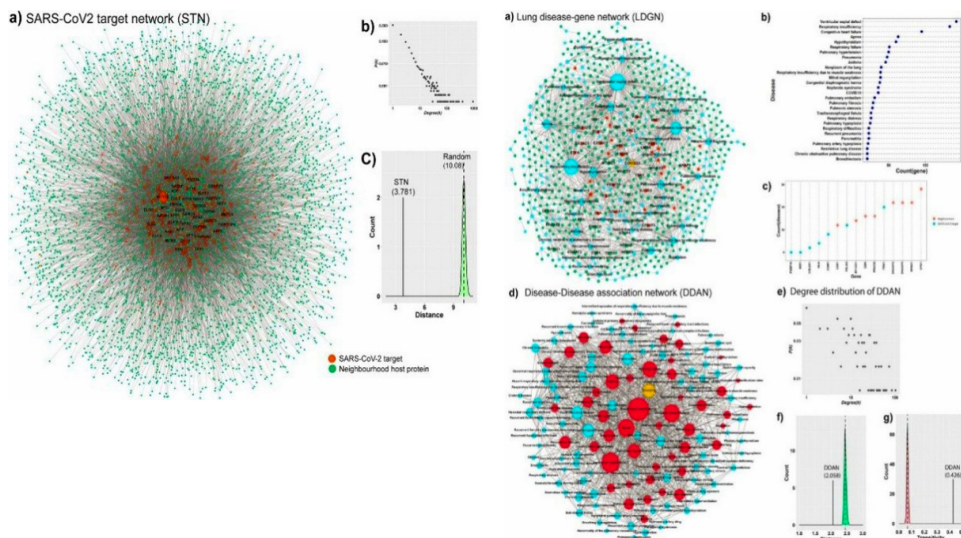


Fig. 21 Using multiple layout algorithms throughout the identical research material – reproduced with permission from (243)

Recent studies on the COVID-19 disease demonstrate that researchers may also employ numerous methods (and algorithms) to provide multiple perspectives for the same network. However, the emphasis is always on medical gain (224). The significance and utility of the infrastructure employed to produce the results cannot be quantified, and as a result, the knowledge and experience are not communicated to the consumers of such studies.

The computer can provide two forms of assistance: a second viewpoint and the visualization and aggregation of data. When choosing an aid, one must select the objective: learning, discovery, or reasoning, and the means of doing this: various predictive analytics or visualization techniques.

6. CHAPTER 2: A NOVEL METHOD FOR LUNG IMAGE PROCESSING USING COMPLEX NETWORKS

6.1. INTRODUCTION

Commonly, pathological problems of the lung interstitium begin with an overly severe inflammatory process that limits alveolus expansion. Over time, the inflammatory strain is replaced by permanent stiffness caused by scar tissue, which in turn generates additional inflammation, resulting in deteriorating clinical consequences. This interstitial lung inflammation and fibrosis cycle is the unifying characteristic of the Diffuse Interstitial Lung Diseases (ILD) group (225).

Historically, this diverse group of more than 200 separate illnesses that damage the lung parenchyma has encountered recurrent difficulties regarding nomenclature, categorization, and staging (2). Due to having the same pathological conditions, the clinical and, to a lesser extent, paraclinical criteria employed in ILD diagnosis tend to overlap; nonetheless, unique disease sources must be distinguished in order to effectively prescribe a treatment plan. There is no better example in this case than Idiopathic Pulmonary Fibrosis (IPF), which has a median survival rate of 2-5 years but whose clinical diagnosis is easily confused with the much more common Chronic Obstructive Pulmonary Disease (COPD), which has a much better prognosis (mild cases have a survival rate of 10-20 years) (226).

The progressive feature of ILD provides the difficulty of an early and precise diagnosis, which nearly doubles the survival rate and enhances life quality when the appropriate therapy is administered (124). As previously stated, clinical signs and symptoms overlap; paraclinical approaches are essential for diagnosing ILD. The commonly used investigations, such as chest X-ray (CXR), peripheral blood tests, and spirometry, must be supplemented with more specialized imagistic tools, such as High-Resolution Computed Tomography (HRCT), lung ultrasound, and, in some cases, bronchoscopy and surgical lung biopsy (126,158).

Since the 2011 update to the imagistic diagnostic guidelines (145), the HRCT has been the principal noninvasive device in analysis (138), providing essential information and insights that can lead to a rapid diagnosis (145). As with any diagnostic instrument, complexities may necessitate a highly skilled professional or further invasive tests. In addition, high inter-observer variation, even among experienced radiologists, complicates the procedure (87)(128,148,149). The current strategy is to enhance human HRCT

interpretation with automated techniques, such as the CALIPER software (150) or different AI-based tools. (153,154).

This study begins with a brief comparison of how computers and humans perform diagnosis. A unique approach is then introduced and evaluated from a biological and system science standpoint.

6.2. USING HRCT – HUMANS & COMPUTERS

In diagnosing ILDs, medical professionals begin with HRCT pattern recognition of a limited number of specific abnormal findings, particular combinations or patterns of these abnormalities, one or more discrete distributions of abnormal findings, and the use of basic clinical and historical information. The radiological diagnosis of ILD is based on patterns and connected to the underlying histology. Future ILD detection is planned to incorporate behavior-based radiological phenotypes, which will determine clinical care (131). A diagnosis may be made by dividing main lesion types into four categories: reticular pattern, nodular pattern, high attenuation, and low attenuation. Their overlap and relationship with other lesions (51) (Figure 23) and their location throughout the lung and in the lung's fundamental anatomical and functional unit - the secondary lobule - are significant.

Thin-section CT, inspiratory, expiratory, and prone sequences are the most sensitive radiologic examination for detecting ILD in the lung parenchyma. The interstitium and secondary pulmonary lobule (SPL) are the primary anatomic components of the lung parenchyma, as evaluated in IPF (66). As a result, histological phenotypes and lesion types (primary lesions and/or their overlapping model) and their lung and SPL distribution may compete and collaborate to reflect an accurate clinical condition. For instance, Usual Interstitial Pneumonia (UIP) is the prototypical progressive fibrotic phenotype; self-sustaining progressive fibrosis is also observed in individuals with progressive Non-Specific Interstitial pneumonia (NSIP) or chronic hypersensitivity pneumonitis (PHc).

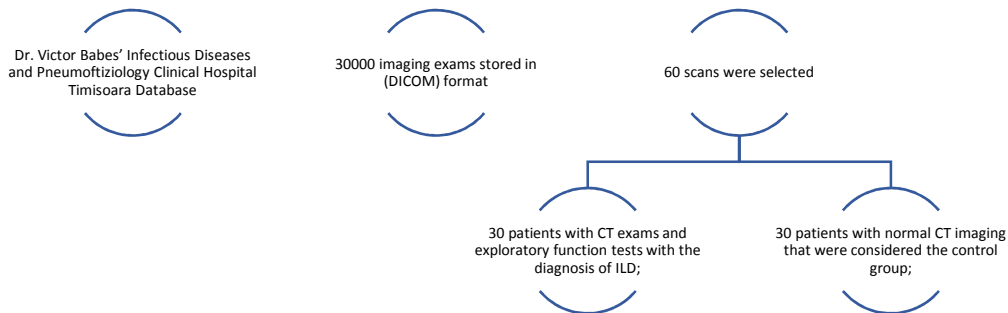
Compared to Computer Aided Diagnosis (CAD), this (human) method is radically different. Most computer-aided design (CAD) systems employ heuristics and machine learning without an analytical process, focusing on appropriate categorization rather than underlying causes. This method, used in (153,154), does not allow for any evaluation of severity or forward-movingness. Commercial and scientific programs that take a more anatomy-based approach (228–230) may require additional input data, such as Pulmonary Function Tests (PFT) (e.g., a caliper). Their output solely reflects the aberrant volume. No

qualification is provided on the severity of the lesion in this publication. Among the benefits of employing such technologies are relatively quick processing times, confirmed findings, good, reproducible accuracy, and the ability to help medical workers effectively.

The HRCT slices contain non-visual apparent information encoded as Hounsfield Units (HU) that can improve the relationship between gradient and textural differences between pixels. The geometric interweaving of varied densities creates textures. In light of the fact that texture recognition has a very high degree of accuracy when a complex network approach is used (146,146,147), this article aims to construct a complex network strategy tailored for ILD.

6.3. MATERIALS AND METHODS

6.3.1. LOT SELECTION



To select the eligible patients, we accessed the 'Dr. Victor Babes' Infectious Diseases and Pneumoftiziology Clinical Hospital Timisoara database was recorded in their private cloud repository. Digital Imaging and Communications in Medicine (DICOM) format was used to store more than 300,000 imaging exams, from which 60 scans were chosen based on the inclusion criteria listed below: 30 patients with CT exams and exploratory function tests for the diagnosis of ILD (diffuse interstitial lung disease); 30 patients with normal CT imaging who served as the control group; all participants gave written approval for the use of their HRCT images. The Ethical Committee also authorized the study.

6.3.2. IMAGING PARAMETERS

General Electrics (GE) Healthcare Optima 520 16-slices with 32-slice reconstruction were used for all examinations. The scanner comprises a 0.5 mm x 16 detector-row, allowing for a total z-axis length of 8 mm. Variable tissue penetration resulted in variations in the radiation dose administered to every patient, whose settings remained constant.

The following HRCT parameters are shown in Fig. 22:

Slice thickness: 1,25mm
Scan time: 1 second
kv: 120
mAs: 130
Collimation: 2,5mm
Matrix size: 768X768
Field of View (FOV): 35 cm
High spatial frequency reconstruction algorithm
Patient position: supine (typically) or prone;
Window: lung window (if ILD is suspected)

Fig. 22 HRCT parameters

The slice is smaller than the 1.5mm advised by the Radiology Working Group of the Pulmonary Fibrosis Foundation to improve lesion detection and increase diagnostic accuracy, both of which are critical for ILD diagnosis. The spatial resolution (pixel spacing) for these settings is 0.74 mm.

The HRCTs were stored in the DICOM format because it is the universal format for encrypted medical imaging with a high transmission capacity. The DICOM technique encodes the patient's personal information, CT data, technical parameters, and medical images, making them difficult to interpret without a specialized application. The primary criterion for analyzing image data was the tissue densities/opacities, which were computed by adopting the principles of the Hounsfield scale. Hounsfield Units (HU) are widely used to quantitatively measure radio density and tissue tensile strength and aid in interpreting CT scans.

Image reconstruction depends on tissue parameters relating to X-ray beam penetration and attenuation to establish a grayscale picture system. According to the attenuation range of tissue absorption, these grayscale intervals span from roughly -1000 HU (air) to 3000 HU (metals such as silver and steel). This transition is represented by grayscale and uses the zero HU density of purified water as a reference point.

Table 6. HU intervals from Lin Li et al. and Maria Paola Belfiore et al. reports

These values are specific for the General Electrics Healthcare Optima 520(9,10,11).

Pulmonary zones	HU intervals
Emphysema	[-1024, -977)
Normal pulmonary parenchyma	[-977, -703)
Ground-glass opacities	[-703, -368)
Others (crazy-paving, pleural fat)	[-368, -100)
Consolidations	[-100, 5)
Others (interstitial vessels)	>5 HU

According to the HU intervals depicted in Table 6, each element of this lesion will have a corresponding value. The honeycombing pattern is a combination of cysts (emphysema) and reticulations (consolidations); the network of reticular fibers is a consolidation analog, as ground-glass opacities are already shown in the table.

The intervals representing emphysema, normal pulmonary parenchyma, ground-glass opacities, and consolidations were chosen for the analyzed diseases.

6.3.3. IMAGE LOT SELECTION

For each HRCT lot, a 65x65 pixel region was manually selected from one of the HRCT slices. The explanation for selecting these regions manually rather than processing the complete image at once is based on the concept of isolating and evaluating the most relevant samples for the selected diseases. After discovering certain trends, applying the findings on a bigger scale would be sensible.

To eliminate intra- and inter-observer variability, the most pertinent area for diagnosis was determined by a majority intersection of selections made by four independent observers: two radiologists (ten + and five years thoracic experience) and two pneumologists (15+ and 5+ years ILD experience), since at least three specialists from the National Fibrosis Center of the 'Dr. Victor Babes' Infectious Diseases and Pneumoftiziologie Clinical Hospital Timisoara had already annotated the photos for the ILD-affected batch; these picks offer an additional diagnosis confirmation.

A combination of factors determined the size of this sample area:

1. The more pixels a sample includes, the more processing power is necessary to convert it into a matrix and a complicated network. This also affects the processing time, ranging between seconds and minutes.

2. This region should be vast enough to capture significant lung tissue for the diagnosis but small enough to avoid any other forms of tissue that might "contaminate" the sample or add unneeded complication.

3. The selected square region must include at least one functioning component of the lung (secondary pulmonary lobule) in its whole and any form of the disease it may be affected with. Given that the area of a secondary lobule ranges between 1 cm^2 and 2.5 cm^2 and that the pixel spacing within the selected HRCTs varies between 0.70 and 0.80 (this setting is machine-dependent and is encoded in the HRCT metadata), a sample rectangle of 65×65 pixels should typically contain at least one secondary lobule. Example: The actual pixel spacing value for the lot is $PS = 0.74 \text{ mm}$, which is obtained as a DICOM parameter. Given that the area of a secondary lobule is $2.5 \text{ cm}^2 \times 2.5 \text{ cm}^2$, the minimum acceptable DICOM sample size for a secondary lobule is $25 / 0.74 = 33.7837 \text{ mm}$. The sample area is nearly doubled to obtain at least one secondary lobule in its entirety. Similar investigations with a cropped DICOM sample of only $11 \times 11 \text{ px}$ have been conducted by other researchers; however, it is unclear why this number was selected (259,263).

6.3.4. IMAGE PROCESSING METHOD

Each selected sample is subsequently processed with the aid of a Python program designed for this specific purpose. The DICOM slices are cropped to the predetermined size ($65 \times 65 \text{ px}$) using a dedicated CT library, pydicom, around the area of interest.

The program is an algorithm designed to carry out the following operations:

1. Iterate across HRCT slice sets (DICOM files);
2. Crop each image to a 65 by 65-pixel square;
3. Analyze the specified topic from three perspectives:
 - a. Convert pixel gradient to Hounsfield Unit value using the following formula: $HU_v = \text{rescaleSlope} * PxGradient + \text{rescaleIntercept}$, where rescale Slope and rescaleIntercept are constant values dependent on the CT equipment and embedded within the DICOM metadata, and PxGradient is the color code of a pixel.
 - b. Separate all emphysema-like tissue, GGO (Ground Glass Opacity), and consolidation densities in the cropped picture while excluding all other tissue types (Figure 22);
 - c. Separate each HU strip from the sample onto its layer (Figure 22);
4. Create complex networks from each layer;
5. Analyze connection, proximity, and node distribution (pixels);
6. Determine patterns of healthy and diseased lungs;

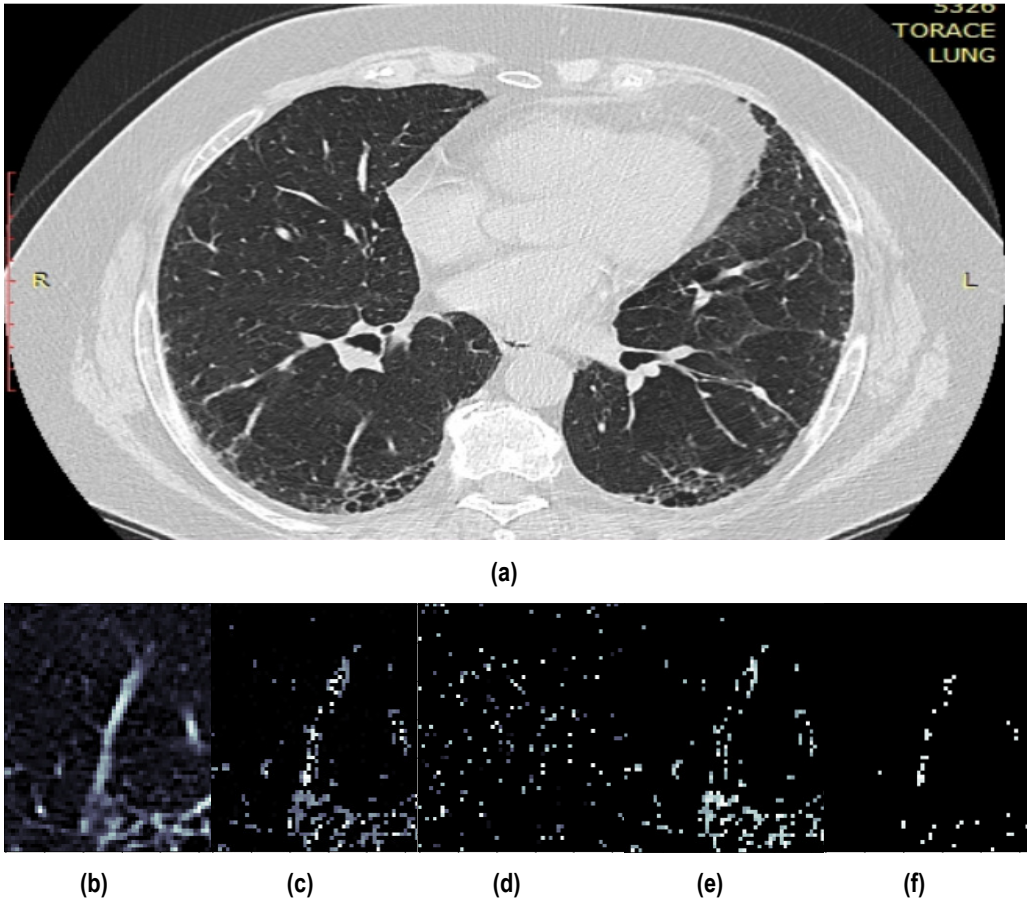


Fig. 23 Splitting CT sample into layers (a) original CT, (b) sample crop, (c) combined Emphysema, GGO, Consolidation layers, (d) Emphysema Layer, (e) GGO layer, (f) Consolidation layer.

Assume the following in order to change each of the crop layers (emphysema tissue, GGO tissue, and consolidation) into complex networks (Step 4):

1. Each pixel represents a network node whose color gradient determines its value.
2. It is assumed that two pixels are linked if the following requirements are met:
 - Within the crop, the radial distance (R_d) between them is $R_d \leq 4$ pixels. Assuming each pixel (P_x) is the origin O of a circle with radius $r = 4$, every other pixel (P_y) within the circle region may be considered linked. Alternatively stated: $E(P_x, P_y) \leq d(P_x, P_y) \leq 4$.
 - The difference between P_x and P_y 's gradient is less than or equal to 50

Given the abovementioned requirements, the algorithm constructs groups of nodes and connecting edges and exports them as different files for each layer. Thus, each lung HU layer is transformed into a complex network and evaluated from the perspective of degree distribution.

Paragraphs 6.3.4.1 and 6.3.4.2 expand on the selection methods for threshold values.

6.3.4.1. Radial distance selection

In order to identify the radial distance at which lesions are single or linked, several tests have been conducted with values ranging from $1 \leq Rd \leq 8$ pixels. Less than three pixels resulted in a sparse network with relatively few connections, indicating that a tiny number of comparable pixels were found in close proximity to one another. This results in a comparatively high number of clusters with less than three nodes. Compared to other Rd values, it does not offer much information on the lung profile.

Alternatively, with Rd values more than 5, while the algorithm is more integrative, it becomes excessively liberal owing to the complicated network process of node attachment, which links comparable nodes without anatomical justification.

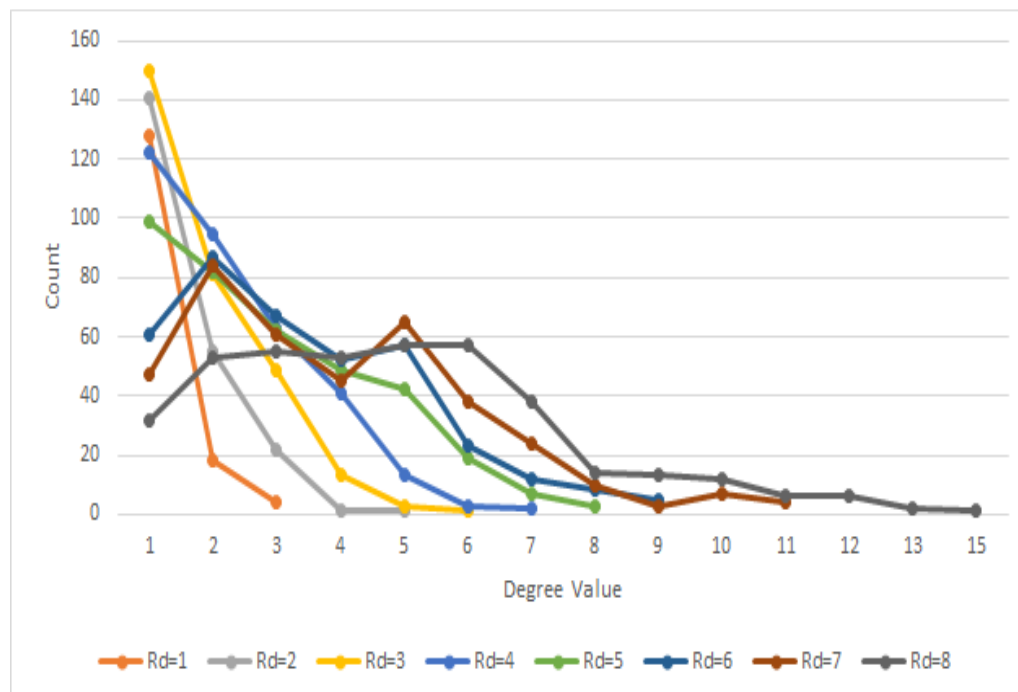


Fig. 24 Degree distributions for various Rd

Defining a circle with a radius between 5 and 8 ($5 < r < 8$) enables a better-linked network, fewer clusters, and a distinct degree distribution (Figure 24).

In light of the previous experiment, it has been determined through multiple trials that the optimal R_d value is $R_d = 4$ pixels, which is large enough to generate dense clusters but small enough to make a difference in the degree distribution, particularly when comparing normal lungs with affected lungs. This is supported by (264), which employs a starting size range of 3–17 mm for detectable lesions in a clinical environment. The observed empirical conclusion accords with their findings because an $R_d = 4$ pixels equals a metric value of $4 \cdot 0.74 = 2.96$ mm. Section 6.3.4.t pertains to model fit in the context of network science; there is more discussion of the distribution fit using a logarithmic or power function.

6.3.4.2. Gradient difference threshold

Regarding gradient difference, the selected delta decides whether two pixels are close enough in grayscale to be considered neighbors. While a delta D value of 50 encompasses the entirety of the Emphysema strip, it assists in clustering the network for the GGO and Condensation strips. This rule is summarized as follows:

$$|G(P_x) - G(P_y)| \leq D,$$

Where $G(P_x)$ and $G(P_y)$ are the gradient values of two pixels, P_x and P_y , respectively, and $D = 50$ is the maximum delta threshold at which two pixels are not considered connected.

Each network layer can ultimately be defined as $N(P, E)$ where $E = \{E(P_x, P_y) | d(P_x, P_y) \leq R_d \text{ and } |G(P_x) - G(P_y)| \leq D\}$, where P is the collection of vertices or pixels, E is the set of edges, $R_d = 4$, and $D = 50$.

6.4. RESULTS

All HRCTs (of both healthy and diseased lungs) were processed using the previous procedure. Subsection 6.4.1 demonstrates the different stages for a single normal and ILD-affected patient (Figure 25), whereas subsection 6.4.2 describes an additional lot analysis.

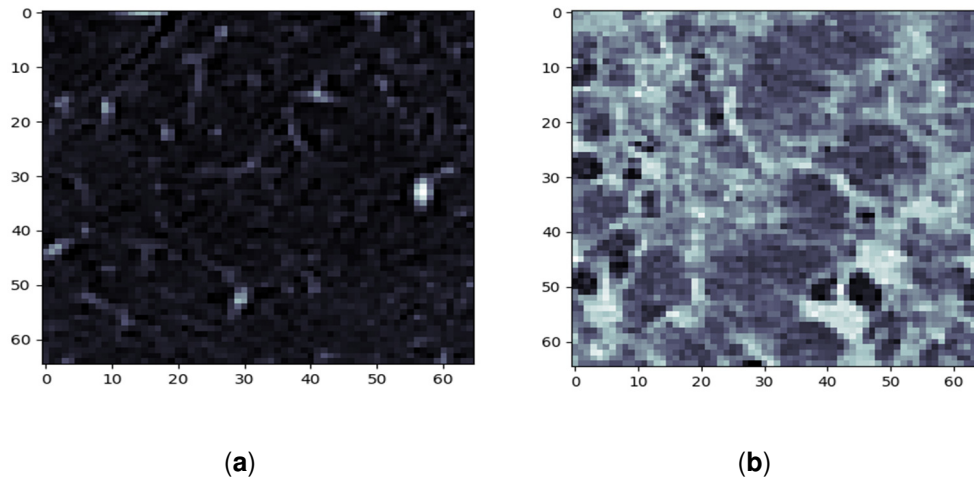
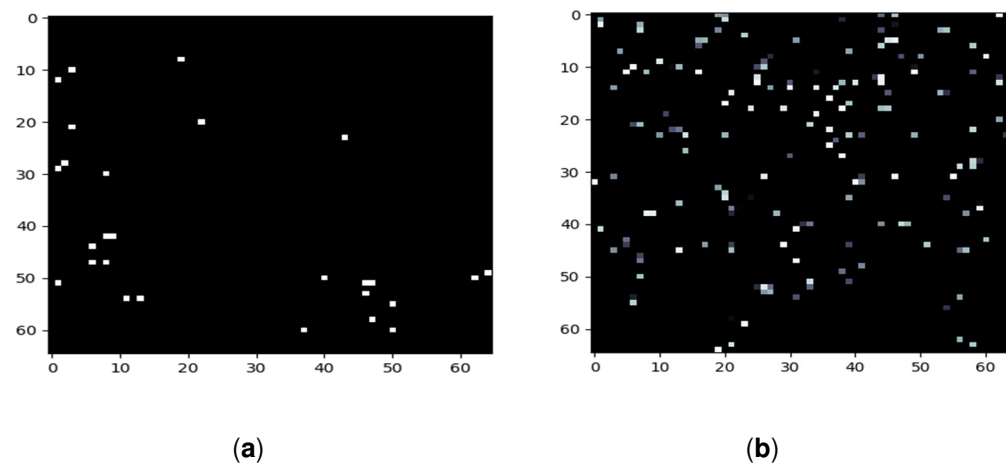


Fig. 25 Algorithm processing -step 1- sample selection (a) Normal sample (b) ILD (IFP) sample

6.4.1. NORMAL AND ILD CASE SAMPLE RESULTS

Sample cropping to 65×65 pixels is the initial stage.

The subsequent phases entail slicing everything into layers and transforming those layers into intricate networks. The emphysema layer is inspected initially (Fig 26).



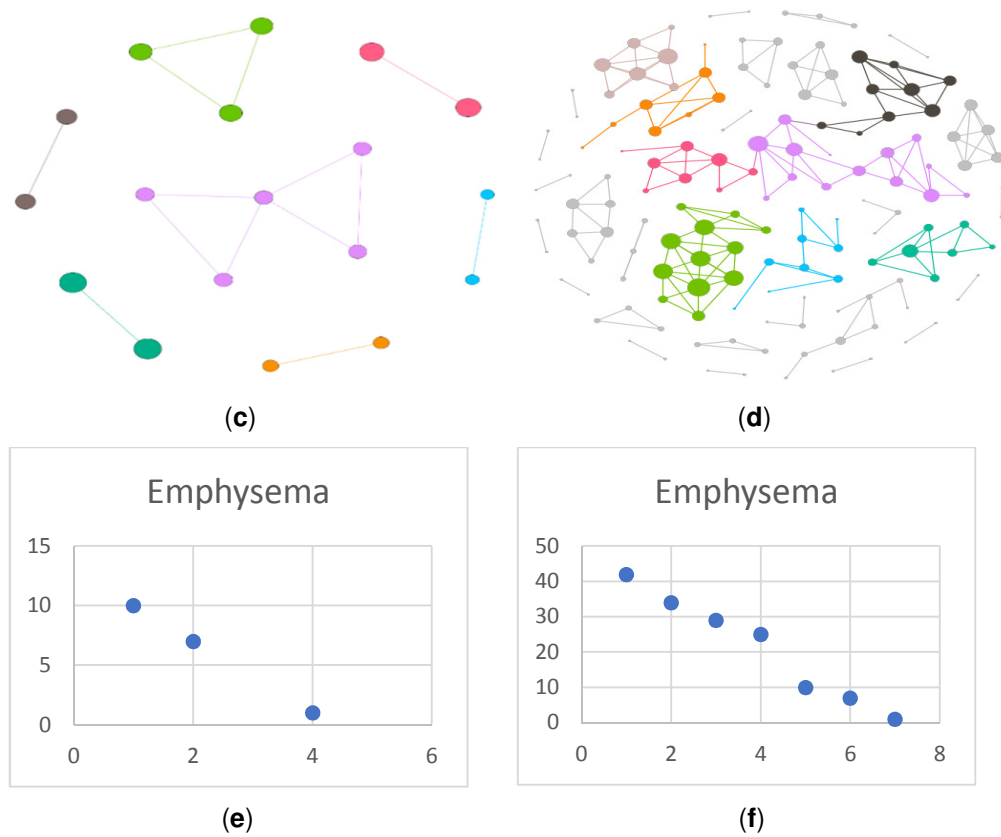


Fig. 26 Emphysema processing

(a) HU filtered layer for the normal sample; (b) HU filtered layer for the ILD sample
 (c) Complex network built according to the proposed algorithm corresponding to the normal sample, Fruchterman Reingold render layout, node sizes proportional to node degrees, edge width invariant (1.5 pixels). (d) The complex network was built according to the proposed ILD sample, Fruchterman Reingold renders layout, node sizes proportional to node degrees, and edge width invariant (1.5 pixels). (e) Degree distribution of the normal sample network (f) Degree distribution of the ILD sample network.

Next comes the ground glass layer, where the most significant variances occur. Visually, the distributions in Figure 27 a and b may appear random, but the network degree distribution reveals an entirely different story: a logarithmic distribution for the normal process and a polynomial distribution for the IFP.

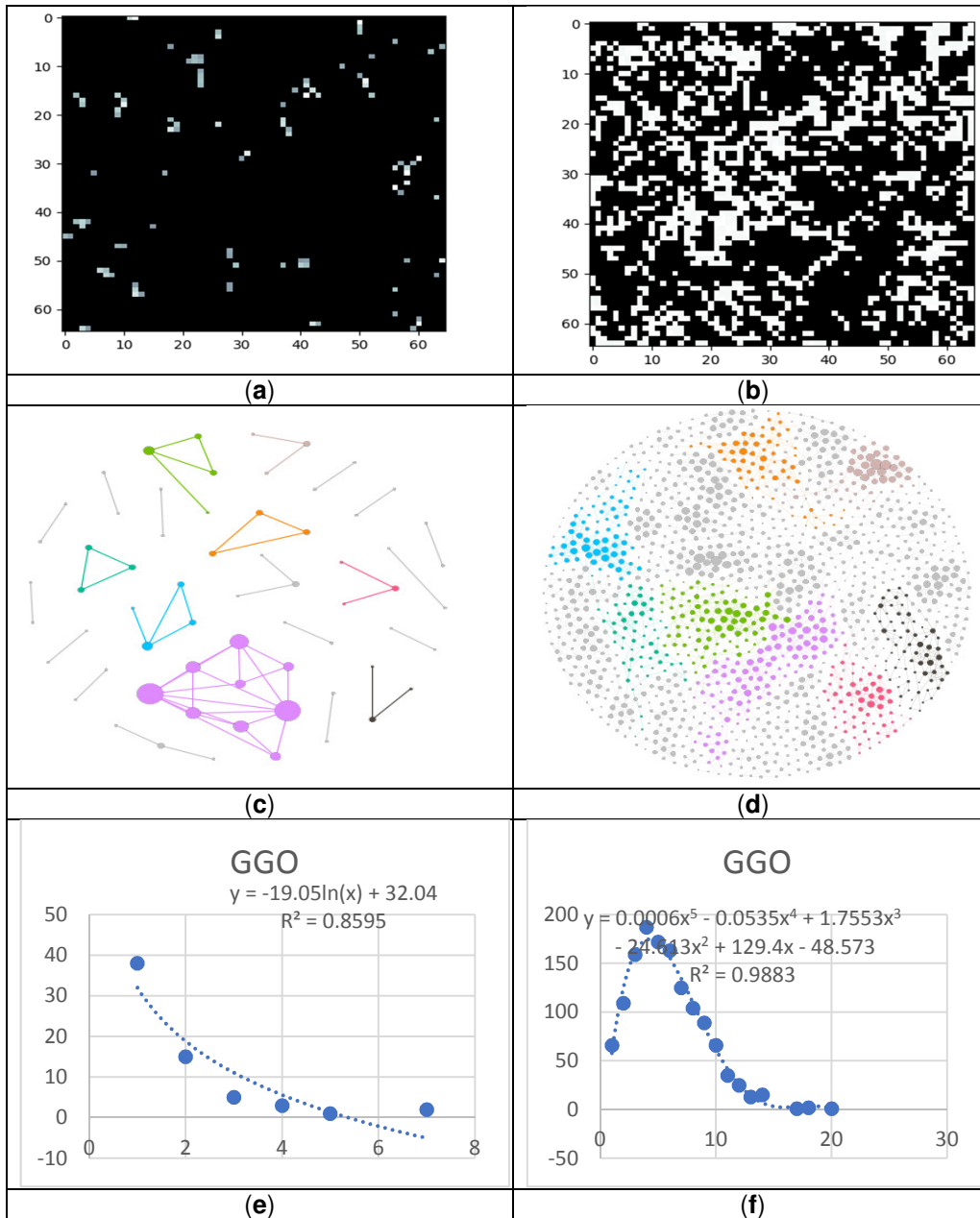


Fig. 27 GGO processing

(a) HU filtered layer for the normal sample; (b) HU filtered layer for the ILD sample; (c) Complex network built according to the proposed algorithm corresponding to the normal sample, Fruchterman Reingold render layout, node sizes proportional to node degrees, edge width invariant (1.5 pixels). (d) The complex network was built according to the proposed ILD sample, Fruchterman Reingold renders layout, node sizes proportional to node degrees, and edge width invariant (1.5 pixels). (e) Degree distribution of the normal sample network (f) Degree distribution of the ILD sample network. Equations for curve fit and R^2 are also presented on the relevant distributions.

Lastly, there is the consolidation layer shown in fig. 28.

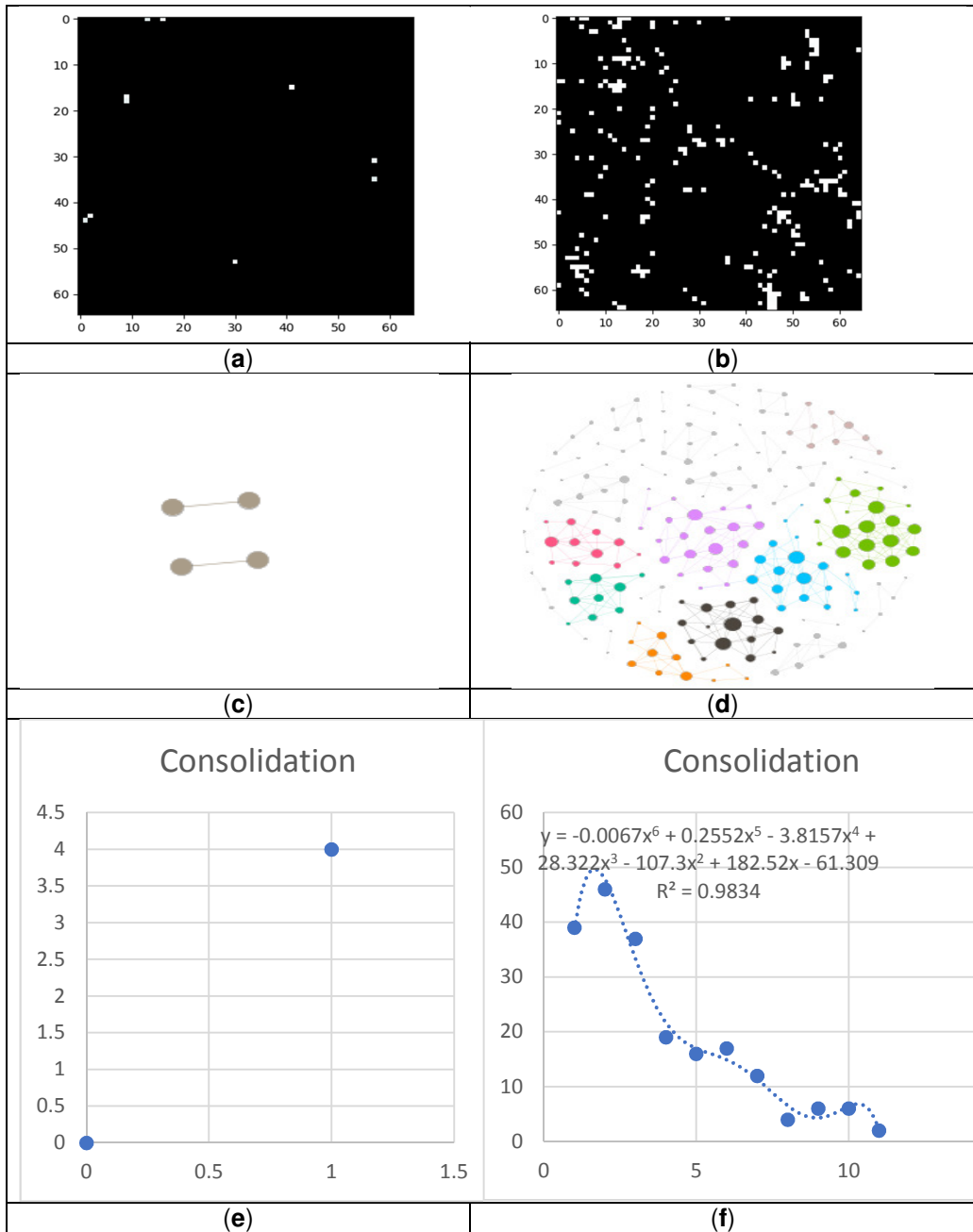


Fig. 28 Consolidation processing

(a) HU filtered layer for the normal sample; (b) HU filtered layer for the ILD sample; (c) Complex network built according to the proposed algorithm corresponding to the normal sample, Fruchterman Reingold render layout, node sizes proportional to node degrees, edge width invariant (1.5 pixels). (d) The complex network was built according to the proposed ILD sample, Fruchterman Reingold renders layout, node sizes proportional to node degrees, and edge width invariant (1.5 pixels). (e) Degree distribution of the normal sample network (f) Degree distribution of the ILD sample network. Equations for curve fit and R^2 are also presented on the relevant distributions.

6.4.2. ADDITIONAL LOT ANALYZATION-RESULTS.

Individually, variations can be rather distinct, and the analysis of the complete image lot offered the difficulty of assessing network metric importance in a larger context.

A metric based on degree sequences is typically preferred for measuring the entropy of network invariants. Adding a measurement for the network size is difficult due to the discrepancies outlined in the previous subsection.

Figure 29 displays three measures for balancing network complexity and size metrics: total count (the degree sum), average count (average degree), and maximum degree.

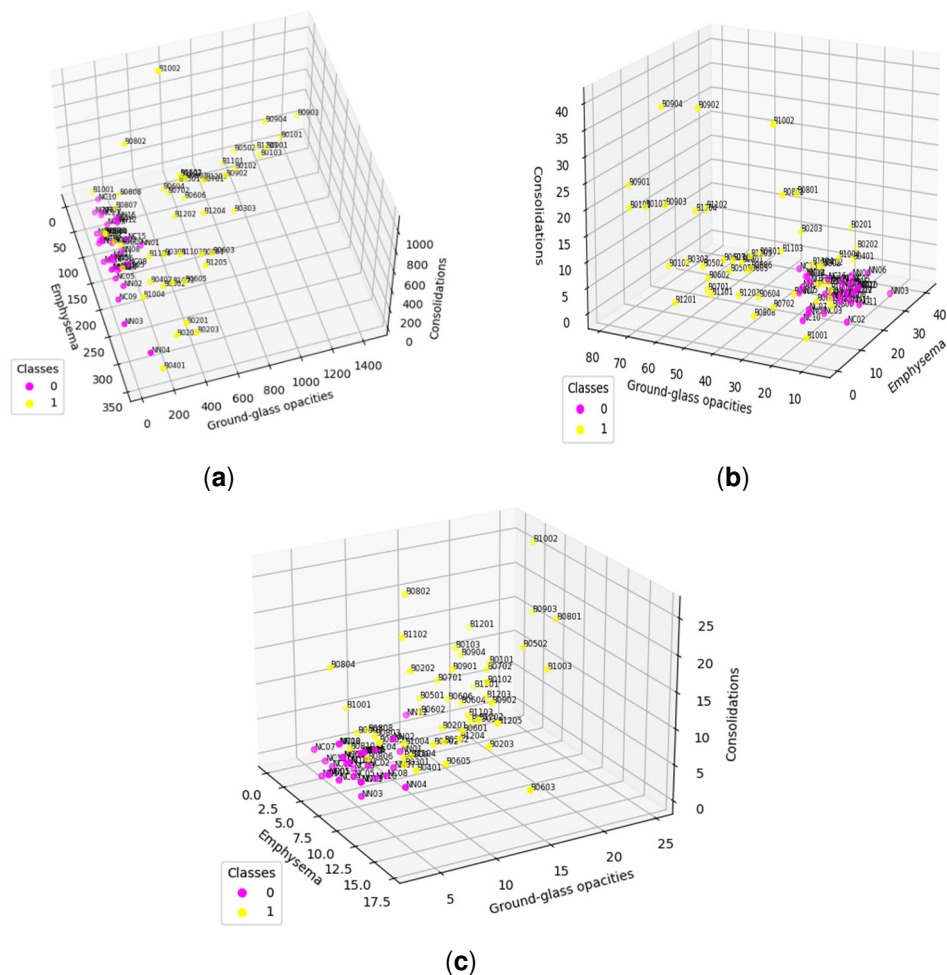


Fig. 29 Population distribution comparison according to specific complex network parameters
 (a) Total count (b) Average count (c) Maximum degree Class 0 (fuchsia) represents normal lungs, while class 0 (fuchsia) represents normal lungs, while class 1 (yellow) is formed of ILD-affected lungs.

To further examine these results, the distributions of normal and ILD patients were displayed individually, adding another data layer (Figure 30). Concerning normal patients, a distinction was made between those diagnosed before and after the covid period. As for those with ILD, particular illness groups were highlighted.

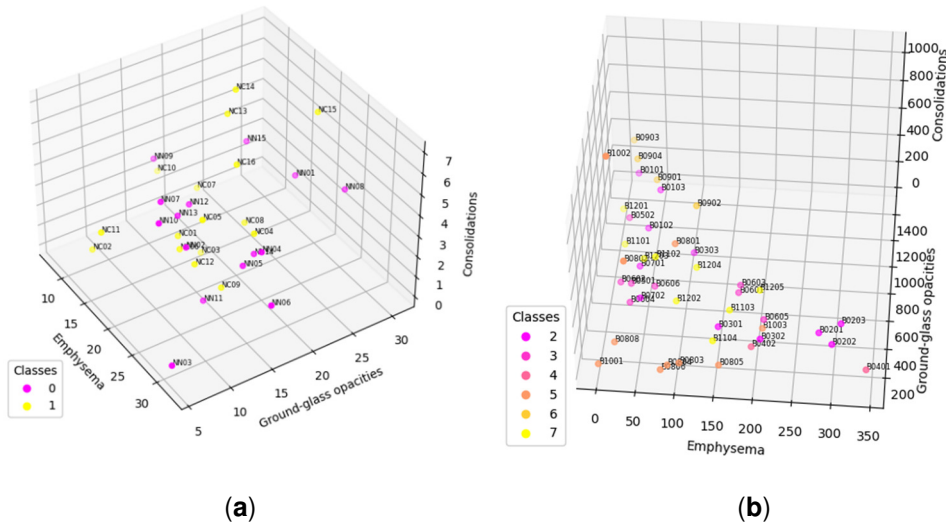


Fig. 30 Distributions of normal and ILD patients

(a) Normal population plotted based on average degree. Class 0 is the normal population investigated prior to COVID-19; class 1 is cases diagnosed as normal in the pandemic era (b) the ILD population plotted based on average degree. Class 2 is UIP, 3 probable UIP, 4 UIP, emphysema, 5 organizing pneumonia (OP), 6 hypersensitivity pneumonitis (HP), and 7 sarcoidosis.

A few outliers in an otherwise highly tight distribution will be evaluated further in the discussion section.

6.5. DISCUSSION

As mentioned at the outset of the research, the objective was to develop a complex network-based model using HRCT lung imaging. Then, an evaluation must be conducted to see how well this model corresponds to Network System Science and Medical Science frameworks.

6.5.1. NETWORK SYSTEM SCIENCE

One method to characterize network systems based on real-world data is by their degree distributions and, more specifically, by the function type that best fits these distributions. Recent studies, such as (231), demonstrate that the power and logarithmic functions characterize these systems. For normal

patients, empirical data, such as those provided in Figure 28, Figure 26e, Figure 27e, and Figure 28e, demonstrate a logarithmic distribution at the appropriate biological resolution ($Rd = 4$). Compared to the logarithmic function, the fit of the power function on all normal patients, even when the radius was varied to account for biological variances, is shallow.

Figure 31 compares the relative distances between lung structures to the different distribution fits. Mathematically accurate but biologically inaccurate because 1 and 2-pixel separation correspond to a 0.74 mm to 1.48 mm gap, which is insignificant.

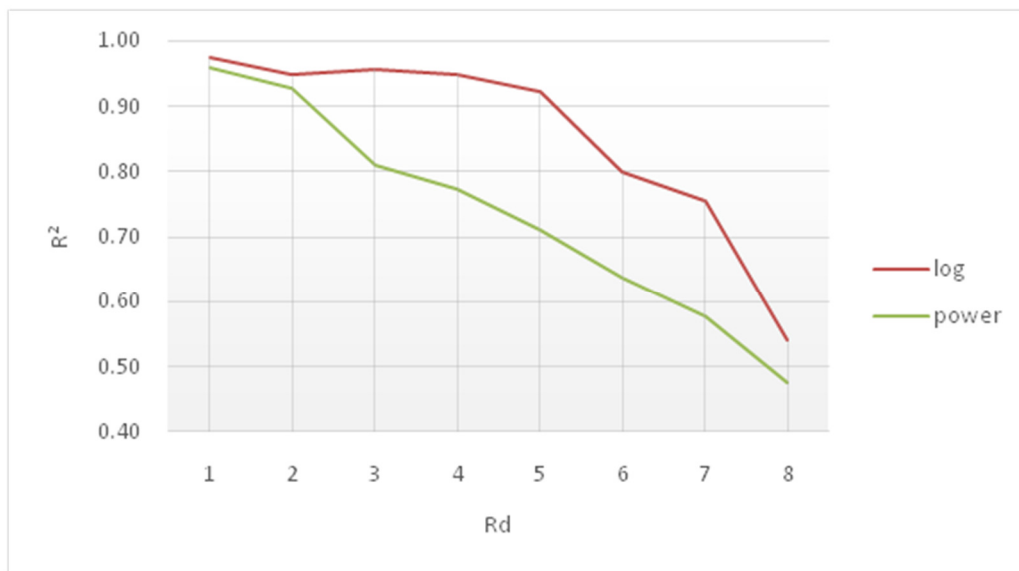


Fig. 31 Average coefficient of determination (R^2) for logarithmic and power distributions relative to radial distance (Rd).

As proposed in (232), one possible explanation for this result is that biological systems with feedback have a power distribution, whereas a logarithmic distribution characterizes those without feedback. As the lung is an open-loop system, its distribution should follow the logarithmic model, as demonstrated by our model.

As seen in Figures 30f, 31f, and 32f, the distribution of pathological lungs is better described by a polynomial function, not a logarithmic one. Literature findings indicate that proliferative processes have polynomial distributions (233,234), and as the investigated ILDs feature proliferative inflammation and fibrosis, they may be compared to the literature processes. Indeed, the origin of proliferation is not always a virus, but histopathological propagation still follows the same rules.

Depending on the type of pulmonary injury, the investigated population's degree of function can range from (138,235) for the study lot. This necessitates more investigation with sufficient data to link the degree of the polynomial function to the type or complexity of disease a patient experiences. Since lung disorders manifest as a composition of the three-axis (Emphysema, GGO (ground glass opacity), consolidation), these three components may change from case to case. Just the existence of a disease has been established, not its particular form. To be able to relate the complexity of a disease to a certain degree of a polynomial function, it is necessary to do a more in-depth investigation using many big datasets.

Figure 29 demonstrates that the discrepancies between ILD-affected and normal networks are distinct and can be measured by calculating a standard deviation for each patient data series. The data are shown in Figure 11 for all three network metrics investigated (highest degree, total count, and average degree) for each HU band, and the combined pathological HU bands demonstrate a distinct distinction between diseased and normal networks.

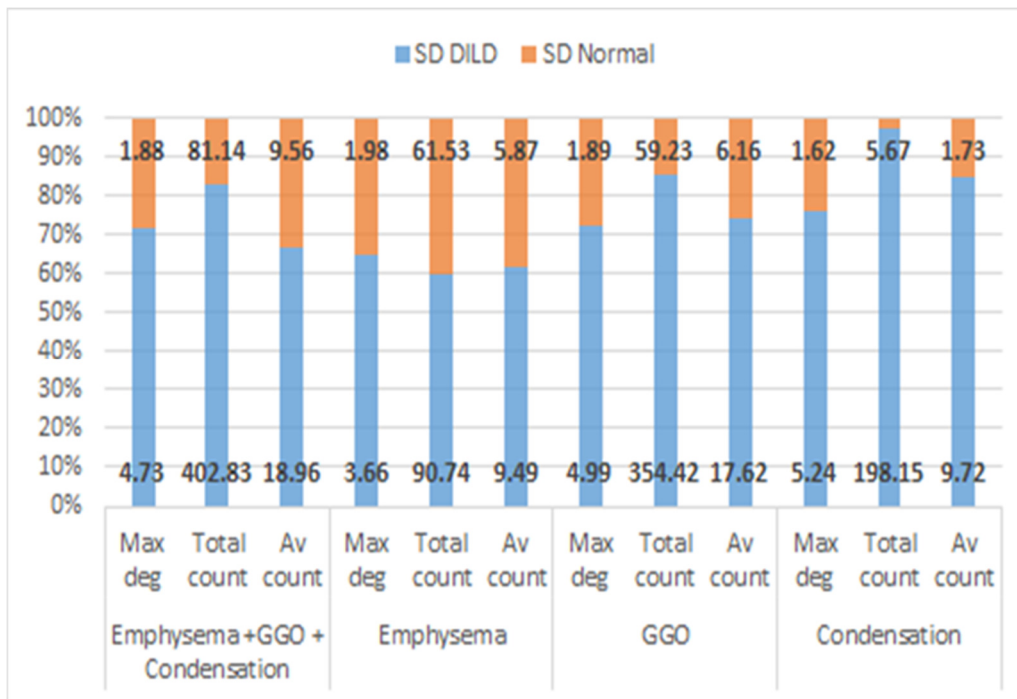


Fig. 32 Relative percentage of standard deviation for ILD vs. normal lungs on all the pathological HU bands Fig.32 shows the maximum degree, total count, and average degree. Absolute values are also given on each data point.

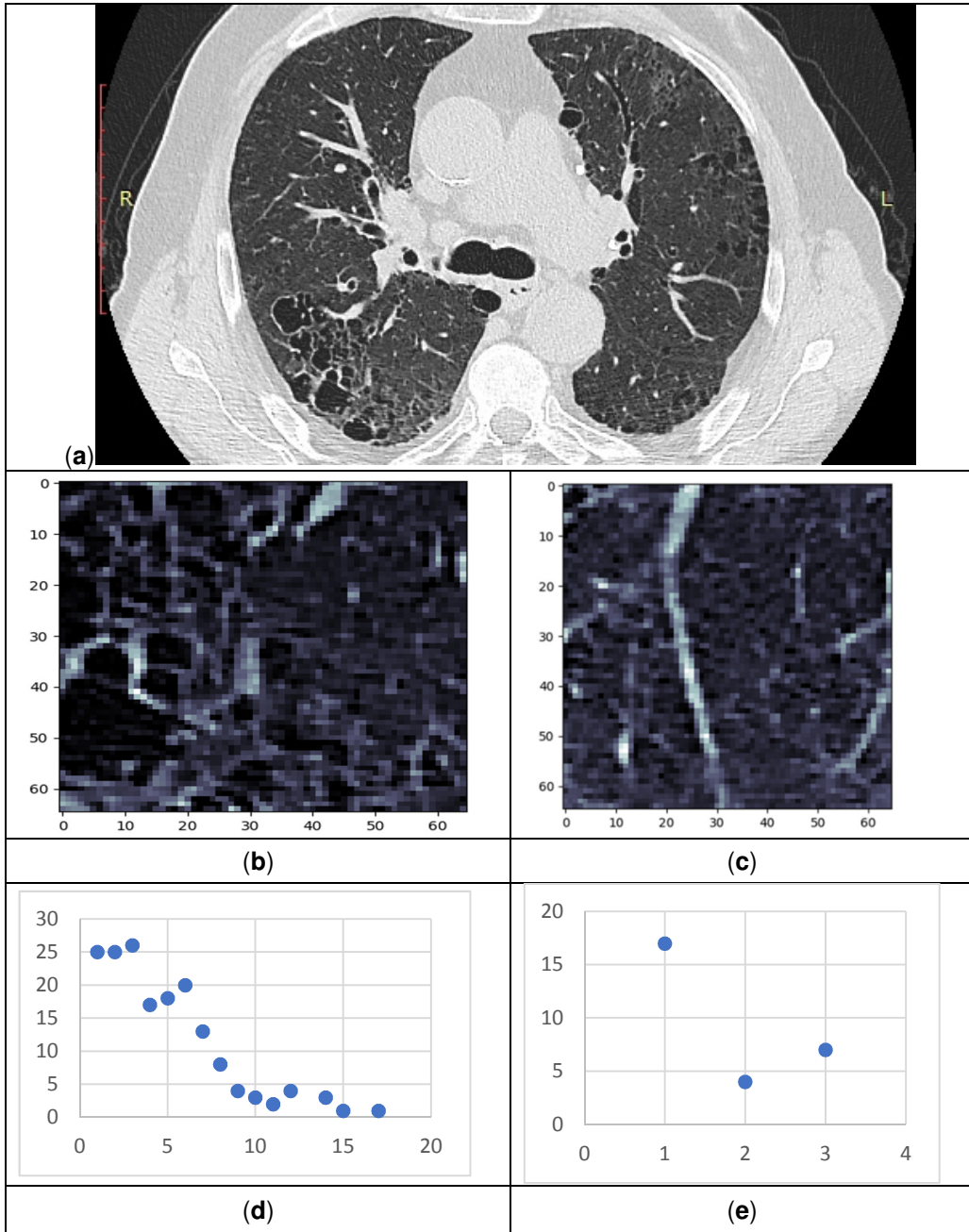
In conclusion, these results demonstrate that the established model is accurate and appropriately reflects the underlying process that determines them from a system science standpoint.

6.5.2. MEDICAL SCIENCE

To accurately mimic the biological system, the suggested technique must account for various anatomical and, more crucially, pathological lung characteristics. In Figure 30a, the normal patients are represented and categorized before or during the pandemic, related to their examined period. There are three post-covid instances with greater GGO and consolidation values: NC13, NC14, and NC15. According to their clinical data, NC13 and NC14 are recovering from severe COVID-19, which would explain their artifacts. NC15, on the other hand, has a unique history, as this inquiry was conducted before the clinical manifestation of COVID-19 when the PCR test was negative. Two days later, the patient had severe COVID, which was verified by a positive PCR test. Despite the doctor's original diagnosis, the system did find an anomaly in this instance. This suggests that such an algorithm may detect early changes in a patient's lung texture and, if necessary, give prompt treatment. The clinical data for the NC group did not reveal any further outliers, as confirmed by our model.

In the pre-covid (NN) group, outliers may emerge from patient characteristics such as smokers, asthmatics, or post-infectious individuals recovering from illness. For example, NN06 and NN03 (Figure 30a) are the only two heavy smokers in the normal group who were certified as normal by the radiology team.

Pathological and non-pathological processes are not discrete but relatively continuous, as demonstrated by the model's depiction of their proximity to the notional boundary of the normal zone. Therefore, the granularity provided by the proposed method improves traditional CT interpretation and includes information that is easily missed by the human eye. To demonstrate the applicability of this model in the disease process, a case of a patient with IPF and emphysema is described below (Figure 33).



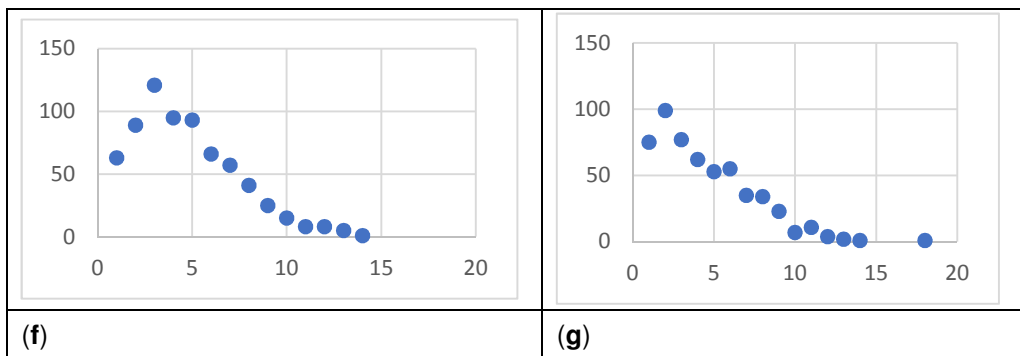


Fig. 33 Stepwise analyze HRCT patterns.

(a)HRCT slice under analysis (b) Sample 1 (c) Sample 2 (d) Degree distribution for sample 1 on the emphysema layer (e) Degree distribution for sample 2 on the emphysema layer (f) Degree distribution for sample 1 on the GGO layer (g) Degree distribution for sample 2 on the GGO layer

The degree distribution of sample 1 reflects the emphysema bubble identified in the same sample. Nonetheless, both samples have comparable inflammation (the GGO layer distributions), demonstrating the underlying illness, IPF. In this instance, the proposed approach has successfully dealt with overlapping patterns.

Regarding the diseased and normal case distributions shown in Figure 29, there are a few instances where the pathological points are pretty close to the normal ones. As demonstrated in Figure 30b, these examples belong to OP upon closer inspection (organizing pneumonitis). The OP is the typical response to lung lesions throughout the healing process, most frequently due to a lung infection, although it can also occur after radiation therapy, inhalation damage, tumor, and medication toxicity. HRTC assessment may reveal a variety of manifestations, including nodular imaging and an uneven GGO pattern. However, peripheral bilateral consolidation is the most common (atoll sign) (64,236). Patients that overlap the normal group are (near to being) cured; therefore, the algorithm grouped them appropriately with the normal patients.

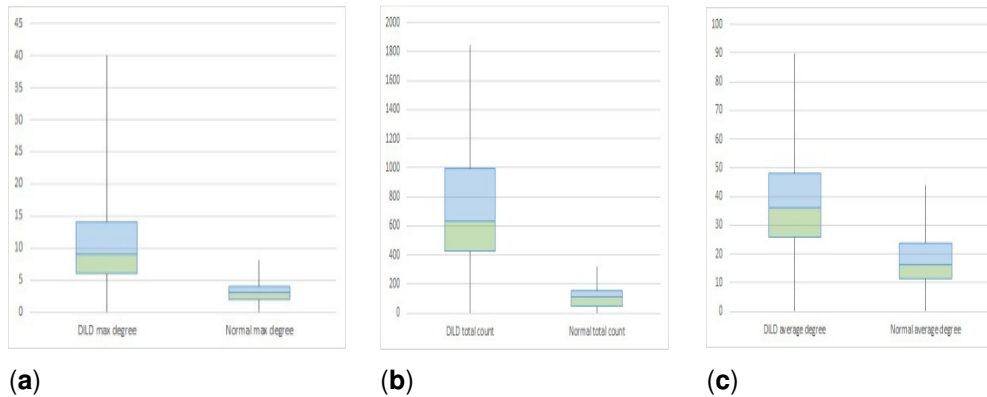


Fig. 34 Box plot for ILD (left) VS Normal (right) for complex network parameters (a) maximum degree (b) total count (c) average degree

Comparing healthy lungs to diseased lungs from a statistical standpoint is difficult due to the diversity of ILD characteristics and the small lot size/disease class. A two-sample t-test assuming unequal variances was undertaken to compare normal and ILD samples to demonstrate the overall validity of the approach and model. The results, summarized in Table 7 and Figure 34, indicate that measured p is less than 0.05 (3.97×10^{-17} , 8.52×10^{-23} , and 5.31×10^{-9}) and observed t is more significant than critical t (1.98, 1.99, and 1.98), thus rejecting the null hypothesis; that is, being 95% CI that differences between groups are not due to chance.

Table 7. Statistical comparison

	Maximum degree		Total count		Average Count	
	ILD	Normal	ILD	Normal	ILD	Normal
Mean	15.96875	7.032258	846.5692	7.1	51.65253	32.53397
Variance	39.45933	3.365591	206084.5	3.334483	362.9068	113.4483
Observations	30	30	30	30	30	30
Hypothesized Mean Difference	0		0		0	
Df	82		64		92	
t Stat	10.49451		14.9084		6.288591	
P(T<=t) one-tail	3.97E-17		8.52E-23		5.31E-09	
t Critical one-tail	1.663649		1.669013		1.661585	
P(T<=t) two-tail	7.93E-17		1.7E-22		1.06E-08	
t Critical two-tail	1.989319		1.99773		1.986086	

A proper comparison of illness phenotypes would require considerably more extensive research. Nevertheless, the objective of this paper was to determine if the complex network model adequately reflects the biological process and whether the quantitative evidence supports this conclusion. Further research is required from a qualitative Medical Science standpoint, although the results are encouraging.

6.5.3. COMPARISON WITH OTHER HRCT ANALYSIS METHODS

This section compares this approach to those that already exist. Compared to the standard, established approach of assessing HRCT by human radiologists and physicians, the suggested method is almost too straightforward. The whole medical study is not restricted to the HRCT; it will almost always require clinical data and, frequently, additional paraclinical procedures. Regarding modality, the human analysis employs a difficult-to-reproduce combination of analytical and empirical methods ("clinical sense"), and its illness progression measurement is mostly subjective (128,128,148).

There are both commercial and research CAD approaches. Caliper (228), the most well-known commercial method, does not rely solely on HRCT; it also requires a method to quantify lung expansion, such as PFT. It is an incredibly efficient, objective, stand-alone method for measuring lung disorders. The suggested approach is significantly slower, taking an estimated median of 2 minutes for each sample for all three layers, or 242 minutes per entire slice and 3872 minutes per patient. The time figures are measured on a typical computer running a single-threaded application. Amdahl's law shows that there is room for improvement with certain restrictions. This deficiency requires improvement to attain maximum analytical potential despite the information provided being more diverse than Caliper because of the complicated network technique.

Research-stemmed approaches, such as those from (229,230), and those based on machine learning, such as (151,154), use only the HRCT, but how they measure the disease is nonexistent in most cases and volumetric in others. Most machine learning techniques focus on accurate categorization and pattern recognition rather than quantifying it. In addition, the time element is undefined mainly for any of these techniques, making evaluation impossible.

Table 8. provides an overview of these comparisons in aggregate.

Table 8. Methodology comparison

	Just HRCT	Analytical	Empirical	Works alone	Measurement
Doctor	N	Y	Y ("clinical sense")	Y	Subjective
Caliper (257),	N, PFT	Y	N	Y	Yes, 1 dimensional size
Zimec (258,259)	Y	Y	N	Mostly	Maybe
Machine learning	Y	N	Y	Maybe	Maybe
Proposed model	Y	Y	N	N	Yes, 3 dimensional

Unlike the methods mentioned, the proposed method provides a mechanism to quantify afflicted lung regions mathematically. Using network features, it can quantify and qualify a pathological process along three axes; it cannot function independently and requires many more examples to enable accurate classification techniques.

7. CHAPTER 3: ENHANCING IMAGISTIC INTERSTITIAL LUNG DISEASE DIAGNOSIS BY USING COMPLEX NETWORKS

7.1. INTRODUCTION

A vast and diverse category, diffuse interstitial lung diseases (ILD), includes about two-hundred different pulmonary diseases that cause inflammation and fibrosis in the lung parenchyma to variable degrees (9,158). Despite the best efforts of a multidisciplinary team, ILD can be challenging to diagnose and treat since they share many symptoms and indications with other conditions but develop in distinct ways (16,237). The most common form of diffuse interstitial lung disease (ILD) is idiopathic pulmonary fibrosis (IPF), a progressive fibrosing intra-alveolar lung disease (PF-ILD) with an abysmal prognosis and an elevated risk of premature mortality without treatment (7,158).

Although high-resolution computer tomography (HRCT) and biopsy should serve as the basis for diagnosis, the absence of the biopsy sometimes necessitates relying exclusively on a vision for an accurate diagnosis (7,158).

Computer enhancements and medical skills are synergistic and precise methods, as are recent advances in computer-aided diagnostic (CAD) procedures (151,153,215). Some patients are challenging to identify due to heterogeneous patterns of lung damage and/or interobserver variability, which is essential even among experienced radiologists (87).

7.2. ILD EARLY DIAGNOSIS

In particular, when relying on a single HRCT, early diagnosis of some diffuse interstitial lung disorders is challenging. Having access to many imaging examinations spread across time allows for particular findings and patterns characteristic of the ILD to form, which improves the accuracy with which the initial diagnosis may be predicted (22). This is complicated because the course of most ILDs varies over time depending on whether inflammation is present (which has a high potential for reversibility) or fibrosis is prominent. In contrast, the course of some, like IPF, is indisputable.

In addition to HRCT imaging, functional lung investigation is essential for ILD diagnosis, monitoring, and prognosis. Spirometry studies for pulmonary function often reveal restrictive dysfunction, with a poor forced vital capacity (FVC), in ILD. Recent research (238), Refs. (239,240) suggests that the DLco of patients with diffuse parenchymal lung disorders corresponds with HRCT results

and is related to the degree of lung involvement (240–242). Notably, DLco diminishes before FVC, giving it a valuable diagnostic tool for the early detection of lung injury.

Although composite index predictions for ILD have been proposed (243,244), such as the modified ILD-GAP score (Gender, Age, Physiology, ILD subtype), integrating clinical-functional elements (respiratory functional tests-DLco, FVC), they typically generate a mortality prediction model (284). They are utilized after the diagnosis has been confirmed rather than as an early diagnostic indicator.

7.3. ILDS EVOLUTION AND IMAGISTIC DIAGNOSIS

ILD is pattern-based and associated with the underlying histology (131). If the progression of IPF is unquestionably fibrosis, the progression of other ILDs is substantially more variable.

Travis et al. (17) categorized longitudinal behavior patterns for ILD progression into five groups. These types of phenotypic clusters in fibrotic ILD can be subdivided into three patterns: stable non-progressive fibrosis following removal of a trigger (e.g., ILD–drug related), irreversible stable under treatment fibrosis (e.g., mycophenolate mofetil therapy in connective tissue disease-associated ILD (24) and chronic hypersensitivity pneumonitis (HPc) (25), and progressive irreversible Other non-fibrotic ILD clusters may be reversible and self-limiting (respiratory bronchiolitis-associated interstitial lung disease (RB-ILD)) or reversible with progression potential (e.g., cellular non-specific interstitial pneumonia (NSIP) and some fibrotic NSIP, desquamative interstitial pneumonia (DIP), and organizing pneumonia (OP)). This most recent longitudinal behavior pattern (9) necessitates short-term observation to validate treatment response and long-term surveillance to guarantee maintained improvements. (245)

Fibrotic phenotypes necessitate regular, long-term monitoring of the evolution of HRCT imaging to appropriately manage the specific case by maintaining the status, avoiding progression, or decreasing progression. The presence of fibrosis is a defining feature of a group of progressive lung disorders, including IPF and progressive pulmonary fibrosis (PPF) (246).

In terms of radiography, ordinary interstitial pneumonia (UIP) is the prototypical progressive fibrotic phenotype, although self-sustaining progressive fibrosis is not limited to patients with IPF; progressive NSIP or HPc phenotypes should also be considered (247). According to the recent consensus from the meeting of the American Thoracic Society, European Respiratory Society,

Japanese Respiratory Society, and Asociación Latinoamericana de Tórax, PPF was defined as the presence of at least two of the three criteria (worsening symptoms, radiological progression, and physiological progression) within the past year in a patient with an ILD other than IPF and no alternative explanation (26).

Despite the current inclination to merge the management of probable UIP and (typical) UIP (26), it is essential to distinguish the various kinds of pulmonary fibrosis when defining the accurate prognosis (e.g., a patient with a probable UIP pattern has fewer acute exacerbations and more prolonged survival compared to patients with a typical UIP pattern (248,249).

7.4. COMPUTER-AIDED DIAGNOSIS

Quite a few techniques-based approaches to computer-aided diagnosis for lung HRCTs are available or in development. Whether based on artificial intelligence, neural networks, or machine learning (153,215), these software solutions cannot capture the dynamics of a pathology's evolution. HRCTs are evaluated statically, with no prognosis of the patient's health condition. In addition, some of them, such as CALIPER, require additional information, such as tests or respiratory data, to produce a correct result (e.g., lung volume affected), albeit extrapolated in a pretty small timescale.

The novel 2022 guide (26) normalizes the use of CAD in disease pattern recognition but emphasizes the need for programs that provide improved prognosis and, most critically, early objective characterization of any sort of lung abnormalities (incidentally identified or otherwise).

Several of these techniques take a more in-depth approach, such as examining lung patches of a specific size (154). Still, none genuinely change the approach to ILD early detection and classification by precisely determining the pace of lung deterioration and/or the affected lung volume.

The complex network approach (146) may give hitherto untapped insights by combining pattern matching and mathematical methods. This paper evaluates a novel complex network technique in ILD-centered imagistic applications.

7.5. HYPOTHESIS TO BE EXPLORED

This research investigates the practical application of a complex networks (CN) strategy based on (159) and its applicability to early detection and/or support/enhance diagnosis by providing a quantifiable progression meter. This is especially noteworthy considering that worldwide guidelines (26) have lately changed the emphasis to antifibrotic medications for nearly all progressive

ILDs, not just IPF. Therefore, early identification of the presence of progression and a measurable and not subjective progression indicator is crucial (35,36).

The first hypothesis asserts that the CN algorithm accurately quantifies ILD progression.

Second Hypothesis: New methods for early detection are made possible by the CN algorithm.

7.6. MATERIALS AND METHODS

7.6.1. LOT SELECTION

The private "Dr. Victor Babes" Infectious Diseases and Pneumoftiziologie Clinical Hospital Timisoara National Fibrosis Center database selected 65 ILD patients with multiple scans and 31 patients with normal lungs.

The following inclusion criteria were in place:

- Each patient was diagnosed by a minimum of three pulmonologists with five or more years of experience in ILD/IPF.
- Each CT satisfies the criteria for HRCT, with constant characteristics across the lot (further described in Section 7.6.2).
- All pathological patients have imagistic surveillance for at least one year.
- Additional data are provided for each investigation, including DLco, FEV₁, age, gender, and clinical outcome.
- All CTs are annotated with comprehensive CT descriptions prepared by center specialists following the MDD.

Exclusion criteria included patients refusing to return annually for imaging follow-up.

- Patients with poor-quality HRCT images exhibit artifacts or slices thicker than 1.5 mm.
- Presence of severe associated pathology, such as liver cirrhosis, neurodegenerative illness, neuropsychiatric disease, severe heart failure, etc.
- Absence of freely expressed consent (observation sheet and/or lack of discernment)

The database query covered the period from 2012 to 2021; all results were confirmed by lung specialists who contributed to developing it.

The ages and sexes of the lots were comparable, and they all legally consented to use their data for academic reasons, and the Ethics Committee approved this research.

For each patient's physiological data (age, sex, smoking status), pulmonary function tests (PFT)—such as forced vital capacity (FVC) by spirometry, were performed. The diffusing capacity of the lungs for DLco was studied alongside HRCT annotations. The quantitative dynamic HRCT pictures of patients were also provided, and four pneumology experts reviewed their case histories.

Since each scan in the database is already annotated by at least three experts, it was possible to define very selective criteria for the ILD lot: typical HRCT appearance of the most frequently encountered interstitial lung diseases in which overlapping primary lesions create models for idiopathic pulmonary fibrosis (IPF), non-specific interstitial pneumonia (NSIP), hypersensitivity pneumonitis (HP), sarcoidosis (S), and organizing pneumonitis (OP) (OP). To reduce the scope, the selected primary lesions were reticulation and consolidation (collectively called band C), emphysema, and cysts (defined together as band E). These lesions exhibit different imagistic absorption rates, allowing for categorization, as described in Section 7.6.3.

The HRCT region of interest was identified by a radiologist with a decade or more of experience in the imagistic diagnosis of ILDs in collaboration with the inputs of other specialists. The selected imagistic characteristics were representative of IPF (29 patients; 44.62%), NSIP (16 patients; 24.62%), OP (8 patients; 12.3%), S (8 patients; 12.3%), and HP (4 patients; 6.15%). Since the morphological pattern of IPFs represents 55% of idiopathic interstitial pneumonia, the selected cases exhibited the typical interstitial pneumonia pattern. Thus, subpleural with peripheric distribution and an apicobasal gradient (predominantly basal) of reticulations, bronchiectasis, and end-stage "honeycombing" cysts with limited ground glass opacification (38,66) were assigned. Combined pulmonary fibrosis and emphysema (CPFE) is a form of IPF characterized by a low survival rate, coupled pulmonary fibrosis, and emphysema (250).

In NSIP cases, a cellular type characterized by subpleural ground glass opacification and fine reticulations was seen (251). Moreover, instances with reticulation, traction bronchiectasis, and architectural distortion due to fibrosis were selected.

Centrilobular or geographical ground glass opacification, poorly defined centrilobular nodules, and air trapping (mosaic attenuation) were lesions observed in acute HP patients (116), with mid- and upper-lung zone

predominance. Chronic HP patients with fibrosis with septal thickening–reticulation, traction bronchiectasis, perhaps honeycombing, and headcheese sign (varying degrees of ground-glass and considerable mosaic attenuation due to sparing of secondary lobules) (117) were selected with caution.

The lot displayed perilymphatic micronodularity in sarcoidosis. In addition, the lot was chosen based on reticulation and/or honeycombing (252) in the sarcoidosis fibrotic stage.

The OP patients presented with bilateral patchy airspace consolidation/ground-glass opacities, with or without tiny nodules, and a characteristic perilobular pattern and fluctuation (97,253).

7.6.2. IMAGING PARAMETERS

On the General Electrics (GE) Healthcare Optima 520 CT, the patients were evaluated with constant settings utilizing sixteen 1.25 mm thick slices reconstructed with high spatial frequency at 32. The scan was completed in 1 second with the following parameters: 120 kV, 130 mAs, and a 2.5 mm collimation. The field of view was 35 cm, and the matrix size was 768. Due to tissue penetration, the radiation dose was altered as required. 90% of the sample was examined in a prone posture, while the remaining 10% was examined in a supine position. Digital Imaging and Communications in Medicine (DICOM) has been used to store examinations in the cloud storage of the aforementioned National Fibrosis Center database.

7.6.3. SELECTING THE PATHOLOGICAL IMAGISTIC ALTERATIONS

The literature defines four categories of pathological imagistic lung alterations: the reticular pattern, the nodular pattern, high attenuation (ground glass opacity, consolidation, atelectasis), and low attenuation (emphysema, cyst, air trapping), whose distribution, overlap, and association with other lesions matter concerning the secondary pulmonary lobule (SPL) and the segmentation of lung regions (51,254).

The attenuation range of X-ray beam tissue absorption, measured in Hounsfield units (HU), and reflected in the grey tones of the image, can aid in stacking various diseases. General Electric Healthcare Optima 520 literature (58,62,255) indicates that, for the employed CT apparatus, three HU bands can contain all of the lung mentioned above alterations: band E [-1024, -977], band GGO [977, 703), and band C [100, 5].

On band E, emphysema appears as polygonal or rounded low-attenuation areas devoid of walls (307). On the same band, cysts are round circumscribed areas of lucency or low attenuation with a diameter greater than

or equal to 1 cm, surrounded by epithelial or fibrous contour and typically presenting discrete walls (67).

GGO refers to a homogenous area of increased lung opacity (a process that partially fills the airspaces) in which the increased opacity does not obscure the underlying bronchial and vascular systems. Due to the presence of fluid, cells, and fibrosis, GGO may be the outcome of air space disease (partial filling of the alveoli) or early interstitial lung disease (fine thickening of the interstitium or alveolar wall, i.e., fibrosis) (82). This design has its own HU band, making it easier to select.

Consolidation is denser than GGO, and from a strictly visual perspective, it appears in ILD (256) as a visually defined compact opacity. The network of intersecting line opacities known as the reticular pattern is on the same HU band as consolidations. The reticulation appears to result from interstitium injury, resulting in the thickening of the intralobular and interlobular septa of the secondary pulmonary lobule (38), which is pathologically mirrored by varying degrees of inflammation and fibrosis.

The primary lesions in the ILD appearance may exist alone in imaging practice. Still, they are typically observed in overlapping combinations, forming genuine models that may be typical or less so for a particular ILD entity (257,258). Mosaicism (259), head cheese pattern (260), and crazy paving pattern (261) are examples of this overlap, but the honeycombing pattern, which is a mixture of cluster cysts (E band) and reticulations (C band) (262), is more significant for this study work.

Pathologically, honeycombing is the ultimate stage in the transition of ILD to fibrosis, accompanied by architectural deformation, traction Bronchiectasis, and the creation of cystic layers (64,82). Therefore, an algorithm that separates these lesions into distinct layers can improve the data.

7.6.4. COMPUTER-ENHANCING THE DATA

Multiple stages comprise the transformation of DICOM pictures by the analyzed algorithm (35): First, DICOM images are evaluated, and each pixel is translated to its equivalent HU unit. Then, depending on the required HU bands, only pixels corresponding to those bands are retained, while all others are eliminated. The remaining pixels are separated into layers based on their respective HU band, resulting in a different image for each layer. The resulting images are then transformed into complex networks according to specific predefined attachment rules, similar to the conversion of grayscale images into complex networks presented in (147,263,264): nodes with similar HU values (within the range of 50 HU units) and closer than 4 px apart are considered to

be linked, whereas all noncompliant nodes are detached. In other words, any two visual locations in the lung that are relatively close together and have a similar color (density) are most likely part of the same type of tissue, regardless of whether it is healthy or diseased. Based on the created network, particular metrics can be produced, allowing for more precise conclusions regarding the architecture of the lung region under study.

From the DICOM format, three complex networks were created for each region of interest, one for each pathologically relevant Hounsfield unit (HU) interval: E for emphysema and cysts, GGO for ground glass opacity, and C for consolidation and reticulations. The device-specific scale for the HU transformation was derived from this implementation (62,65,255).

7.6.5. SELECTING RELEVANT METRICS

To evaluate the efficacy of the suggested CN method, the measurements must reflect the underlying biological processes and their dynamic evolution. A CN can be defined by various metrics, ranging from those that quantify its interconnections to those that assess information flow or clustering (265).

Since the objective of this paper can be translated biologically into a method for measuring lesions and their growth, the accompanying CN measurements should reflect their interconnectedness and size. His chosen metrics are maximum degree number (the most significant number of network connections for a single node), total degree count (the number of network connections), and average degree count (the average number of connections per node—how sparse the network is). Depending on how the method is implemented, a network node can represent either a single pixel or a small region; for the purposes of this section, it represents a pixel.

Figure 35 illustrates these precise measures with examples. A micronodule (Figure 35a) is graphically represented (Figure 35d) as a node or cluster of nodes (e.g., Figure 35d, node number 13, purple) with the highest degree in the examined window. The total number of edges (interconnections) in a sarcoidosis or honeycomb network (Figures 35b and 35c) may be comparable, but their average degree metrics differ dramatically. One (S—Figure 35b) has many nodes with a median of roughly two connections (representing the typical micronodules perilymphatic distribution of linearly attached nodules, like a string). In contrast, the other (Figure 35c) has fewer nodes but with many connections, averaging at 5.8. (reflecting the cyst wall, which is linearly homogenous). Loosely translated, the total count indicates how "damaged" the sample is per total, the average count indicates how localized these lesions are, and the highest degree indicates the peak

severity of the pathological alteration. Therefore, it can be argued that these values indicate interconnectivity and size, the two necessary characteristics examined individually on each of the three HU bands.

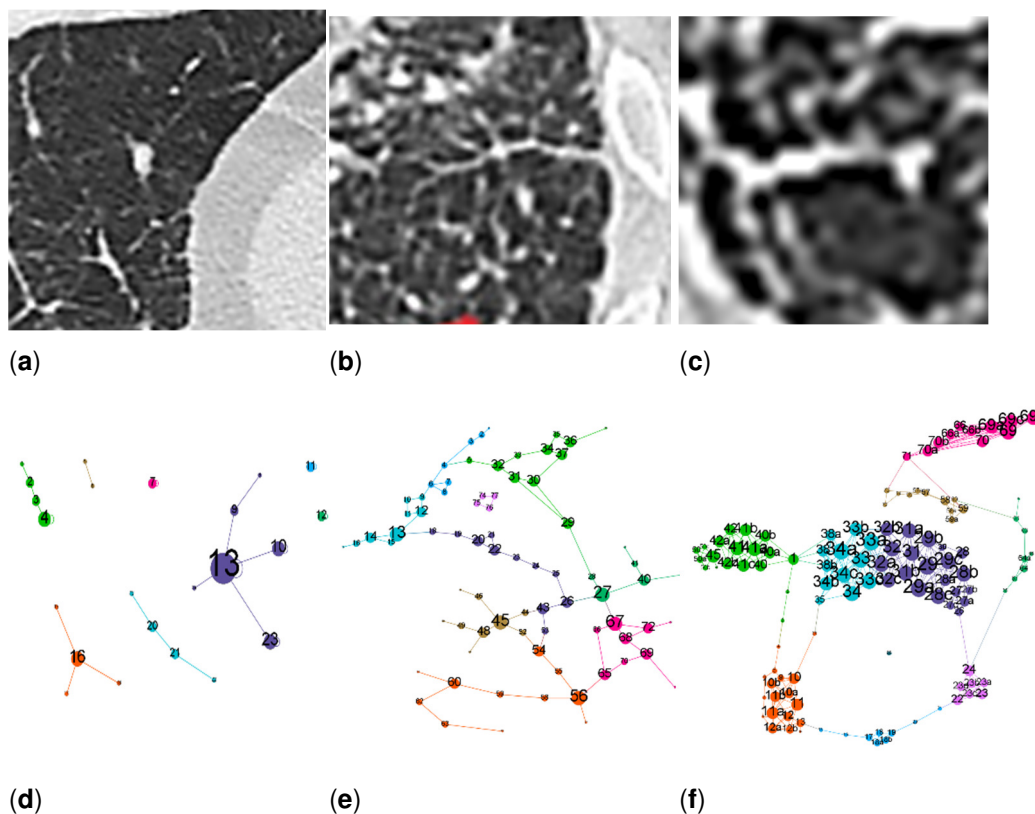


Fig. 35. Simple example to illustrate CN measurements and biological counterparts
 (a) CT section with a micronodule in the center (b) CT section with sarcoidosis (perilymphatic micronodules) (c) CT section with honeycombing cysts (d) CN depicting micronodule CT (e) CN depicting sarcoidosis CT (f) CN depicting honeycombing CT For all CNs, node positions mimic light color entities on the CT above them, node size is proportional to node degree and on each node a numeric label is provided. Label size is proportional to node size. Maximum, minimum, and scaling for node size are constant in all three CNs. Node color reflects clusterization, provided for visual interest only. Edge width depiction is constant. CT slice scale between a, b, and c is not the same as this, which is intended for CN exemplification only.

In order to evaluate the efficacy of the suggested CN method, the measurements must reflect the underlying biological processes and their dynamic evolution. A CN can be defined by a variety of metrics, including those that quantify its interconnections, information flow, and clustering (265). Since the underlying objective of this paper may be biologically translated into a method to evaluate lesions and their expansion, the accompanying CN measurements should represent interconnectedness and size. Therefore, the

chosen metrics are maximum degree number (the maximum number of network connections for a single node), total degree count (the total number of network connections), and average degree count (the average number of connections per node—how sparse the network is). A network node can represent a single pixel or a small region, depending on how the method is implemented. For the purposes of this section, it represents a pixel.

Figure 35 illustrates concrete examples of various dimensions. A micronodule (Figure 35a) can be visually interpreted (Figure 35d) as a node or cluster of nodes (e.g., Figure 35d, node number 13, purple) with the highest degree in the analyzed window.

A sarcoidosis or honeycombing network (Figures 35b and 35c) may have a comparable total number of edges (interconnections), but their average degree metrics are drastically dissimilar. One (S—Figure 35b) has many nodes with a median of around two connections (representing the usual micronodules perilymphatic distribution of linearly attached nodules, like a string), whereas the other (honeycombing, Figure 35c) has fewer nodes but more connections, averaging 5.8. (reflecting the cyst wall, which is linearly homogenous). Loosely translated, the total count indicates how "damaged" the sample is as a whole, the average count indicates how widespread these lesions are, and the maximum degree depicts the highest intensity of the pathological alteration.

Consequently, it can be inferred that these measures reflect interconnectivity and size, the two parameters that needed to be assessed and evaluated individually across all three HU bands.

$$v = \begin{cases} \frac{(s-s_0)}{s_0 \times t}, & \text{for } s_0 \neq 0 \\ \frac{s}{t}, & \text{in rest} \end{cases}.$$

The s value from equation (1) is the studied metric, while s_0 is the normalization point corresponding to the reference sample.

In Equation (1), t is stated in years because patients with ILD require annual examinations (317). Counting the number of days (for example, using the Excel function DAY ()) between the oldest HRCT (at time t_0) and the one now evaluated (at time t_1) and normalizing it using a 365-day year is an easy technique to calculate its value.

$$T = \text{DAY}(\text{DATE}(t_1) - \text{DATE}(t_0))/365.$$

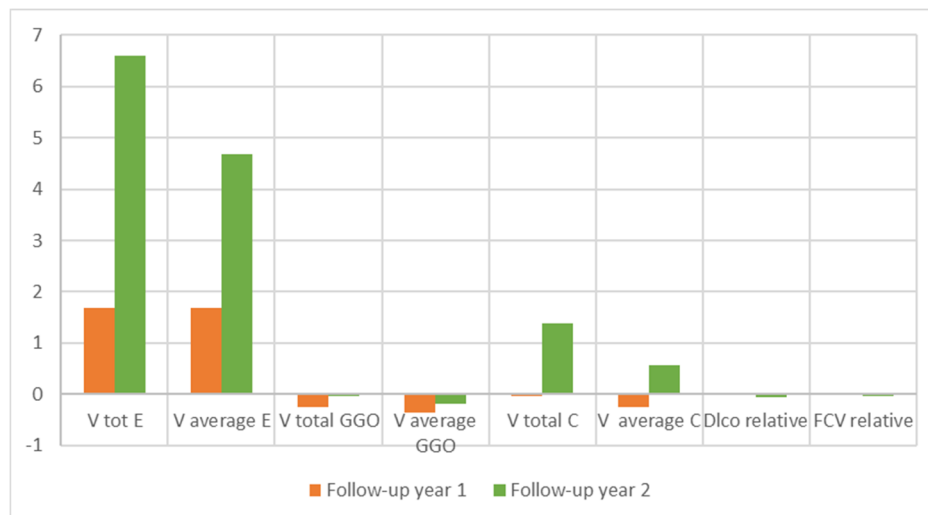
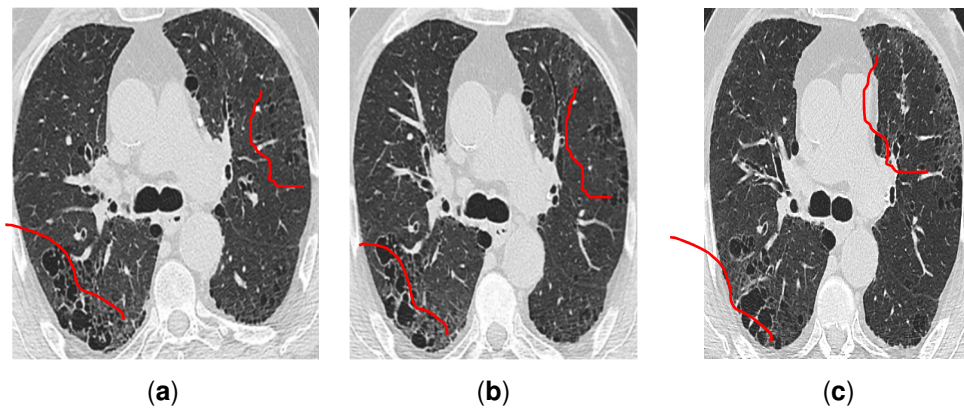
Another viable alternative is to normalize the year to 360 days, as is typical in certain financial calculations; nonetheless, the most critical factor is the consistency of the normalization type. This article applied the normalization suggested by Formula (2).

7.7. RESULTS

7.7.1. CASE REPORTS

This section illustrates sample locations from two completely different patients throughout the analysis process in order to clarify the approach.

Figure 36 depicts the results of a patient diagnosed with a typical UIP following a heated dispute among the doctors at our center for cystic fibrosis. This patient's atypical honeycombing pattern may bias the diagnosis towards likely UIP. Age and gender strongly influenced the ultimate diagnosis. This scenario is suitable for evaluating the algorithm's detecting capabilities. The course of this case with UIP+ emphysema (CPFE phenotype) is illustrated below.



(d)

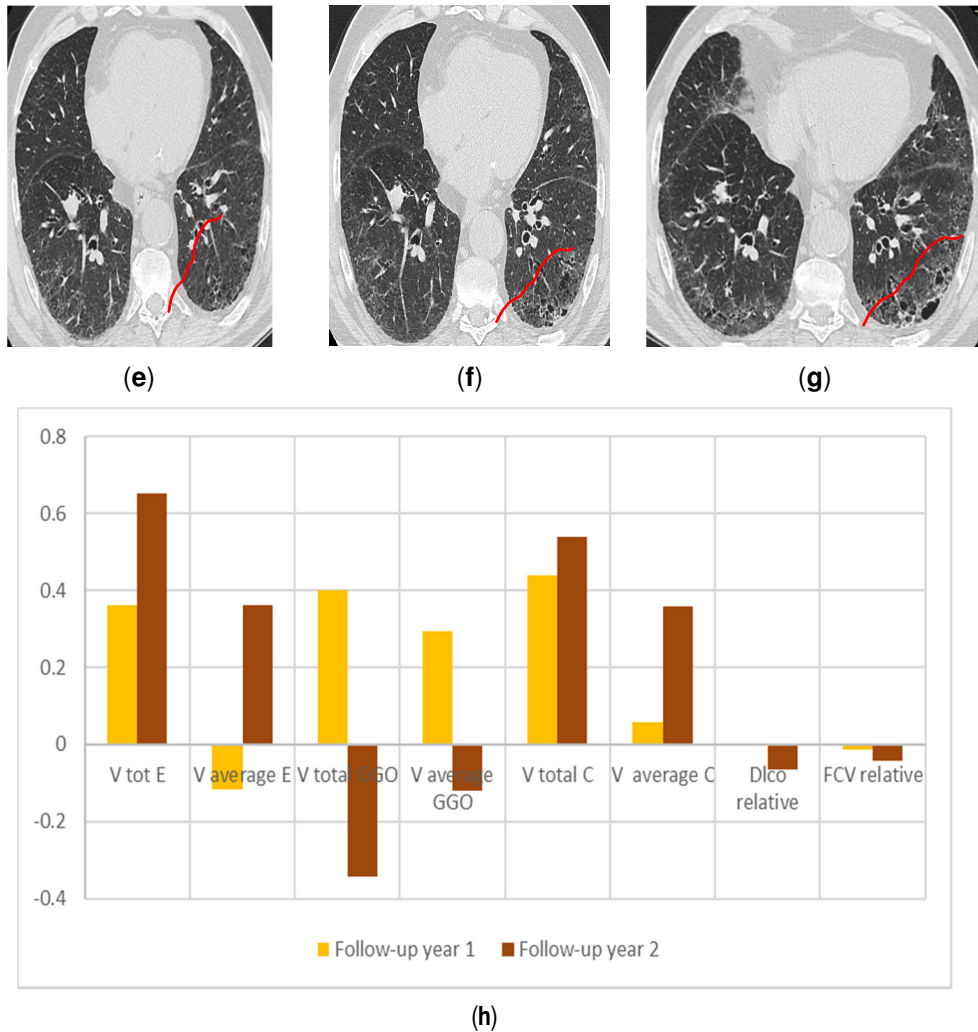
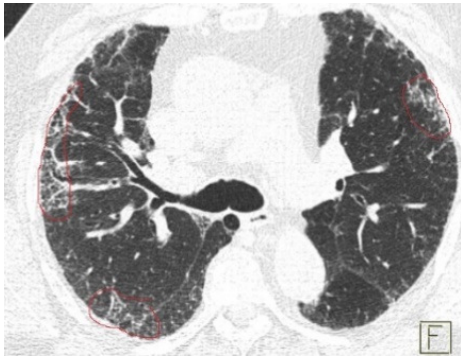


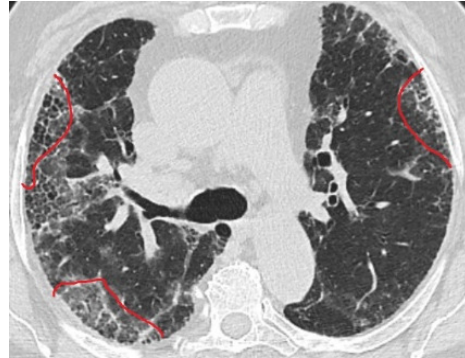
Fig. 36 Case report for a lung axial HRCT, UIP + E pattern (CPFE) patient progression

(a) Superior lung region HRCT slice in initial t_0 year, (b) Superior lung region HRCT slice in next year- t_1 . (c) Superior lung region HRCT slice in second year- t_2 . (d) Relative speed variations on the superior lung slice for all three bands. Speed is computed using Equation 1. (e) Basal lung region HRCT slice in initial t_0 year. (f) Basal lung region HRCT slice next year- t_1 . (g) Basal lung region HRCT slice in second year- t_2 . (h) Relative speed variations on the basal lung slice for all three bands. Speed is computed using Equation 1.

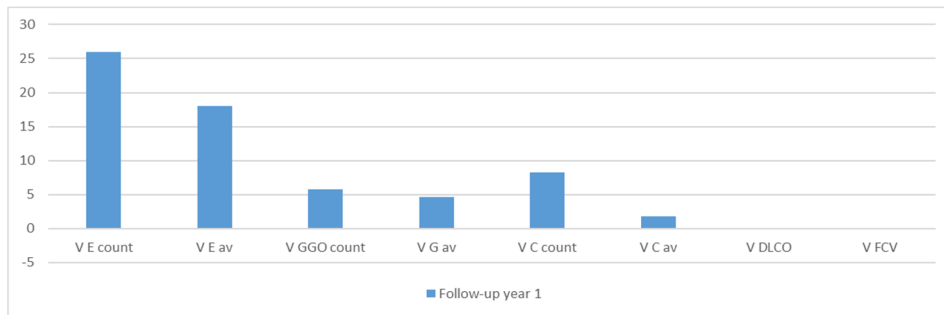
The results in Figure 36 present a typical NSIP pattern in evolution.



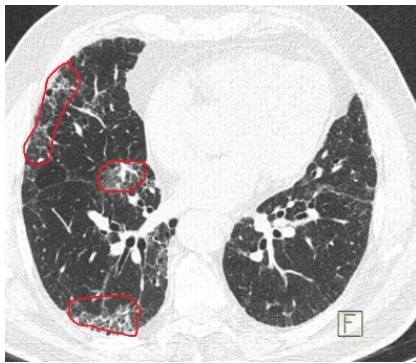
(a)



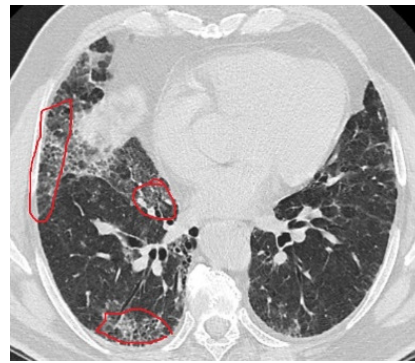
(b)



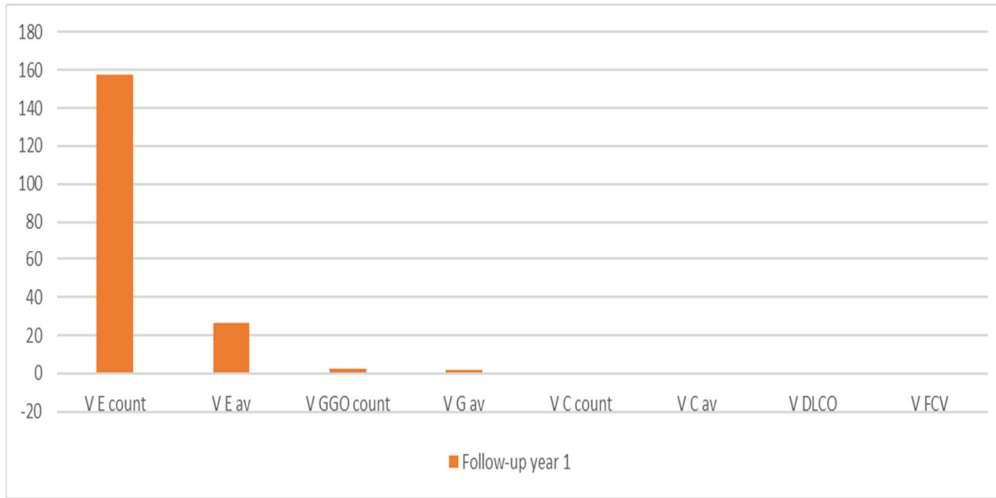
(c)



(d)



(e)



(f)

Fig. 37 Case report for a NSIP + E patient progression.

- (a) Superior lung region axial HRCT slice in initial t_0 year. (b) Superior lung region axial HRCT slice in next year- t_1 .
- (c) Relative speed variations on the superior lung slice for all three bands. Speed is computed using Equation (1).
- (d) Basal lung region axial HRCT slice in initial t_0 year. (e) Basal lung region axial HRCT slice in next year- t_1 . (f) Relative speed variations on the basal lung slice for all three bands. Speed is computed using Equation (1).

7.7.2. PROGRESSION SPEED

The entire lot was evaluated compared to what was discussed in the previous section. Table 9 displays the t-test analysis of the defined relative speed versus DLco relative variation for every HU band and CN. This test was performed on the complete lot, including normal and ILD patients. It should be highlighted that even though the maximum degree can be studied because the sought-after assessment is progression, the peak singular lesion is less meaningful.

Table 9. t-test results for relative speed in HU bands parameters VS DLco.

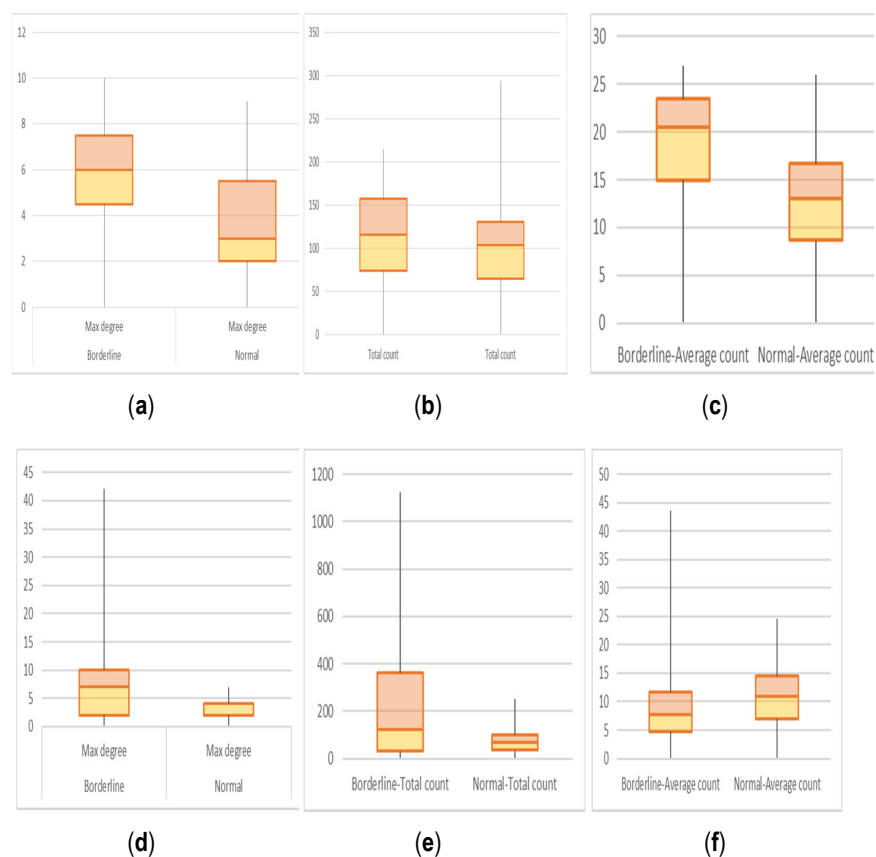
HU Layer	Total Count VS DLCO	Average Count VS DLco	Parameters
E	1.81144865	2.297734923	t Stat
	0.038529988	0.013194925	P(T ≤ t) one-tail
	2.016692199	2.015367574	t Critical two-tail
GGO	-1.334981884	-1.82528253	t Stat
	0.092702764	0.035714932	P(T ≤ t) one-tail
	1.987934206	1.987934206	t Critical two-tail
C	-1.334981884	-1.82528253	t Stat
	0.093421672	0.035996812	P(T ≤ t) one-tail
	1.999623585	1.992543495	t Critical two-tail

The null hypothesis is maintained for all selected series except one. The average count VS DLco test for the E band rejects the null hypothesis, as indicated by the italic font in Table 9.

7.7.3. TESTING FOR EARLY DETECTION

To seek for early identification, the lot was divided into normal instances and cases with incipient ILD and relatively good functional characteristics (0–3 GAP-ILD points, DLco values of 70–85%). The DLco values were selected as an interval centered on the lower standard limit (80%) to permit the inclusion of early impairment in the alveolar-capillary membrane.

The cases were evaluated using the same three axes, with the results presented in Figure 38 as box plots and summarized in Table 10.



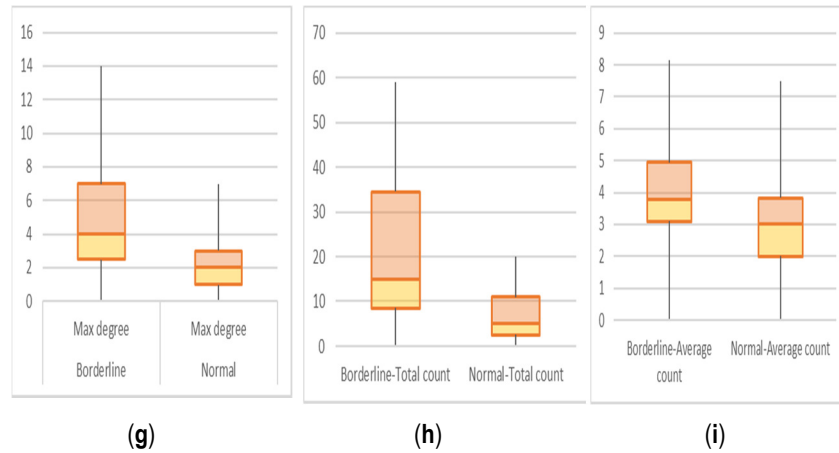


Fig. 38 CNs on Borderline normal versus normal layer distribution;
 Layer E values with (a) maximum degree (b) total count (c) average count; Layer GGO values with (d) maximum degree (e) total count (f) average count; Layer C with (g) maximum degree (h) total count (i) average count.

The *t*-test data presented in Table 10 is written in italics for the series rejecting the null hypothesis.

Table 10. Statistical t-tests results between borderline and normal lungs.

Layer	Max Degree	Total Count	Average Count	Parameters
E	<i>-0.357327012</i>	<i>-0.33960631</i>	<i>-1.194455411</i>	t Stat
	<i>0.361362738</i>	<i>0.367964892</i>	<i>0.119667428</i>	P(T ≤ t) one-tail
	<i>2.02107539</i>	<i>2.02107539</i>	<i>2.02107539</i>	t Critical two-tail
GGO	<i>2.362901118</i>	<i>2.496174465</i>	<i>2.132901092</i>	t Stat
	<i>0.016568972</i>	<i>0.012345754</i>	<i>0.023097162</i>	P(T ≤ t) one-tail
	<i>2.144786688</i>	<i>2.131449546</i>	<i>2.093024054</i>	t Critical two-tail
C	<i>2.787128882</i>	<i>2.910253494</i>	<i>1.723111496</i>	t Stat
	<i>0.006593367</i>	<i>0.005384188</i>	<i>0.048371727</i>	P(T ≤ t) one-tail
	<i>2.119905299</i>	<i>2.131449546</i>	<i>2.055529439</i>	t Critical two-tail

7.8. DISCUSSION

Figure 36 depicts two levels of axial HRCT slices (superior and basal lung region) chosen to illustrate the evolution of disputed UIP pattern+ emphysema (CPFE phenotype). Even though all of the results in this work belong to the axial lung plane, their applicability is not limited. A technical examination illustrating the equivalence in sagittal, coronal, and axial plane results would overstate the goal of this paper, which is to highlight the uses of the CN model in imagistic contexts. Returning to the UIP + emphysema case, an imagistic interpretation of the progression begins with the initial to the point, which in the superior lung region

indicates the presence of fine reticulation, bullous emphysema, and slight subpleural honeycombing cysts, and in the basal lung, region is characterized by sparse reticulation and honeycombing lesions.

According to the HU ranges, as previously noted, reticulations and consolidations have comparable values. Still, in this context, the values are read as reticulations. In specified regions, the CN model provides data for relative speed variation on each layer. This speed is unique to a particular location and represents a relative change in characteristics over time. It is not an absolute value; its significance is tied to the rate of change, therefore identifying places that are fast deteriorating. Since the CN conversion algorithm considers lesions as tiny as 3 mm (320), the default speed is more granular than the human eye.

The CN model's relative speed on the E layer shows an increase in follow-up in years 1 and 2. However, the magnitude varies significantly between the superior (Figure 36d) and basal (Figure 36h) slices. The superior region is almost 10 times more rapidly degrading than the basal slice, as measured by the superior lobe's emphysema lesion expansion and honeycombing cyst layer growth (Figure 36a–c), as compared with the basal lobe, in which emphysema is not as prominently exhibited (Figure 36e–g). C layer grows in both the superior and inferior slices, demonstrating the degenerative course of the lesion with lung architectural deformation, reticulation, and multilayer cysts of varying sizes. The model reveals modest fluctuations in the GGO, particularly in the basal plane (Figure 36e–h), indicating the presence of an acute substrate in that particular region. This image is heavily annotated (it is part of the national ILD database, has already been reviewed by at least three lung specialists, and five other lung specialists have assessed all of the images utilized in this study), but the GGO difference is imperceptible. Upon examination of the patients' data, the symptoms of the first year of follow-up are curiously somewhat worse than those of the second. This verifies the CN relative speed light variation and its early detection capability. In both follow-up years, the relative variation of functional parameters is nearly zero, indicating a fixed functional status and precluding the early identification of the proposed CN model.

Figure 37 depicts imagistic axial HRCT lung lesion progression in an instance of NSIP pattern. On the E band, relative speed indicates a significant rise in the number of emphysema focal points (total count) but only a moderate increase in their intensity (average) for both sample sites, which the accumulation of honeycombing cysts layers can explain. GGO in t0 (Figure 37a,d) exhibits a modest rise in the follow-up sample, correlating with the interpretation of the imaging slice HRCT (Figure 37c,f). The C layer only slightly increases in the superior regions (Figure 37a,b), as indicated by the well-defined

multilayer cysts and their defining borders. Functional parameters have essentially no fluctuation, supporting the early identification of the suggested CN model based on functional parameter data.

Table 9's results support the testing of hypothesis 1, which asserts that the CN algorithm accurately and quantitatively characterizes the progression of ILD. Hypothesis 1 is sustained because most statistical comparisons between DLco and CN measurements reveal essential similarities. The lone exception is the comparison of average count and DLco in the E band (marked with italics in the table). Some persons categorized as normal have compensatory chronic obstructive lung pathology and/or are active or former smokers. Since CN measurements represent biological terms, this indicates that the number of E-layer regions of interest is the same, but the median intensity of these regions is statistically significant and greater than the variance of their corresponding functional parameter.

The statistical comparisons between the borderline and normal groups, depicted in Figure 38 and Table 10, require further investigation. There is no statistical difference on the E layer between the early diagnostic and normal sets; hence, the CN model prohibits early detection on this layer. The data demonstrate that, from a biological standpoint, early ILD diagnosis with emphysema phenotype is nearly equivalent to emphysema lesions in smokers. On the GGO layer, there is a statistically significant difference, the null hypothesis is rejected, and the proposed model successfully detects ILD early. Maximum degree and total count detect early ILD on the C band, while average count does not. Pathologically, the suggested model accurately identifies well-defined consolidation lesions but cannot identify early diffuse consolidations with blurred edges. As a result, hypothesis 2, stating that the CN method permits early detection, is correct for the GGO, largely valid for the C layer, and untrue for the E layer.

Various types of ILDs that present PPF, such as idiopathic interstitial pneumonia, autoimmune ILDs, exposure-related, ILDs with cysts and/or airspace filling, or sarcoidosis, should apply an antifibrotic therapy according to the current guidelines (26). In order to maximize therapeutic benefits in terms of the patient's life quality and duration, it is necessary to discover the progressive feature as soon as feasible. This leaves practitioners in a difficult position, as they must rely on their practical "medical sense" or CAD-based approaches to evaluate the likelihood of initiating treatment.

Previous CAD approaches, such as those that implement simple mathematical-based techniques in one or more dimensions (66–69) or more complex machine and deep learning algorithms (8–10,69–71) or even the

commercially available CALIPER do not provide a method to objectively assess the aggressive aspect of a lung disease that can serve as an indicator for the initiation of an antifibrotic protocol.

The investigated method can do this, which utilizes a speed measurement influenced by physics. The proposed speed assessment does not indicate the severity of the disease but rather its aggressiveness. For instance, a simple insert disease name here> in its early stages might advance swiftly, resulting in a high observed velocity. Although the superior region in Figure 36 has a less severe appearance, it deteriorates faster, as measured by the speed test. However, a severe aspect can remain relatively static, indicating another component to be considered (the medication is working, the phenotype is slowly progressive, the disease is remissive, or it has shifted towards other areas).

CONCLUSION AND PERSONAL CONTRIBUTION

CONCLUSIONS STUDY 1

In this article, we cover the recent developments in deep learning algorithms and their applications in medicine, primarily in the field of ILD diagnosis.

We concentrated on the problems and the methods to repair them so that the early detection of ILDs could become a common practice with clinical implications. The next step in the early diagnosis of IPF is the development of a CAD that can be implemented on any computer and is accessible to non-academic centers.

CONCLUSIONS STUDY 2

This study presents a novel approach to transforming HRCT images of the lung by using complicated network structures. In the section on technique, a greater level of profundity is devoted to the phases of the algorithm and the reason for each selected parameter. The secondary pulmonary lobule's anatomical boundaries support the sample size, making it acceptable; the radius that influences network connection is connected with injury granularity, and the Hounsfield unit intervals depend upon the device and resolution. In the section on the results, the processing processes for two sample patients (one normal and one with a pathological condition) are presented in parallel, in addition to a whole-lot perspective. In the section titled "Discussion," the correctness of this model is explained from a System Science point of view by employing the degree distributions as the primary instrument for system description. This is performed to demonstrate the model's accuracy. In addition, the network measurement clusterization has been defined, and it has been shown that, as a consequence, substantial disparities have been produced between the normal and diseased lots.

From the point of view of Medical Science, it is demonstrated how the selected model matches clinical data and how the low granularity of the model provides an advantage when it comes to the diagnostic procedure. A comparison between this method and others that already exist reveals its benefit, namely the ability to provide a detailed qualitative and quantitative measurement. Inadequacies of the model that have been proposed, such as its incapacity to function independently as of yet and the relatively small lot on which it has been tested, will need to be addressed in a subsequent study.

In conclusion, it can be said that the stated purpose has been accomplished because it demonstrated how a complex network model might be utilized to transform lung HRCT into a quantifiable and qualifiable structure that can improve ILD diagnosis.

CONCLUSION STUDY 3

To effectively treat ILDs, two concerns must be resolved, which are well known to all practitioners: early recognition and accurate progression evaluation. Traditional medical and computer-based approaches based on artificial intelligence, machine learning, etc., have failed thus far despite the crucial need for effective treatments for diseases such as IPF. This work aimed to determine if a CN-based computer-assisted diagnosis can offer the necessary data to effectively manage ILDs.

Two hypotheses were looked at in order to achieve this: the first studied progression, while the second examined early detection. In terms of development, the CN CAD was nearly a complete success. Its precision in testing lesions as tiny as 3 mm enabled correlation with the clinical status beyond the granularity of conventional functional tests. The only issue with the average count measurement type was on the E band, but the other five measurement axes readily compensate for this.

For early detection, the GGO layer of inflammation proved crucial. Inflammation and fibrosis are the two most common ILD states, and the CN algorithm performed well on both GGO-defined HU bands and C-defined HU bands. This demonstrates the practical capabilities of this algorithm type, which is particularly well-suited to ILDs and has not been met by any other tool, such as Caliper.

As a disadvantage, the CN technique has a lengthy runtime that grows exponentially with the size of the investigated window. It also requires prior segmentation of the lungs, which can be obtained manually or using other CAD systems.

The authors believe this technique should be incorporated into a much bigger CAD system, combining the faster machine learning segmentation and pattern identification capabilities with the slower but more accurate CN local analysis.

PERSONAL CONTRIBUTION

The scientific research objectives have been achieved because the aim to provide a viable CAD algorithm for ILD patient imaging alternative diagnosis was obtained;

Regarding personal contribution, they were achieved step-by-step as follows:

- In this research paper, I proposed and identified a new direction for lung imaging thin section CT processing based on a complex network mechanism.
- I begin this interdisciplinary research paper by offering an in-depth analysis of how virtual AI improves ILD diagnosis, studying all the existing CAD case approaches and then identifying the burns. Identified an opportunity to integrate a new method that has not been done so far. I guided the selection of such algorithms for the specific field of ILD management, emphasizing the visual-based complex network method.
- Participating in creating a CN algorithm to model a lung HRCT accurately
- I have taken care that the specific reality of HRCT is reflected in the CN-based analytical algorithm, namely:
 - segmentation on specific pathological house field unit bands, with impact in HRCT imaging analysis for interstitial lung pathology. Thus, GGO, consolidation (considered equal to reticulation), and emphysema (equal to cyst) bands were converted with the help of the algorithm into complex networks, reported, and correlated with the values of HU corresponding to each tissue.
 - -correlation of the form of pathological variation identified following the CN algorithm process with the medical imaging analysis of the CTs provided as a database validated by experts in the field.
- Participating in creating the optimum window size to analyze the lung with the previously mentioned algorithm. Translating anatomically lung-specific measurements into the algorithm allows a secondary pulmonary lobule to be analyzed. Considering the idea of capturing at

least one entire secondary lobule, we chose the smallest valid DICOM sample, a rectangle area of 65X65 pixels.

- I validated the provided algorithm method from a biological system perspective. This was possible based on analyzing the HRCTs of both normal and affected lungs by all three measurements considered for this proposed network (total count, average degree, and maximum degree) and proving a solid separation between the normal and pathological network.
- The next step was analyzing ILD patients dynamically (successive scans) by clustering them by HRCT patterns (UIP, NSIP, HP, OP, and sarcoidosis) using the algorithm output. Two cases of ILD (UIP plus emphysema phenotype and NSIP) reports highlighted early detection and accurate progression evaluation.
- Participating in defining a new measurement type for pulmonary fibrosis progression customarily flowed. Because progression is explained as a variation over time, the relative variation speed measurement emerged to translate the engineering notion.
- In the end, validating the previous measurement on an ILD cohort dynamic was analyzed by correlating mathematical values with medical reality.

Although this Ph.D. paper includes a rigorous and complicated research process, there are still issues to be solved, such as:

- The need for an automated system of lung pre-segmentation by CAD techniques, not manuals - as we used;
- Integration of a classifier AI technique for marking the region of interest to be studied;
- Graphical interface intuitive and friendly to the non-technical user;
- Processing (cloud) that would allow increased speed and access from mobile devices.

The technical advantage of the proposed algorithm is the identification of minor HRCT lesions, which leaked the classical technique of humans validation, and which predicts the evolution towards a disease (detection of fine lesions on an HRCT imaging considered normal by human validation, later the patient being diagnosed with covid 19). In any case, future research

is needed. The burden to be considered is that the algorithm is now in a proof of concept (POC) version, which requires advanced technical personnel. Also, expensive and high-performance equipment is needed for numerical processing.

Therefore, as closing lines, a future perspective is to link this technical domain, IT, and medicine as strongly as possible. Together, they can lead to great results, especially in the case of this vast and ambiguous entity, which is ILD.

BIBLIOGRAPHY

1. Baughman RP, du Bois RM, editors. Diffuse Lung Disease: A Practical Approach [Internet]. New York, NY: Springer New York; 2012 [cited 2022 Sep 27]. Available from: <http://link.springer.com/10.1007/978-1-4419-9771-5>
2. Guler SA, Corte TJ. Interstitial Lung Disease in 2020: A History of Progress. *Clin Chest Med*. 2021 Jun;42(2):229–39.
3. Fiddler C, Parfrey H. Diffuse parenchymal lung disease. *Medicine (Baltimore)*. 2020 Jun 1;48(6):373–80.
4. Raghu G, Weycker D, Edelsberg J, Bradford WZ, Oster G. Incidence and prevalence of idiopathic pulmonary fibrosis. *Am J Respir Crit Care Med*. 2006 Oct 1;174(7):810–6.
5. Renzoni EA, Poletti V, Mackintosh JA. Disease pathology in fibrotic interstitial lung disease: is it all about usual interstitial pneumonia? *The Lancet*. 2021 Oct 16;398(10309):1437–49.
6. Bagnato G, Harari S. Cellular interactions in the pathogenesis of interstitial lung diseases. *Eur Respir Rev*. 2015 Mar 1;24(135):102–14.
7. American Thoracic Society. Idiopathic pulmonary fibrosis: diagnosis and treatment. International consensus statement. American Thoracic Society (ATS), and the European Respiratory Society (ERS). *Am J Respir Crit Care Med*. 2000 Feb;161(2 Pt 1):646–64.
8. American Thoracic Society, European Respiratory Society. American Thoracic Society/European Respiratory Society International Multidisciplinary Consensus Classification of the Idiopathic Interstitial Pneumonias. This joint statement of the American Thoracic Society (ATS), and the European Respiratory Society (ERS) was adopted by the ATS board of directors, June 2001 and by the ERS Executive Committee, June 2001. *Am J Respir Crit Care Med*. 2002 Jan 15;165(2):277–304.
9. Travis WD, Costabel U, Hansell DM, King TE, Lynch DA, Nicholson AG, et al. An Official American Thoracic Society/European Respiratory Society Statement: Update of the International Multidisciplinary Classification of the Idiopathic Interstitial Pneumonias. *Am J Respir Crit Care Med*. 2013 Sep 15;188(6):733–48.
10. Raghu G, Remy-Jardin M, Myers JL, Richeldi L, Ryerson CJ, Lederer DJ, et al. Diagnosis of Idiopathic Pulmonary Fibrosis. An Official ATS/ERS/JRS/ALAT Clinical Practice Guideline. *Am J Respir Crit Care Med*. 2018 Sep 1;198(5):e44–68.

11. Kondoh Y, Johkoh T, Fukuoka J, Arakawa H, Tanaka T, Watanabe N, et al. Broader criteria of undifferentiated connective tissue disease in idiopathic interstitial pneumonias. *Respir Med*. 2015 Mar;109(3):389–96.
12. Luckhardt TR, Müller-Quernheim J, Thannickal VJ. Update in Diffuse Parenchymal Lung Disease 2011. *Am J Respir Crit Care Med*. 2012 Jul 1;186(1):24–9.
13. Mira-Avendano I, Abril A, Burger CD, Dellaripa PF, Fischer A, Gotway MB, et al. Interstitial Lung Disease and Other Pulmonary Manifestations in Connective Tissue Diseases. *Mayo Clin Proc*. 2019 Feb;94(2):309–25.
14. Kalchiem-Dekel O, Galvin JR, Burke AP, Atamas SP, Todd NW. Interstitial Lung Disease and Pulmonary Fibrosis: A Practical Approach for General Medicine Physicians with Focus on the Medical History. *J Clin Med*. 2018 Nov 24;7(12):E476.
15. Skeoch S, Weatherley N, Swift AJ, Oldroyd A, Johns C, Hayton C, et al. Drug-Induced Interstitial Lung Disease: A Systematic Review. *J Clin Med*. 2018 Oct 15;7(10):356.
16. Guo B, Wang L, Xia S, Mao M, Qian W, Peng X, et al. The interstitial lung disease spectrum under a uniform diagnostic algorithm: a retrospective study of 1,945 individuals. *J Thorac Dis*. 2020 Jul;12(7):3688–96.
17. Fischer A, Antoniou KM, Brown KK, Cadranel J, Corte TJ, Bois RM du, et al. An official European Respiratory Society/American Thoracic Society research statement: interstitial pneumonia with autoimmune features. *Eur Respir J*. 2015 Oct 1;46(4):976–87.
18. Ley B, Bradford WZ, Weycker D, Vittinghoff E, Bois RM du, Collard HR. Unified baseline and longitudinal mortality prediction in idiopathic pulmonary fibrosis. *Eur Respir J*. 2015 May 1;45(5):1374–81.
19. Nakamura H, Aoshiba K, editors. *Idiopathic Pulmonary Fibrosis: Advances in Diagnostic Tools and Disease Management* [Internet]. Tokyo: Springer Japan; 2016 [cited 2022 Oct 2]. Available from: <http://link.springer.com/10.1007/978-4-431-55582-7>
20. Desai SR, Prosch H, Galvin JR. Plain Film and HRCT Diagnosis of Interstitial Lung Disease. In: Hodler J, Kubik-Huch RA, von Schulthess GK, editors. *Diseases of the Chest, Breast, Heart and Vessels 2019-2022: Diagnostic and Interventional Imaging* [Internet]. Cham (CH): Springer; 2019 [cited 2022 Feb 6]. (IDKD Springer Series). Available from: <http://www.ncbi.nlm.nih.gov/books/NBK553872/>
21. Pediatric interstitial lung disease revisited - Fan - 2004 - Pediatric Pulmonology - Wiley Online Library [Internet]. [cited 2022 Oct 2]. Available from: <https://onlinelibrary.wiley.com/doi/10.1002/ppul.20114>

22. Hatabu H, Hunninghake GM, Lynch DA. Interstitial Lung Abnormality: Recognition and Perspectives. *Radiology*. 2019 Apr 1;291(1):1–3.
23. Wallis A, Spinks K. The diagnosis and management of interstitial lung diseases. *BMJ*. 2015 May 7;350:h2072.
24. Mycophenolate mofetil improves lung function in connective tissue disease-associated interstitial lung disease - PubMed [Internet]. [cited 2022 Jun 20]. Available from: <https://pubmed.ncbi.nlm.nih.gov/23457378/>
25. Morisset J, Johannson KA, Vittinghoff E, Aravena C, Elicker BM, Jones KD, et al. Use of Mycophenolate Mofetil or Azathioprine for the Management of Chronic Hypersensitivity Pneumonitis. *Chest*. 2017 Mar;151(3):619–25.
26. Idiopathic Pulmonary Fibrosis (an Update) and Progressive Pulmonary Fibrosis in Adults: An Official ATS/ERS/JRS/ALAT Clinical Practice Guideline [Internet]. [cited 2022 Aug 23]. Available from: <https://www.atsjournals.org/doi/epdf/10.1164/rccm.202202-0399ST>
27. Elicker BM, Kallianos KG, Henry TS. The role of high-resolution computed tomography in the follow-up of diffuse lung disease: Number 2 in the Series “Radiology” Edited by Nicola Sverzellati and Sujal Desai. *Eur Respir Rev Off J Eur Respir Soc*. 2017 Jun 30;26(144):170008.
28. SOCIETATEA ROMÂNĂ DE PNEUMOLOGIE, GRUPUL DE LUCRU PENTRU PNEUMOPATII INTERSTIPIALE DIFUZE, ^{a1} SARCOIDOZĂ. Ghid de diagnostic si tratament al PID [Internet]. 2015 [cited 2022 Feb 6]. Available from: <https://www.srp.ro/ghiduri/Ghid%20de%20diagnostic%20si%20tratament%20al%20PID.pdf>
29. Bartholmai BJ, Raghunath S, Karwoski RA, Moua T, Rajagopalan S, Maldonado F, et al. Quantitative CT Imaging of Interstitial Lung Diseases. *J Thorac Imaging*. 2013 Sep;28(5):10.1097/RTI.0b013e3182a21969.
30. Weatherley ND, Eaden JA, Stewart NJ, Bartholmai BJ, Swift AJ, Bianchi SM, et al. Experimental and quantitative imaging techniques in interstitial lung disease. *Thorax*. 2019 Jun;74(6):611–9.
31. Brown KK, Martinez FJ, Walsh SLF, Thannickal VJ, Prasse A, Schlenker-Herceg R, et al. The natural history of progressive fibrosing interstitial lung diseases. *Eur Respir J* [Internet]. 2020 Jun 1 [cited 2022 Oct 3];55(6). Available from: <https://erj.ersjournals.com/content/55/6/2000085>
32. High-resolution CT findings in fibrotic idiopathic interstitial pneumonias with little honeycombing: serial changes and prognostic implications - PubMed [Internet]. [cited 2022 Oct 3]. Available from: <https://pubmed.ncbi.nlm.nih.gov/23096169/>

33. Silva CIS, Müller NL, Hansell DM, Lee KS, Nicholson AG, Wells AU. Nonspecific interstitial pneumonia and idiopathic pulmonary fibrosis: changes in pattern and distribution of disease over time. *Radiology*. 2008 Apr;247(1):251–9.
34. Serial CT analysis in idiopathic pulmonary fibrosis: comparison of visual features that determine patient outcome | *Thorax* [Internet]. [cited 2022 Oct 3]. Available from: <https://thorax.bmj.com/content/75/8/648>
35. Nintedanib in Progressive Fibrosing Interstitial Lung Diseases | *NEJM* [Internet]. [cited 2022 Aug 26]. Available from: <https://www.nejm.org/doi/full/10.1056/NEJMoa1908681>
36. Wells AU, Brown KK, Flaherty KR, Kolb M, Thannickal VJ. What's in a name? That which we call IPF, by any other name would act the same. *Eur Respir J* [Internet]. 2018 May 1 [cited 2022 Aug 26];51(5). Available from: <https://erj.ersjournals.com/content/51/5/1800692>
37. Putman RK, Gudmundsson G, Axelsson GT, Hida T, Honda O, Araki T, et al. Imaging Patterns Are Associated with Interstitial Lung Abnormality Progression and Mortality. *Am J Respir Crit Care Med*. 2019 Jul 15;200(2):175–83.
38. Lynch DA, Sverzellati N, Travis WD, Brown KK, Colby TV, Galvin JR, et al. Diagnostic criteria for idiopathic pulmonary fibrosis: a Fleischner Society White Paper. *Lancet Respir Med*. 2018 Feb;6(2):138–53.
39. Cottin V, Hirani NA, Hotchkiss DL, Nambiar AM, Ogura T, Otaola M, et al. Presentation, diagnosis and clinical course of the spectrum of progressive-fibrosing interstitial lung diseases. *Eur Respir Rev Off J Eur Respir Soc*. 2018 Dec 31;27(150):180076.
40. A Phase 3 Trial of Pirfenidone in Patients with Idiopathic Pulmonary Fibrosis | *NEJM* [Internet]. [cited 2022 Oct 1]. Available from: <https://www.nejm.org/doi/full/10.1056/nejmoa1402582>
41. Pharmacological management of progressive-fibrosing interstitial lung diseases: a review of the current evidence | *European Respiratory Society* [Internet]. [cited 2022 Oct 1]. Available from: <https://err.ersjournals.com/content/27/150/180074>
42. Mikolasch TA, Garthwaite HS, Porter JC. Update in diagnosis and management of interstitial lung disease. *Clin Med*. 2017 Apr;17(2):146–53.
43. Maher TM, Streck ME. Antifibrotic therapy for idiopathic pulmonary fibrosis: time to treat. *Respir Res*. 2019 Sep 6;20(1):205.

44. Practice guidelines for interstitial lung diseases: Widening... : Lung India [Internet]. [cited 2022 Oct 3]. Available from: https://journals.lww.com/lungindia/Fulltext/2020/37040/Practice_guidelines_for_interstitial_lung.1.aspx
45. Jacobs SS, Krishnan JA, Lederer DJ, Ghazipura M, Hossain T, Tan AYM, et al. Home Oxygen Therapy for Adults with Chronic Lung Disease. An Official American Thoracic Society Clinical Practice Guideline. *Am J Respir Crit Care Med*. 2020 Nov 15;202(10):e121–41.
46. De Oliveira NC, Osaki S, Maloney J, Cornwell RD, Meyer KC. Lung transplant for interstitial lung disease: outcomes for single versus bilateral lung transplantation. *Interact Cardiovasc Thorac Surg*. 2012 Mar;14(3):263–7.
47. Leung AN, Staples CA, Müller NL. Chronic diffuse infiltrative lung disease: comparison of diagnostic accuracy of high-resolution and conventional CT. *AJR Am J Roentgenol*. 1991 Oct;157(4):693–6.
48. Remy-Jardin M, Remy J, Deffontaines C, Duhamel A. Assessment of diffuse infiltrative lung disease: comparison of conventional CT and high-resolution CT. *Radiology*. 1991 Oct;181(1):157–62.
49. Hochegger B, Marchiori E, Zanon M, Rubin AS, Fragomeni R, Altmayer S, et al. Imaging in idiopathic pulmonary fibrosis: diagnosis and mimics. *Clin Sao Paulo Braz*. 2019 Feb 4;74:e225.
50. Amador C, Weber C, Varacallo M. Anatomy, Thorax, Bronchial. In: *StatPearls* [Internet]. Treasure Island (FL): StatPearls Publishing; 2022 [cited 2022 Feb 6]. Available from: <http://www.ncbi.nlm.nih.gov/books/NBK537353/>
51. Signs and Patterns of Lung Disease - Chest Radiology: The Essentials, 2nd Edition [Internet]. [cited 2022 Feb 6]. Available from: <https://doctorlib.info/medical/chest/2.html>
52. The Radiology Assistant : Basic Interpretation [Internet]. [cited 2022 Feb 6]. Available from: <https://radiologyassistant.nl/chest/hrct/basic-interpretation>
53. Cristian Oancea Ovidiu Fira-Mlădinescu Voicu Tudorache V. *Tratat de Pneumologie pentru medici rezidenti*. In: *Capitolul 3 Metode de investigatie imagistica a patologiei pulmonare*. p. 42–59.
54. Fleischner Society: Glossary of Terms for Thoracic Imaging | Radiology [Internet]. [cited 2022 Feb 6]. Available from: <https://pubs.rsna.org/doi/abs/10.1148/radiol.2462070712?journalCode=radiology>

55. Verschakelen JA, De Wever W. Nodular Pattern. In: Verschakelen JA, De Wever W, editors. *Computed Tomography of the Lung: A Pattern Approach* [Internet]. Berlin, Heidelberg: Springer; 2018 [cited 2022 Feb 6]. p. 81–101. (Medical Radiology). Available from: https://doi.org/10.1007/978-3-642-39518-5_6
56. Akira M, Kozuka T, Yamamoto S, Sakatani M. Computed tomography findings in acute exacerbation of idiopathic pulmonary fibrosis. *Am J Respir Crit Care Med*. 2008 Aug 15;178(4):372–8.
57. Kim DS, Park JH, Park BK, Lee JS, Nicholson AG, Colby T. Acute exacerbation of idiopathic pulmonary fibrosis: frequency and clinical features. *Eur Respir J*. 2006 Jan;27(1):143–50.
58. Li L, Qin L, Xu Z, Yin Y, Wang X, Kong B, et al. Using Artificial Intelligence to Detect COVID-19 and Community-acquired Pneumonia Based on Pulmonary CT: Evaluation of the Diagnostic Accuracy. *Radiology*. 2020 Aug;296(2):E65–71.
59. Collins Jannette and Stern Eric J. Alveolar Lung Disease - Chest Radiology: The Essentials, 2nd Edition [Internet]. [cited 2022 Feb 6]. Available from: <https://doctorlib.info/medical/chest/4.html>
60. Organizing Pneumonia - an overview | ScienceDirect Topics [Internet]. [cited 2022 Feb 12]. Available from: <https://www.sciencedirect.com/topics/pharmacology-toxicology-and-pharmaceutical-science/organizing-pneumonia>
61. Dhagat PK, Singh S, Jain M, Singh SN, Sharma RK. Thoracic Sarcoidosis: Imaging with High Resolution Computed Tomography. *J Clin Diagn Res JCDR*. 2017 Feb;11(2):TC15–8.
62. Grassi R, Belfiore MP, Montanelli A, Patelli G, Urraro F, Giacobbe G, et al. COVID-19 pneumonia: computer-aided quantification of healthy lung parenchyma, emphysema, ground glass and consolidation on chest computed tomography (CT). *Radiol Med (Torino)*. 2021 Apr;126(4):553–60.
63. Hovinga M, Sprengers R, Kauczor HU, Schaefer-Prokop C. CT Imaging of Interstitial Lung Diseases. *Multidetector-Row CT Thorax*. 2016 Feb 27;105–30.
64. Desai SR, Prosch H, Galvin JR. Plain Film and HRCT Diagnosis of Interstitial Lung Disease. In: Hodler J, Kubik-Huch RA, von Schulthess GK, editors. *Diseases of the Chest, Breast, Heart and Vessels 2019-2022: Diagnostic and Interventional Imaging* [Internet]. Cham (CH): Springer; 2019 [cited 2022 Feb 6]. (IDKD Springer Series). Available from: <http://www.ncbi.nlm.nih.gov/books/NBK553872/>

65. Takahashi M, Fukuoka J, Nitta N, Takazakura R, Nagatani Y, Murakami Y, et al. Imaging of pulmonary emphysema: A pictorial review. *Int J Chron Obstruct Pulmon Dis*. 2008 Jun;3(2):193–204.
66. Hobbs S, Chung JH, Leb J, Kaproth-Joslin K, Lynch DA. Practical Imaging Interpretation in Patients Suspected of Having Idiopathic Pulmonary Fibrosis: Official Recommendations from the Radiology Working Group of the Pulmonary Fibrosis Foundation. *Radiol Cardiothorac Imaging*. 2021 Feb 1;3(1):e200279.
67. Caltabiano DC, Costanzo V, Mammino L, Vindigni V, Torrisi S, Rosso R, et al. Cystic pattern in lung diseases: a simplified HRCT guide based on free-hand drawings [Internet]. ECR 2017 EPOS. European Congress of Radiology - ECR 2017; 2017 [cited 2022 Feb 13]. Available from: <https://epos.myesr.org/poster/esr/ecr2017/C-2141>
68. Muzio BD. Air trapping | Radiology Reference Article | Radiopaedia.org [Internet]. Radiopaedia. [cited 2022 Sep 30]. Available from: <https://radiopaedia.org/articles/air-trapping>
69. Gupta N, Vassallo R, Wikenheiser-Brokamp KA, McCormack FX. Diffuse Cystic Lung Disease. Part II. *Am J Respir Crit Care Med*. 2015 Jul 1;192(1):17–29.
70. Galvin JR, Frazier AA, Franks TJ. Collaborative radiologic and histopathologic assessment of fibrotic lung disease. *Radiology*. 2010 Jun;255(3):692–706.
71. Piciocchi S, Tomassetti S, Ravaglia C, Gurioli C, Gurioli C, Dubini A, et al. From “traction bronchiectasis” to honeycombing in idiopathic pulmonary fibrosis: A spectrum of bronchiolar remodeling also in radiology? *BMC Pulm Med*. 2016 May 23;16(1):87.
72. Watadani T, Sakai F, Johkoh T, Noma S, Akira M, Fujimoto K, et al. Interobserver variability in the CT assessment of honeycombing in the lungs. *Radiology*. 2013 Mar;266(3):936–44.
73. Johkoh T, Sumikawa H, Fukuoka J, Tanaka T, Fujimoto K, Takahashi M, et al. Do you really know precise radiologic-pathologic correlation of usual interstitial pneumonia? *Eur J Radiol*. 2014 Jan;83(1):20–6.
74. Torres PPTES, Rabahi MF, Moreira MA do C, Escuissato DL, Meirelles G de SP, Marchiori E. Importance of chest HRCT in the diagnostic evaluation of fibrosing interstitial lung diseases. *J Bras Pneumol Publicacao Of Soc Bras Pneumol E Tisiologia*. 2021;47(3):e20200096.
75. Dalpiaz G, Cancellieri A. Alveolar Pattern. *Atlas Diffuse Lung Dis*. 2016 Dec 8;145–62.
76. Ridge CA, Bankier AA, Eisenberg RL. Mosaic attenuation. *AJR Am J Roentgenol*. 2011 Dec;197(6):W970-977.

77. Henson N. Mosaic attenuation pattern in lung | Radiology Reference Article | Radiopaedia.org [Internet]. Radiopaedia. [cited 2022 Sep 30]. Available from: <https://radiopaedia.org/articles/mosaic-attenuation-pattern-in-lung>
78. Gaillard F. Head cheese sign (lungs) | Radiology Reference Article | Radiopaedia.org [Internet]. Radiopaedia. [cited 2022 Feb 12]. Available from: <https://radiopaedia.org/articles/head-cheese-sign-lungs>
79. Meira Dias O, Baldi B, Pennati F, Aliverti A, Chate R, Sawamura MVY, et al. Computed tomography in hypersensitivity pneumonitis: main findings, differential diagnosis and pitfalls. *Expert Rev Respir Med*. 2018 Jan 2;12:5–13.
80. Rossi SE, Erasmus JJ, Volpacchio M, Franquet T, Castiglioni T, McAdams HP. “Crazy-Paving” Pattern at Thin-Section CT of the Lungs: Radiologic-Pathologic Overview. *RadioGraphics*. 2003 Nov;23(6):1509–19.
81. De Wever W, Meersschaert J, Coolen J, Verbeken E, Verschakelen JA. The crazy-paving pattern: a radiological-pathological correlation. *Insights Imaging*. 2011 Apr;2(2):117–32.
82. Hansell DM, Bankier AA, MacMahon H, McLoud TC, Müller NL, Remy J. Fleischner Society: glossary of terms for thoracic imaging. *Radiology*. 2008 Mar;246(3):697–722.
83. Walsh SLF, Robertson BJ. The atoll sign. *Thorax*. 2010 Nov 1;65(11):1029–30.
84. Godoy MCB, Viswanathan C, Marchiori E, Truong MT, Benveniste MF, Rossi S, et al. The reversed halo sign: update and differential diagnosis. *Br J Radiol*. 2012 Sep;85(1017):1226–35.
85. Verri G, Lyberis P, Solidoro P, Mercante L, Bardessono MM, Roffinella M, et al. Correlation between HRTC appearance and histopathological features in the diagnosis of interstitial lung diseases. *Eur Respir J* [Internet]. 2018 Sep 15 [cited 2022 Oct 1];52(suppl 62). Available from: https://erj.ersjournals.com/content/52/suppl_62/PA2935
86. Kebbe J, Abdo T. Interstitial lung disease: the diagnostic role of bronchoscopy. *J Thorac Dis*. 2017 Sep;9(Suppl 10):S996–1010.
87. Trusculescu AA, Manolescu D, Tudorache E, Oancea C. Deep learning in interstitial lung disease-how long until daily practice. *Eur Radiol*. 2020 Nov;30(11):6285–92.
88. Nathan SD, Pastre J, Ksovreli I, Barnett S, King C, Aryal S, et al. HRCT evaluation of patients with interstitial lung disease: comparison of the 2018 and 2011 diagnostic guidelines. *Ther Adv Respir Dis*. 2020 Dec;14:1753466620968496.

89. Raghu G, Collard HR, Egan JJ, Martinez FJ, Behr J, Brown KK, et al. An official ATS/ERS/JRS/ALAT statement: idiopathic pulmonary fibrosis: evidence-based guidelines for diagnosis and management. *Am J Respir Crit Care Med*. 2011 Mar 15;183(6):788–824.
90. Nonspecific Interstitial Pneumonia - Pulmonary Disorders [Internet]. MSD Manual Professional Edition. [cited 2022 Feb 13]. Available from: <https://www.msmanuals.com/professional/pulmonary-disorders/interstitial-lung-diseases/nonspecific-interstitial-pneumonia>
91. Weerakkody Y. Non-specific interstitial pneumonia | Radiology Reference Article | Radiopaedia.org [Internet]. Radiopaedia. [cited 2022 Feb 13]. Available from: <https://radiopaedia.org/articles/non-specific-interstitial-pneumonia-1>
92. Travis WD, Matsui K, Moss J, Ferrans VJ. Idiopathic nonspecific interstitial pneumonia: prognostic significance of cellular and fibrosing patterns: survival comparison with usual interstitial pneumonia and desquamative interstitial pneumonia. *Am J Surg Pathol*. 2000 Jan;24(1):19–33.
93. Nayfeh AS, Chippa V, Moore DR. Nonspecific Interstitial Pneumonitis. In: StatPearls [Internet]. Treasure Island (FL): StatPearls Publishing; 2022 [cited 2022 Sep 29]. Available from: <http://www.ncbi.nlm.nih.gov/books/NBK518974/>
94. Katzenstein AL, Myers JL, Mazur MT. Acute interstitial pneumonia. A clinicopathologic, ultrastructural, and cell kinetic study. *Am J Surg Pathol*. 1986 Apr;10(4):256–67.
95. Ichikado K. High-resolution computed tomography findings of acute respiratory distress syndrome, acute interstitial pneumonia, and acute exacerbation of idiopathic pulmonary fibrosis. *Semin Ultrasound CT MR*. 2014 Feb;35(1):39–46.
96. Robertson BJ, Hansell DM. Organizing pneumonia: a kaleidoscope of concepts and morphologies. *Eur Radiol*. 2011 Nov;21(11):2244–54.
97. Baque-Juston M, Pellegrin A, Leroy S, Marquette CH, Padovani B. Organizing pneumonia: What is it? A conceptual approach and pictorial review. *Diagn Interv Imaging*. 2014 Sep 1;95(9):771–7.
98. Hellemons ME, Moor CC, Thüsen J von der, Rossius M, Odink A, Thorgersen LH, et al. Desquamative interstitial pneumonia: a systematic review of its features and outcomes. *Eur Respir Rev* [Internet]. 2020 Jun 30 [cited 2022 Feb 10];29(156). Available from: <https://err.ersjournals.com/content/29/156/190181>

99. Diken ÖE, Şengül A, Beyan AC, Ayten Ö, Mutlu LC, Okutan O. Desquamative interstitial pneumonia: Risk factors, laboratory and bronchoalveolar lavage findings, radiological and histopathological examination, clinical features, treatment and prognosis. *Exp Ther Med*. 2019 Jan;17(1):587–95.
100. Gaillard F. Respiratory bronchiolitis-interstitial lung disease | Radiology Reference Article | Radiopaedia.org [Internet]. Radiopaedia. [cited 2022 Feb 13]. Available from: <https://radiopaedia.org/articles/respiratory-bronchiolitis-interstitial-lung-disease-2>
101. Gaillard F. Respiratory bronchiolitis-interstitial lung disease | Radiology Reference Article | Radiopaedia.org [Internet]. Radiopaedia. 2022 [cited 2022 Feb 13]. Available from: <https://radiopaedia.org/articles/respiratory-bronchiolitis-interstitial-lung-disease-2>
102. Sieminska A, Kuziemska K. Respiratory bronchiolitis-interstitial lung disease. *Orphanet J Rare Dis*. 2014 Jul 11;9:106.
103. Ryu JH, Colby TV, Hartman TE, Vassallo R. Smoking-related interstitial lung diseases: a concise review. *Eur Respir J*. 2001 Jan;17(1):122–32.
104. Kumar A, Cherian SV, Vassallo R, Yi ES, Ryu JH. Current Concepts in Pathogenesis, Diagnosis, and Management of Smoking-Related Interstitial Lung Diseases. *CHEST*. 2018 Aug 1;154(2):394–408.
105. Margaritopoulos GA, Vasarmidi E, Jacob J, Wells AU, Antoniou KM. Smoking and interstitial lung diseases. *Eur Respir Rev*. 2015 Sep 1;24(137):428–35.
106. Konopka KE, Myers JL. A Review of Smoking-Related Interstitial Fibrosis, Respiratory Bronchiolitis, and Desquamative Interstitial Pneumonia: Overlapping Histology and Confusing Terminology. *Arch Pathol Lab Med*. 2018 Oct 1;142(10):1177–81.
107. Basset F, Corrin B, Spencer H, Lacronique J, Roth C, Soler P, et al. Pulmonary histiocytosis X. *Am Rev Respir Dis*. 1978 Nov;118(5):811–20.
108. Avila NA, Kelly JA, Dwyer AJ, Johnson DL, Jones EC, Moss J. Lymphangioliomyomatosis: correlation of qualitative and quantitative thin-section CT with pulmonary function tests and assessment of dependence on pleurodesis. *Radiology*. 2002 Apr;223(1):189–97.
109. Zaveri J, La Q, Yarmish G, Neuman J. More than Just Langerhans Cell Histiocytosis: A Radiologic Review of Histiocytic Disorders. *RadioGraphics*. 2014 Nov;34(7):2008–24.
110. Chitnis A, Vyas PK, Chaudhary P, Ghatavat G. Case-based discussion: Lymphocytic interstitial pneumonia a rare presentation in an immunocompetent adult male. *Lung India Off Organ Indian Chest Soc*. 2015;32(5):500–4.

111. Narula N, Iannuzzi M. Sarcoidosis: Pitfalls and Challenging Mimickers. *Front Med*. 2021 Jan 11;7:594275.
112. Tana C, Donatiello I, Coppola MG, Ricci F, Maccarone MT, Ciarambino T, et al. CT Findings in Pulmonary and Abdominal Sarcoidosis. Implications for Diagnosis and Classification. *J Clin Med*. 2020 Sep 20;9(9):3028.
113. Raouf S, Amchentshev A, Vlahos I, Goud A, Naidich DP. Pictorial essay: multinodular disease: a high-resolution CT scan diagnostic algorithm. *Chest*. 2006 Mar;129(3):805–15.
114. Maller VG. Sarcoidosis (thoracic manifestations) | Radiology Reference Article | Radiopaedia.org [Internet]. Radiopaedia. [cited 2022 Sep 30]. Available from: <https://radiopaedia.org/articles/sarcoidosis-thoracic-manifestations-2>
115. Oh SJ, Choo JY, Lee KY, Kim JH, Yeom SK. Localized Pulmonary Alveolar Proteinosis: Two Case Reports. *Balk Med J*. 2014 Sep;31(3):257–60.
116. Tateishi T, Ohtani Y, Takemura T, Akashi T, Miyazaki Y, Inase N, et al. Serial high-resolution computed tomography findings of acute and chronic hypersensitivity pneumonitis induced by avian antigen. *J Comput Assist Tomogr*. 2011 Apr;35(2):272–9.
117. Selman M. Hypersensitivity pneumonitis: a multifaceted deceiving disorder. *Clin Chest Med*. 2004 Sep;25(3):531–47, vi.
118. Problem Solving in Chest Imaging - 1st Edition [Internet]. [cited 2022 Feb 6]. Available from: <https://www.elsevier.com/books/problem-solving-in-chest-imaging/digumarthy/978-0-323-04132-4>
119. Wallis A, Spinks K. The diagnosis and management of interstitial lung diseases. *BMJ*. 2015 May 7;350:h2072.
120. Pleuroparenchymal fibroelastosis in patients with idiopathic pulmonary fibrosis - Lee - 2020 - Respirology - Wiley Online Library [Internet]. [cited 2022 Oct 5]. Available from: <https://onlinelibrary.wiley.com/doi/10.1111/resp.13796>
121. Oda T, Ogura T, Kitamura H, Hagiwara E, Baba T, Enomoto Y, et al. Distinct Characteristics of Pleuroparenchymal Fibroelastosis With Usual Interstitial Pneumonia Compared With Idiopathic Pulmonary Fibrosis. *CHEST*. 2014 Nov 1;146(5):1248–55.
122. Aburto M, Herráez I, Iturbe D, Jiménez-Romero A. Diagnosis of Idiopathic Pulmonary Fibrosis: Differential Diagnosis. *Med Sci*. 2018 Sep 4;6(3):73.
123. Indeterminate for UIP Pattern – IPF Radiology Rounds [Internet]. [cited 2022 Oct 5]. Available from: <https://www.ipfradiologyrounds.com/hrct-ild-diagnosis/indeterminate-uip-pattern/>

124. Kolb M, Richeldi L, Behr J, Maher TM, Tang W, Stowasser S, et al. Nintedanib in patients with idiopathic pulmonary fibrosis and preserved lung volume. *Thorax*. 2017 Apr;72(4):340–6.
125. Meyer KC. Diagnosis and management of interstitial lung disease. *Transl Respir Med*. 2014 Feb 13;2:4.
126. Manolescu D, Davidescu L, Traila D, Oancea C, Tudorache V. The reliability of lung ultrasound in assessment of idiopathic pulmonary fibrosis. *Clin Interv Aging*. 2018;13:437–49.
127. Raghu G, Chen SY, Yeh WS, Maroni B, Li Q, Lee YC, et al. Idiopathic pulmonary fibrosis in US Medicare beneficiaries aged 65 years and older: incidence, prevalence, and survival, 2001–11. *Lancet Respir Med*. 2014 Jul 1;2(7):566–72.
128. Walsh SLF, Calandriello L, Sverzellati N, Wells AU, Hansell DM, UIP Observer Consort. Interobserver agreement for the ATS/ERS/JRS/ALAT criteria for a UIP pattern on CT. *Thorax*. 2016 Jan;71(1):45–51.
129. Nicholson A, Addis B, Bharucha H, Clelland C, Corrin B, Gibbs A, et al. Inter-observer variation between pathologists in diffuse parenchymal lung disease. *Thorax*. 2004 Jun;59(6):500–5.
130. Prasad R, Gupta N, Singh A, Gupta P. Diagnosis of idiopathic pulmonary fibrosis: Current issues. *Intractable Rare Dis Res*. 2015 May;4(2):65–9.
131. Walsh SLF, Kolb M. Radiological diagnosis of interstitial lung disease: is it all about pattern recognition? *Eur Respir J [Internet]*. 2018 Aug 1 [cited 2022 Feb 12];52(2). Available from: <https://erj.ersjournals.com/content/52/2/1801321>
132. Xaubet A, Ancochea J, Bollo E, Fernández-Fabrellas E, Franquet T, Molina-Molina M, et al. Guidelines for the Diagnosis and Treatment of Idiopathic Pulmonary Fibrosis. *Arch Bronconeumol*. 2013 Aug 1;49(8):343–53.
133. Piotrowski WJ, Bestry I, Białas AJ, Boros PW, Grzanka P, Jassem E, et al. Guidelines of the Polish Respiratory Society for diagnosis and treatment of idiopathic pulmonary fibrosis. *Adv Respir Med*. 2020;88(1):41–93.
134. Wong AW, Fidler L, Marcoux V, Johannson KA, Assayag D, Fisher JH, et al. Practical Considerations for the Diagnosis and Treatment of Fibrotic Interstitial Lung Disease During the Coronavirus Disease 2019 Pandemic. *Chest*. 2020 Sep;158(3):1069–78.
135. Hernández-González F, Lucena CM, Ramírez J, Sánchez M, Jimenez MJ, Xaubet A, et al. Cryobiopsy in the diagnosis of diffuse interstitial lung disease: yield and cost-effectiveness analysis. *Arch Bronconeumol*. 2015 Jun;51(6):261–7.

136. Cottin V, Crestani B, Cadranet J, Cordier JF, Marchand-Adam S, Prévot G, et al. French practical guidelines for the diagnosis and management of idiopathic pulmonary fibrosis - 2017 update. Full-length version. *Rev Mal Respir.* 2017 Oct;34(8):900–68.
137. Robalo Cordeiro C, Campos P, Carvalho L, Campinha S, Clemente S, Figueiredo L, et al. Consensus document for the diagnosis and treatment of idiopathic pulmonary fibrosis: Joint Consensus of Sociedade Portuguesa de Pneumologia, Sociedade Portuguesa de Radiologia e Medicina Nuclear e Sociedade Portuguesa de Anatomia Patológica. *Rev Port Pneumol.* 2016 Apr;22(2):112–22.
138. du Bois RM. An earlier and more confident diagnosis of idiopathic pulmonary fibrosis. *Eur Respir Rev Off J Eur Respir Soc.* 2012 Jun 1;21(124):141–6.
139. Utility of a Lung Biopsy for the Diagnosis of Idiopathic Pulmonary Fibrosis | *American Journal of Respiratory and Critical Care Medicine* [Internet]. [cited 2022 Oct 7]. Available from: https://www.atsjournals.org/doi/10.1164/ajrccm.164.2.2101090?url_ver=Z39.88-2003&rfr_id=ori:rid:crossref.org&rfr_dat=cr_pub%20%20pubmed
140. Wells A. Clinical usefulness of high resolution computed tomography in cryptogenic fibrosing alveolitis. *Thorax.* 1998 Dec 1;53(12):1080–7.
141. Fibrotic idiopathic interstitial pneumonias: HRCT findings that predict mortality | *SpringerLink* [Internet]. [cited 2022 Oct 7]. Available from: <https://link.springer.com/article/10.1007/s00330-011-2098-2>
142. Interstitial Lung Disease in Systemic Sclerosis | A Simple Staging System | *American Journal of Respiratory and Critical Care Medicine* [Internet]. [cited 2022 Oct 7]. Available from: https://www.atsjournals.org/doi/10.1164/rccm.200706-877OC?url_ver=Z39.88-2003&rfr_id=ori:rid:crossref.org&rfr_dat=cr_pub%20%20pubmed
143. An integrated clinicroadiological staging system for pulmonary sarcoidosis: a case-cohort study - *The Lancet Respiratory Medicine* [Internet]. [cited 2022 Oct 7]. Available from: [https://www.thelancet.com/journals/lanres/article/PIIS2213-2600\(13\)70276-5/fulltext](https://www.thelancet.com/journals/lanres/article/PIIS2213-2600(13)70276-5/fulltext)
144. Transbronchial Lung Cryobiopsy in Patients with Interstitial Lung Disease: A Systematic Review - *PubMed* [Internet]. [cited 2022 Oct 7]. Available from: <https://pubmed.ncbi.nlm.nih.gov/35499855/>
145. Sverzellati N. Highlights of HRCT imaging in IPF. *Respir Res.* 2013;14 Suppl 1:S3.

146. de Lima GVL, Castilho TR, Bugatti PH, Saito PTM, Lopes FM. A Complex Network-Based Approach to the Analysis and Classification of Images. In: Pardo A, Kittler J, editors. *Progress in Pattern Recognition, Image Analysis, Computer Vision, and Applications*. Cham: Springer International Publishing; 2015. p. 322–30.
147. Mourchid Y, Hassouni ME, Cherifi H. A General Framework for Complex Network-Based Image Segmentation. *Multimed Tools Appl*. 2019 Jul;78(14):20191–216.
148. Inomata M, Jo T, Kuse N, Awano N, Tone M, Yoshimura H, et al. Clinical impact of the radiological indeterminate for usual interstitial pneumonia pattern on the diagnosis of idiopathic pulmonary fibrosis. *Respir Investig*. 2021 Jan;59(1):81–9.
149. Walsh SLF, Wells AU, Desai SR, Poletti V, Piciocchi S, Dubini A, et al. Multicentre evaluation of multidisciplinary team meeting agreement on diagnosis in diffuse parenchymal lung disease: a case-cohort study. *Lancet Respir Med*. 2016 Jul;4(7):557–65.
150. Crews MS, Bartholmai BJ, Adegunsoye A, Oldham JM, Montner SM, Karwoski RA, et al. Automated CT Analysis of Major Forms of Interstitial Lung Disease. *J Clin Med*. 2020 Nov 23;9(11):E3776.
151. Simonyan K, Zisserman A. Very Deep Convolutional Networks for Large-Scale Image Recognition. *ArXiv14091556 Cs [Internet]*. 2015 Apr 10 [cited 2022 Feb 6]; Available from: <http://arxiv.org/abs/1409.1556>
152. Li Q, Cai W, Wang X, Zhou Y, Feng DD, Chen M. Medical image classification with convolutional neural network. In: 2014 13th International Conference on Control Automation Robotics Vision (ICARCV). 2014. p. 844–8.
153. Walsh SLF, Calandriello L, Silva M, Sverzellati N. Deep learning for classifying fibrotic lung disease on high-resolution computed tomography: a case-cohort study. *Lancet Respir Med*. 2018 Nov 1;6(11):837–45.
154. Li Q, Cai W, Feng DD. Lung image patch classification with automatic feature learning. *Annu Int Conf IEEE Eng Med Biol Soc IEEE Eng Med Biol Soc Annu Int Conf*. 2013;2013:6079–82.
155. Doi K. Computer-aided diagnosis in medical imaging: historical review, current status and future potential. *Comput Med Imaging Graph Off J Comput Med Imaging Soc*. 2007 Jul;31(4–5):198–211.
156. Takahashi R, Kajikawa Y. Computer-aided diagnosis: A survey with bibliometric analysis. *Int J Med Inf*. 2017 May;101:58–67.
157. Hamet P, Tremblay J. Artificial intelligence in medicine. *Metabolism*. 2017 Apr;69S:S36–40.

158. Meyer KC. Diagnosis and management of interstitial lung disease. *Transl Respir Med*. 2014;2:4.
159. Broască L, Truşculescu AA, Ancuşa VM, Ciocârlie H, Oancea CI, Stoicescu ER, et al. A Novel Method for Lung Image Processing Using Complex Networks. 2022 Jul 11 [cited 2022 Jul 13]; Available from: <https://www.preprints.org/manuscript/202207.0156/v1>
160. Truşculescu A, Broască L, Ancuşa VM, Manolescu D, Tudorache E, Oancea C. Managing Interstitial Lung Diseases with Computer-Aided Visualization. In: Kumar Bhoi A, Mallick PK, Narayana Mohanty M, Albuquerque VHC de, editors. *Hybrid Artificial Intelligence and IoT in Healthcare* [Internet]. Singapore: Springer; 2021 [cited 2022 Oct 8]. p. 245–71. (Intelligent Systems Reference Library). Available from: https://doi.org/10.1007/978-981-16-2972-3_12
161. Lecun Y, Bengio Y, Hinton G. Deep learning. *Nat Cell Biol* [Internet]. 2015 May 27 [cited 2022 Jul 6];521(7553):436–44. Available from: <http://www.scopus.com/inward/record.url?scp=84930630277&partnerID=8YFLogxK>
162. Schmidhuber J. Deep Learning in Neural Networks: An Overview. *Neural Netw* [Internet]. 2015 Jan [cited 2022 Jul 8];61:85–117. Available from: <http://arxiv.org/abs/1404.7828>
163. Murphy A, Skalski M, Gaillard F. The utilisation of convolutional neural networks in detecting pulmonary nodules: a review. *Br J Radiol*. 2018 Oct;91(1090):20180028.
164. Sutskever I, Vinyals O, Le QV. Sequence to Sequence Learning with Neural Networks [Internet]. arXiv; 2014 [cited 2022 Jul 6]. Available from: <http://arxiv.org/abs/1409.3215>
165. Mikolov T, Deoras A, Povey D, Burget L, Cernocky J. Strategies for training large scale neural network language models. In: 2011 IEEE Workshop on Automatic Speech Recognition & Understanding [Internet]. Waikoloa, HI, USA: IEEE; 2011 [cited 2022 Jul 6]. p. 196–201. Available from: <http://ieeexplore.ieee.org/document/6163930/>
166. Ciregan D, Meier U, Schmidhuber J. Multi-column deep neural networks for image classification. In: 2012 IEEE Conference on Computer Vision and Pattern Recognition. 2012. p. 3642–9.
167. Lecun Y, Boser B, Denker JS, Henderson D, Howard RE, Hubbard W, et al. Handwritten digit recognition with a back-propagation network. Touretzky D, editor. *Adv Neural Inf Process Syst NIPS 1989 Denver CO*. 1990;2.

168. Krizhevsky A, Sutskever I, Hinton GE. ImageNet Classification with Deep Convolutional Neural Networks. In: *Advances in Neural Information Processing Systems* [Internet]. Curran Associates, Inc.; 2012 [cited 2022 Jul 6]. Available from: <https://proceedings.neurips.cc/paper/2012/hash/c399862d3b9d6b76c8436e924a68c45b-Abstract.html>
169. Lee JG, Jun S, Cho YW, Lee H, Kim GB, Seo JB, et al. Deep Learning in Medical Imaging: General Overview. *Korean J Radiol.* 2017 Aug;18(4):570–84.
170. Soffer S, Ben-Cohen A, Shimon O, Amitai MM, Greenspan H, Klang E. Convolutional Neural Networks for Radiologic Images: A Radiologist's Guide. *Radiology.* 2019 Mar;290(3):590–606.
171. Lo SCB, Lin JS, Freedman MT, Mun SK. Computer-assisted diagnosis of lung nodule detection using artificial convolution neural network. In: *Medical Imaging 1993: Image Processing.* SPIE; 1993. p. 859–69.
172. Sahiner B, Chan HP, Petrick N, Wei D, Helvie MA, Adler DD, et al. Classification of mass and normal breast tissue: a convolution neural network classifier with spatial domain and texture images. *IEEE Trans Med Imaging.* 1996 Oct;15(5):598–610.
173. Döhler F, Mormann F, Weber B, Elger C, Lehnertz K. A cellular neural network based method for classification of magnetic resonance images: Towards an automated detection of hippocampal sclerosis. *J Neurosci Methods.* 2008 Jun 1;170:324–31.
174. Christodoulidis S, Anthimopoulos M, Ebner L, Christe A, Mougiakakou S. Multisource Transfer Learning With Convolutional Neural Networks for Lung Pattern Analysis. *IEEE J Biomed Health Inform.* 2017 Jan;21(1):76–84.
175. Bar Y, Diamant I, Wolf L, Greenspan H. Deep learning with non-medical training used for chest pathology identification. In: *Medical Imaging 2015: Computer-Aided Diagnosis* [Internet]. SPIE; 2015 [cited 2022 Jul 6]. p. 215–21. Available from: <https://www.spiedigitallibrary.org/conference-proceedings-of-spie/9414/94140V/Deep-learning-with-non-medical-training-used-for-chest-pathology/10.1117/12.2083124.full>
176. Suzuki K. Overview of deep learning in medical imaging. *Radiol Phys Technol.* 2017 Sep;10(3):257–73.
177. Esteva A, Kuprel B, Novoa RA, Ko J, Swetter SM, Blau HM, et al. Dermatologist-level classification of skin cancer with deep neural networks. *Nature* [Internet]. 2017 Feb [cited 2022 Jul 6];542(7639):115–8. Available from: <https://www.nature.com/articles/nature21056>

178. Prasoon A, Petersen K, Igel C, Lauze F, Dam E, Nielsen M. Deep Feature Learning for Knee Cartilage Segmentation Using a Triplanar Convolutional Neural Network. In: Mori K, Sakuma I, Sato Y, Barillot C, Navab N, editors. *Medical Image Computing and Computer-Assisted Intervention – MICCAI 2013*. Berlin, Heidelberg: Springer; 2013. p. 246–53. (Lecture Notes in Computer Science).
179. Pereira S, Pinto A, Alves V, Silva CA. Brain Tumor Segmentation Using Convolutional Neural Networks in MRI Images. *IEEE Trans Med Imaging*. 2016 May;35(5):1240–51.
180. Han S, Kang HK, Jeong JY, Park MH, Kim W, Bang WC, et al. A deep learning framework for supporting the classification of breast lesions in ultrasound images. *Phys Med Biol*. 2017 Sep 15;62(19):7714–28.
181. Kooi T, Litjens G, van Ginneken B, Gubern-Mérida A, Sánchez CI, Mann R, et al. Large scale deep learning for computer aided detection of mammographic lesions. *Med Image Anal*. 2017 Jan;35:303–12.
182. Ciompi F, de Hoop B, van Riel SJ, Chung K, Scholten ET, Oudkerk M, et al. Automatic classification of pulmonary peri-fissural nodules in computed tomography using an ensemble of 2D views and a convolutional neural network out-of-the-box. *Med Image Anal*. 2015 Dec;26(1):195–202.
183. Tu X, Xie M, Gao J, Ma Z, Chen D, Wang Q, et al. Automatic Categorization and Scoring of Solid, Part-Solid and Non-Solid Pulmonary Nodules in CT Images with Convolutional Neural Network. *Sci Rep* [Internet]. 2017 Sep 1 [cited 2022 Jul 6];7(1):8533. Available from: <https://www.nature.com/articles/s41598-017-08040-8>
184. Lopes UK, Valiati JF. Pre-trained convolutional neural networks as feature extractors for tuberculosis detection. *Comput Biol Med*. 2017 Oct 1;89:135–43.
185. Cicero M, Bilbily A, Colak E, Dowdell T, Gray B, Perampaladas K, et al. Training and Validating a Deep Convolutional Neural Network for Computer-Aided Detection and Classification of Abnormalities on Frontal Chest Radiographs. *Invest Radiol*. 2017 May;52(5):281–7.
186. Kim GB, Jung KH, Lee Y, Kim HJ, Kim N, Jun S, et al. Comparison of Shallow and Deep Learning Methods on Classifying the Regional Pattern of Diffuse Lung Disease. *J Digit Imaging*. 2018 Aug;31(4):415–24.
187. Wang Q, Zheng Y, Yang G, Jin W, Chen X, Yin Y. Multiscale Rotation-Invariant Convolutional Neural Networks for Lung Texture Classification. *IEEE J Biomed Health Inform*. 2018 Jan;22(1):184–95.

188. Anthimopoulos M, Christodoulidis S, Ebner L, Christe A, Mougiakakou S. Lung Pattern Classification for Interstitial Lung Diseases Using a Deep Convolutional Neural Network. *IEEE Trans Med Imaging*. 2016 May;35(5):1207–16.
189. Gao M, Bagci U, Lu L, Wu A, Buty M, Shin HC, et al. Holistic classification of CT attenuation patterns for interstitial lung diseases via deep convolutional neural networks. *Comput Methods Biomech Biomed Eng Imaging Vis*. 2018;6(1):1–6.
190. Wang Z, Gu S, Leader JK, Kundu S, Tedrow JR, Sciruba FC, et al. Optimal threshold in CT quantification of emphysema. *Eur Radiol*. 2013 Apr;23(4):975–84.
191. Bae HJ, Kim CW, Kim N, Park B, Kim N, Seo JB, et al. A Perlin Noise-Based Augmentation Strategy for Deep Learning with Small Data Samples of HRCT Images. *Sci Rep*. 2018 Dec 6;8(1):17687.
192. Gruden JF. CT in idiopathic pulmonary fibrosis: diagnosis and beyond. *Am J Roentgenol*. 2016;206(3):495–507.
193. Szegedy C, Ioffe S, Vanhoucke V, Alemi A. Inception-v4, Inception-ResNet and the Impact of Residual Connections on Learning. *Proc AAAI Conf Artif Intell [Internet]*. 2017 Feb 12 [cited 2022 Jul 6];31(1). Available from: <https://ojs.aaai.org/index.php/AAAI/article/view/11231>
194. He K, Zhang X, Ren S, Sun J. Deep Residual Learning for Image Recognition. In: 2016 IEEE Conference on Computer Vision and Pattern Recognition (CVPR). 2016. p. 770–8.
195. Richeldi L, du Bois RM, Raghu G, Azuma A, Brown KK, Costabel U, et al. Efficacy and safety of nintedanib in idiopathic pulmonary fibrosis. *N Engl J Med*. 2014 May 29;370(22):2071–82.
196. Costabel U, Albera C, Lancaster LH, Lin CY, Hormel P, Hulter HN, et al. An Open-Label Study of the Long-Term Safety of Pirfenidone in Patients with Idiopathic Pulmonary Fibrosis (RECAP). *Respir Int Rev Thorac Dis*. 2017;94(5):408–15.
197. Crestani B, Huggins JT, Kaye M, Costabel U, Glaspole I, Ogura T, et al. Long-term safety and tolerability of nintedanib in patients with idiopathic pulmonary fibrosis: results from the open-label extension study, INPULSIS-ON. *Lancet Respir Med*. 2019 Jan;7(1):60–8.
198. Costabel U, Albera C, Glassberg MK, Lancaster LH, Wuyts WA, Petzinger U, et al. Effect of pirfenidone in patients with more advanced idiopathic pulmonary fibrosis. *Respir Res*. 2019 Mar 12;20(1):55.

199. Raghu G, van den Blink B, Hamblin MJ, Brown AW, Golden JA, Ho LA, et al. Long-term treatment with recombinant human pentraxin 2 protein in patients with idiopathic pulmonary fibrosis: an open-label extension study. *Lancet Respir Med*. 2019 Aug;7(8):657–64.
200. Armstrong N, Hilton P. Doing diagnosis: whether and how clinicians use a diagnostic tool of uncertain clinical utility. *Soc Sci Med* 1982. 2014 Nov;120:208–14.
201. Grote T, Berens P. On the ethics of algorithmic decision-making in healthcare. *J Med Ethics*. 2020 Mar;46(3):205–11.
202. Wernick MN, Yang Y, Brankov JG, Yourganov G, Strother SC. Machine Learning in Medical Imaging. *IEEE Signal Process Mag*. 2010 Jul;27(4):25–38.
203. Netto SMB, Leite VRC, Silva AC, Paiva AC de, Neto A de A. Application on Reinforcement Learning for Diagnosis Based on Medical Image [Internet]. *Reinforcement Learning*. IntechOpen; 2008 [cited 2022 Aug 8]. Available from: <https://www.intechopen.com/chapters/undefined/state.item.id>
204. Ker J, Wang L, Rao J, Lim T. Deep Learning Applications in Medical Image Analysis. *IEEE Access*. 2018;6:9375–89.
205. Yu C, Liu J, Nemati S, Yin G. Reinforcement learning in healthcare: A survey. *ACM Comput Surv CSUR*. 2021;55(1):1–36.
206. Chin M, Johns C, Currie BJ, Weatherley N, Hill C, Elliot C, et al. Pulmonary Artery Size in Interstitial Lung Disease and Pulmonary Hypertension: Association with Interstitial Lung Disease Severity and Diagnostic Utility. *Front Cardiovasc Med* [Internet]. 2018 [cited 2022 Aug 8];5. Available from: <https://www.frontiersin.org/articles/10.3389/fcvm.2018.00053>
207. Hamzah MFM, Kasim RM, Yunus A, Rijal OM, Noor NM. Detection of Interstitial Lung Disease using correlation and regression methods on texture measure. In: 2017 IEEE International Conference on Imaging, Vision & Pattern Recognition (icIVPR). 2017. p. 1–4.
208. Taooka Y, Takezawa G, Ohe M, Sutani A, Isobe T. Multiple logistic regression analysis of risk factors in elderly pneumonia patients: QTc interval prolongation as a prognostic factor. *Multidiscip Respir Med* [Internet]. 2014 Nov 22 [cited 2022 Aug 8];9(1):59. Available from: <https://doi.org/10.1186/2049-6958-9-59>
209. Jiang F, Jiang Y, Zhi H, Dong Y, Li H, Ma S, et al. Artificial intelligence in healthcare: past, present and future. *Stroke Vasc Neurol*. 2017 Dec;2(4):230–43.

210. Ayer T, Chhatwal J, Alagoz O, Kahn CE, Woods RW, Burnside ES. Comparison of Logistic Regression and Artificial Neural Network Models in Breast Cancer Risk Estimation. *Radiographics* [Internet]. 2010 Jan [cited 2022 Aug 8];30(1):13–22. Available from: <https://www.ncbi.nlm.nih.gov/pmc/articles/PMC3709515/>
211. Pathological lung segmentation based on random forest combined with deep model and multi-scale superpixels | SpringerLink [Internet]. [cited 2022 Aug 8]. Available from: <https://link.springer.com/article/10.1007/s11063-020-10330-8>
212. Pikoula M, Quint JK, Nissen F, Hemingway H, Smeeth L, Denaxas S. Identifying clinically important COPD sub-types using data-driven approaches in primary care population based electronic health records. *BMC Med Inform Decis Mak* [Internet]. 2019 Apr 18 [cited 2022 Aug 8];19(1):86. Available from: <https://doi.org/10.1186/s12911-019-0805-0>
213. Powell GA, Verma A, Luo Y, Stephens D, Buckeridge D. Modeling Chronic Obstructive Pulmonary Disease Progression Using Continuous-Time Hidden Markov Models. *Stud Health Technol Inform*. 2019 Aug 21;264:920–4.
214. Kwon BC, Anand V, Severson KA, Ghosh S, Sun Z, Frohnert BI, et al. DPVis: Visual Analytics With Hidden Markov Models for Disease Progression Pathways. *IEEE Trans Vis Comput Graph*. 2021 Sep;27(9):3685–700.
215. Li Q, Cai W, Wang X, Zhou Y, Feng DD, Chen M. Medical image classification with convolutional neural network. In: 2014 13th International Conference on Control Automation Robotics & Vision (ICARCV). 2014. p. 844–8.
216. Weeks J, Pardee R. Learning to Share Health Care Data: A Brief Timeline of Influential Common Data Models and Distributed Health Data Networks in U.S. Health Care Research. *eGEMs* [Internet]. [cited 2022 Oct 4];7(1):4. Available from: <https://www.ncbi.nlm.nih.gov/pmc/articles/PMC6437693/>
217. Ancusa V, Broasca L. A method to pinpoint undiscovered links in genetic and protein networks. In: *Digital Healthcare Empowering Europeans*. IOS Press; 2015. p. 771–5.
218. Danese MD, Halperin M, Duryea J, Duryea R. The generalized data model for clinical research. *BMC Med Inform Decis Mak*. 2019;19(1):1–13.
219. Li J, Chen Q, Liu B. Classification and disease probability prediction via machine learning programming based on multi-GPU cluster MapReduce system. *J Supercomput*. 2017;73(5):1782–809.

220. Vulliard L, Menche J. Complex Networks in Health and Disease. *Syst Med*. 2021;26–33.
221. Lanzoni G, Cardinale V, Carpino G. The hepatic, biliary, and pancreatic network of stem/progenitor cell niches in humans: A new reference frame for disease and regeneration. *Hepatology*. 2016 Jul;64(1):277–86.
222. Broasca L, Ancusa VM, Ciocarlie H. A qualitative analysis on force directed network visualization tools in the context of large complex networks. In: 2019 23rd International Conference on System Theory, Control and Computing (ICSTCC). IEEE; 2019. p. 656–61.
223. Broască L, Ancușa V, Ciocârliie H. Bioinformatics visualisation tools: An unbalanced picture. In: *Exploring Complexity in Health: An Interdisciplinary Systems Approach*. IOS Press; 2016. p. 760–4.
224. Das AB. Lung disease network reveals the impact of comorbidity on SARS-CoV-2 infection. *bioRxiv*. 2020;
225. Ryu JH, Daniels CE, Hartman TE, Yi ES. Diagnosis of interstitial lung diseases. *Mayo Clin Proc*. 2007 Aug;82(8):976–86.
226. Molina-Molina M, Aburto M, Acosta O, Ancochea J, Rodríguez-Portal JA, Sauleda J, et al. Importance of early diagnosis and treatment in idiopathic pulmonary fibrosis. *Expert Rev Respir Med*. 2018 Jul;12(7):537–9.
227. Trusculescu AA, Manolescu D, Tudorache E, Oancea C. Deep learning in interstitial lung disease—how long until daily practice. *Eur Radiol*. 2020 Nov 1;30(11):6285–92.
228. Chen A, Karwoski RA, Gierada DS, Bartholmai BJ, Koo CW. Quantitative CT Analysis of Diffuse Lung Disease. *Radiogr Rev Publ Radiol Soc N Am Inc*. 2020 Feb;40(1):28–43.
229. Tatjana Z, Busayarat S. Computer-aided Analysis and Interpretation of HRCT Images of the Lung. *Theory Appl CT Imaging Anal*. 2011;26.
230. Depeursinge A, Zrimec T, Busayarat S, Müller H. 3D lung image retrieval using localized features. In: *Medical Imaging 2011: Computer-Aided Diagnosis*. SPIE; 2011. p. 701–14.
231. Smith KM. Explaining the emergence of complex networks through log-normal fitness in a Euclidean node similarity space. *Sci Rep*. 2021;11(1):1–14.
232. Adler M, Mayo A, Alon U. Logarithmic and power law input-output relations in sensory systems with fold-change detection. *PLoS Comput Biol*. 2014;10(8):e1003781.
233. Shang Y. Degree distribution dynamics for disease spreading with individual awareness. *J Syst Sci Complex*. 2015;28(1):96–104.

234. Pastor-Satorras R, Castellano C, Van Mieghem P, Vespignani A. Epidemic processes in complex networks. *87 (3): 925–979. ArXiv Prepr ArXiv14082701. 2015;*
235. Guler SA, Corte TJ. Interstitial Lung Disease in 2020: A History of Progress. *Clin Chest Med. 2021 Jun;42(2):229–39.*
236. Hovinga M, Sprengers R, Kauczor HU, Schaefer-Prokop C. CT Imaging of Interstitial Lung Diseases. *Multidetector-Row CT Thorax. 2016 Feb 27;105–30.*
237. Tomassetti S, Ravaglia C, Poletti V. Diffuse parenchymal lung disease. *Eur Respir Rev. 2017;26(144).*
238. Hieba EG, Shaimaa EE, Dina SS, Noha AO. Diffusion lung capacity for carbon monoxide correlates with HRCT findings in patients with diffuse parenchymal lung disease. *Egypt J Bronchol [Internet]. 2020 Nov 10 [cited 2022 Sep 25];14(1):39. Available from: <https://doi.org/10.1186/s43168-020-00042-x>*
239. Kim HC, Lee JH, Chae EJ, Song JS, Song JW. Long-term clinical course and outcome of interstitial pneumonia with autoimmune features. *Respirol Carlton Vic. 2020 Jun;25(6):636–43.*
240. Brown KK, Inoue Y, Flaherty KR, Martinez FJ, Cottin V, Bonella F, et al. Predictors of mortality in subjects with progressive fibrosing interstitial lung diseases. *Respirol Carlton Vic. 2022 Apr;27(4):294–300.*
241. Hussein K, Shaaban LH, Mohamed E. Correlation of high resolution CT patterns with pulmonary function tests in patients with interstitial lung diseases. *Egypt J Chest Dis Tuberc [Internet]. 2016 [cited 2022 Sep 25];65(3). Available from: <https://cyberleninka.org/article/n/1206630>*
242. Cristian Oancea Ovidiu Fira-Mlădinescu Voicu Tudorache V. *Tratat de Pneumologie pentru medici rezidenti. In: Capitolul 3 Metode de investigatie imagistica a patologiei pulmonare. p. 42–59.*
243. Lee SH, Park JS, Kim SY, Kim DS, Kim YW, Chung MP, et al. Comparison of CPI and GAP models in patients with idiopathic pulmonary fibrosis: a nationwide cohort study. *Sci Rep. 2018 Mar 19;8(1):4784.*
244. Hyltdgaard C, Hilberg O, Bendstrup E. Validation of GAP score in Danish patients diagnosed with idiopathic pulmonary fibrosis. *Eur Respir J [Internet]. 2013 Sep 1 [cited 2022 Sep 25];42(Suppl 57). Available from: https://erj.ersjournals.com/content/42/Suppl_57/P2367*
245. GHID DE DIAGNOSTIC AI TRATAMENT AL PNEUMOPATIILOR INTERSTIAIALE DIFUZE. GRUPUL DE LUCRU PENTRU PNEUMOPATII INTERSTIPIALE DIFUZE ȘI SARCOIDOZĂ. 2015.

246. Wells AU, Brown KK, Cottin V. The progressive fibrotic phenotype in current clinical practice. *Curr Opin Pulm Med* [Internet]. 2021 Sep 1 [cited 2022 Sep 25];27(5):368–73. Available from: <https://doi.org/10.1097/MCP.0000000000000805>
247. Differential diagnosis of usual interstitial pneumonia: when is it truly idiopathic? | European Respiratory Society [Internet]. [cited 2022 Sep 25]. Available from: <https://err.ersjournals.com/content/23/133/308>
248. Possible UIP pattern on high-resolution computed tomography is associated with better survival than definite UIP in IPF patients - PubMed [Internet]. [cited 2022 Sep 25]. Available from: <https://pubmed.ncbi.nlm.nih.gov/28947036/>
249. Probable usual interstitial pneumonia pattern on chest CT: is it sufficient for a diagnosis of idiopathic pulmonary fibrosis? | European Respiratory Society [Internet]. [cited 2022 Sep 25]. Available from: <https://erj.ersjournals.com/content/55/4/1802465>
250. Alsumrain M, De Giacomi F, Nasim F, Koo CW, Bartholmai BJ, Levin DL, et al. Combined pulmonary fibrosis and emphysema as a clinicoradiologic entity: Characterization of presenting lung fibrosis and implications for survival. *Respir Med*. 2019 Jan;146:106–12.
251. Silva M, Nunes H, Valeyre D, Sverzellati N. Imaging of Sarcoidosis. *Clin Rev Allergy Immunol*. 2015 Aug;49(1):45–53.
252. Imaging of Sarcoidosis - Document - Gale OneFile: Health and Medicine [Internet]. [cited 2022 Sep 25]. Available from: <https://go.gale.com/ps/i.do?id=GALE%7CA426188134&sid=googleScholar&v=2.1&it=r&linkaccess=abs&issn=10800549&p=HRCA&sw=w&userGroup=anon%7Ef4af421b>
253. Cryptogenic organizing pneumonia | Radiology Reference Article | Radiopaedia.org [Internet]. [cited 2022 Sep 25]. Available from: <https://radiopaedia.org/articles/cryptogenic-organising-pneumonia-1>
254. The Radiology Assistant : HRCT - Basic Interpretation [Internet]. [cited 2022 Sep 25]. Available from: <https://radiologyassistant.nl/chest/hrct/basic-interpretation>
255. Belfiore MP, Urraro F, Grassi R, Giacobbe G, Patelli G, Cappabianca S, et al. Artificial intelligence to codify lung CT in Covid-19 patients. *Radiol Med (Torino)*. 2020 May;125(5):500–4.
256. Collins J, Stern EJ. *Chest radiology: the essentials*. Lippincott Williams & Wilkins; 2008.
257. Dalpiaz G, Cancellieri A. Alveolar pattern. In: *Atlas of Diffuse Lung Diseases*. Springer; 2017. p. 145–62.

258. Torres PPTES, Rabahi MF, Moreira MA do C, Escuissato DL, Meirelles G de SP, Marchiori E. Importance of chest HRCT in the diagnostic evaluation of fibrosing interstitial lung diseases. *J Bras Pneumol Publicacao Of Soc Bras Pneumol E Tisiologia*. 2021;47(3):e20200096.
259. Ridge CA, Bankier AA, Eisenberg RL. Mosaic attenuation. *AJR Am J Roentgenol*. 2011 Dec;197(6):W970-977.
260. Gaillard F. Respiratory bronchiolitis-interstitial lung disease | Radiology Reference Article | Radiopaedia.org [Internet]. Radiopaedia. 2022 [cited 2022 Feb 13]. Available from: <https://radiopaedia.org/articles/respiratory-bronchiolitis-interstitial-lung-disease-2>
261. Rossi SE, Erasmus JJ, Volpacchio M, Franquet T, Castiglioni T, McAdams HP. “Crazy-paving” pattern at thin-section CT of the lungs: radiologic-pathologic overview. *Radiographics*. 2003;23(6):1509–19.
262. Gupta N, Vassallo R, Wikenheiser-Brokamp KA, McCormack FX. Diffuse Cystic Lung Disease. Part II. *Am J Respir Crit Care Med*. 2015 Jul 1;192(1):17–29.
263. Costa L da F, Rodrigues FA, Travieso G, Villas Boas PR. Characterization of complex networks: A survey of measurements. *Adv Phys*. 2007;56(1):167–242.
264. Nambiar AM, Walker CM, Sparks JA. Monitoring and management of fibrosing interstitial lung diseases: a narrative review for practicing clinicians. *Ther Adv Respir Dis*. 2021;15:17534666211039772.
265. Best AC, Lynch AM, Bozic CM, Miller D, Grunwald GK, Lynch DA. Quantitative CT Indexes in Idiopathic Pulmonary Fibrosis: Relationship with Physiologic Impairment. *Radiology* [Internet]. 2003 Aug [cited 2022 Sep 25];228(2):407–14. Available from: <https://pubs.rsna.org/doi/abs/10.1148/radiol.2282020274>